UNDERSTANDING THE INFLUENCE OF THE ELECTRODE MATERIAL ON MICROBIAL FUEL CELL PERFORMANCE

by

David V. P. Sanchez

B.S. in Civil Engineering, University of Portland, 2006

M.S. in Civil Engineering, University of Pittsburgh, 2010

Submitted to the Graduate Faculty of

Swanson School of Engineering in partial fulfillment

of the requirements for the degree of

Doctor of Philosophy

University of Pittsburgh

2013

UNIVERSITY OF PITTSBURGH

SWANSON SCHOOL OF ENGINEERING

This dissertation was presented

by

David V. P. Sanchez

It was defended on

May 30, 2013

and approved by

Kyle J. Bibby, PhD, Assistant Professor, Department of Civil and Environmental Engineering

Kelvin B. Gregory, PhD, Associate Professor, Department of Civil and Environmental Engineering Carnegie Mellon University

Leonard W. Casson, PhD, Associate Professor, Department of Civil and Environmental Engineering

Kent Harries, PhD, Associate Professor, Department of Civil and Environmental Engineering

Dissertation Co-Director: Radisav D. Vidic, PhD, Professor, Department of Civil and Environmental Engineering

Dissertation Co-Director: Minhee Yun, PhD, Associate Professor, Department of Electrical and Computer Engineering

UNDERSTANDING THE INFLUENCE OF THE ELECTRODE MATERIAL ON MICROBIAL FUEL CELL PERFORMANCE

David V. P. Sanchez, Ph.D.

University of Pittsburgh, 2013

In this thesis, I deploy sets of electrodes into microbial fuel cells (MFC), characterize their performance, and evaluate the influence of both platinum catalysts and carbon-based electrodes on current production. The platinum work centers on improving current production by optimizing the use of the catalyst using nano-fabrication techniques. The carbon-electrode work seeks to determine the influence of the bare electrode on biofilm-anode current production.

The development of electrodes for MFCs has boomed over the past decade, however, experiments aimed at identifying how catalyst deposition methods and electrode properties influence current production have been limited. The research conducted here is an attempt to expand this knowledge base for platinum catalysts and carbon electrodes. In the initial chapters (4 and 5), I discuss our attempt to decrease catalyst loadings while increasing current production through the use of platinum nanoparticles. The results demonstrate that incorporating platinum nanoparticles throughout the anode and cathode is an efficient means of increasing MFC current production relative to surface deposition because it increases catalyst surface area.

The later chapters (chapters 6 and 7) develop an understanding of the importance of electrode properties (i.e. surface area, activation resistance, conductivity, surface morphology) by electrochemically evaluating well-studied anode-respiring pure cultures on different carbon

electrode architectures. Two different architectures are produced by using tubular and platelet shaped constituent materials (i.e. carbon fibers and graphene nanoplatelets) and the morphologies of the electrodes are varied by altering the size of the constituent material.

The electrodes are characterized and evaluated in MFCs using either *Shewanella oneidensis* MR-1 or *Geobacter sulfurreducens* as the innoculant because their bioelectrochemical physiologies are the most documented in the literature. Using the electrochemical results, the electrode characterizations and previous studies on their physiology I am able to extrapolate that it is the difference in the electrode morphology that significantly alters current production. For the carbon fiber, smaller constituent materials create a tighter mesh and spacing that is more amenable to biofilm colonization and increases current production. In the second experiment, the larger graphene-nanoplatelet constituents provided a morphology that better promoted biofilm-growth, after the initial colonization, which enabled significantly higher current production.

TABLE OF CONTENTS

LIST OF TABLES

LIST OF FIGURES

PREFACE

Looking back at my time here at the University of Pittsburgh I am humbled by the generosity and privileges I have been afforded. I pray for the grace and virtue to continually pay it forward. I would like to thank my co-advisors Dr. Minhee Yun and Dr. Radisav Vidic for allowing me to pursue interdisciplinary research and for their support and guidance. I want to thank my committee members Dr. Kelvin Gregory, Dr. Kyle Bibby, and Dr. Kent Harries for their time, invaluable insight and suggestions and express my gratitude to the Mascaro Center for Sustainable Innovation's IGERT program, the National Science Foundation Graduate Research Fellowship Program and the Alfred P. Sloan Foundation's NACME program for the financial and logistical support they've consistently provided throughout my studies .

I have received an extensive amount of support from multiple collaborators and colleagues and I want to thank them for their help namely; Xuyen Nguyen and Dr. Younghee Lee from Sungkyunkwan University in Suwon, South Korea, Mikhail Kozlov and Dr. Ray Baughman at the University of Texas-Dallas, Dr. Jeff Lawrence, Dr. Kristen Butella, and Brian Goddard from Pitt Biosciences, Dr. Jeff Gralnick at the University of Minnesota, Dr. Kelly Nevin, Trevor Woodward, Dr. Nikhil Malvenkar and Dr. Derek Lovley from the University of Massachusetts-Amherst, Dr. Ho Il Park, Dr. Yushi Hu, Dr. Innam Lee, Dr. Dave Perello, Dan Jacobs, and Jiyong Huang from the Nanoelectronics Device Laboratory and the other IGERT fellows in my program.

Finally, from the bottom of my heart, I would like to thank God, my family and my friends who have supported me throughout my journey with love and encouragement. To Grandma and Grandpa Kotla, Nana and Grandpa Sanchez, Mom, Dad, siblings, cousins, aunts, uncles, nieces, nephews, Godchildren and friends, Si Yu'us Ma'ase. This dissertation is dedicated to Our Blessed Mother in honor of all of you, our ancestors and all those generations still to come.

1.0 INTRODUCTION

Using bacterial biofilms as catalysts to convert our waste into electricity is an attempt to tap into a natural wastewater-energy nexus to produce both clean energy and clean water. A microbial fuel cell (MFCs) is a technology used to harness this process because wastewater often contains more energy than is used to treat it. As a result, improving MFC technology to generate electricity via the degradation of our organic waste, could decrease our energy costs for treating wastewater (i.e. less aeration in wastewater treatment), transform a waste stream into an energy feedstock and convert a wastewater treatment plant into a net energy producer. This would fundamentally change the sector currently responsible for 2% of our national energy consumption.[1]

While the current state of the art for MFCs is insufficient for wastewater treatment applications, the benefits of improving our fundamental understanding of biofilm-anodes expand well beyond MFC development. The interaction between electricity producing biofilms and electrodes will allow researches from various fields such as material science, chemistry, biophysics, and environmental engineering to extrapolate these concepts to improve other biotechnologies (i.e. environmental sensing, remote power generation, and bioremediation) all of which are crucial to the future of water quality monitoring and treatment.

Two of the main research objectives associated with the development of MFCs are increasing current production and understanding the influence of the bare electrode on the biofilm-electrode interface. In this thesis, I focus on increasing the efficient use of a metal catalyst using nanofabrication methods and on understanding what aspects of the bare carbon electrode are most important for biofilm-electrode current production. For the catalyst, I chose platinum as a catalyst because it is a common fuel cell catalyst and it has been characterized sufficiently (i.e. well defined cyclic voltammograms, catalyst poisons are known). While it is impractical from a cost perspective save for space missions, the following studies and fabrication methods can serve as a foundation for future aimed at understanding the role of a metal catalyst in an MFC electrode or as a framework for optimizing inexpensive alternatives.

I employ different deposition methods (e.g. e-beam evaporation, adsorption and sublimation, co-deposition) to load platinum onto the electrode in order to determine what aspects of the catalyst (location, thickness, and surface area) are most important for current production from the biofilm-anode and the cathode. I use material characterization methods to confirm the nature of our deposits and evaluate the electrodes in MFCs. When the effect of changing the thickness of the surface deposited platinum is shown to be negligible the focus shifts to efficiently increasing the surface area of platinum through the use of nanoparticles incorporated throughout the electrode. The metric used to determine whether I am increasing the efficient use of the catalyst is the mass-specific current density (current/mg of Pt).

In order to understand what aspects (i.e. surface area, activation resistance, conductivity, surface morphology) of the bare electrode are most important for biofilm-anode current production I use carbon-based electrodes whose constituent material sizes could be modified. Carbon is chosen because it is relatively abundant, is inexpensive, has many phases, is generally

non-toxic and can be manipulated to have different surface areas. Being able to adjust the size of the constituent material is important because it allows one to start engineering the electrode. However, it is important to note that changing the size of the constituent material often results in changes to the electrode surface area, electron transfer kinetics, electrode conductivity, and electrode surface morphology. The challenge of isolating the effects of each of these parameters on biofilm-anode current production is compounded by the fact that the physiologies of the bacteria that form the biofilm are not completely understood and that the complexity of a biofilm's physiological profile increases with increasingly mixed communities. I address these challenges by using dissimiliatory-metal-reducing bacteria whose physiologies have been extensively studied in bioelectrochemical systems such as microbial fuel cells. I chose *Shewanella oneidensis* MR-1 and *Geobacter sulfurreducens* because the nature of their electron transfer mechanisms to electrodes are well documented in the literature and the numerous studies on their physiology in bioelectrochemical systems provide an insight into the formation and health of the biofilm-anode. Along with electrochemical techniques (i.e. amperometry and cyclic voltammetry) and experimental designs that take into account biofilm kinetics, bioelectrochemistry, and the physiology of the respective strain this is important to understanding how the electrode is interfacing with the biofilm and influencing the current production from the biofilm-anode.

1.1 WHAT IS A MICROBIAL FUEL CELL?

Microbial fuel cells are devices that convert chemical energy to electrical energy using the metabolisms of bacteria as catalysts. The reactor is often divided by a proton exchange membrane into two compartments, the anode and cathode compartments containing the anode and cathode electrodes respectively. As substrate (i.e. organic biodegradable matter) is fed into the anode compartment bacteria (typically set in a biofilm) oxidize the substrate. In the absence of soluble thermodynamically favorable electron acceptors (i.e. oxygen, nitrate, sulfate) electrons are transferred to the anode via a protein-based electron transport chain. Essentially the bacteria are performing respiration on a solid conductor. These bacteria are collectively known as Electrochemically Active Bacteria (EAB) , Electricigens, or Anode-Respiring Bacteria (ARB).

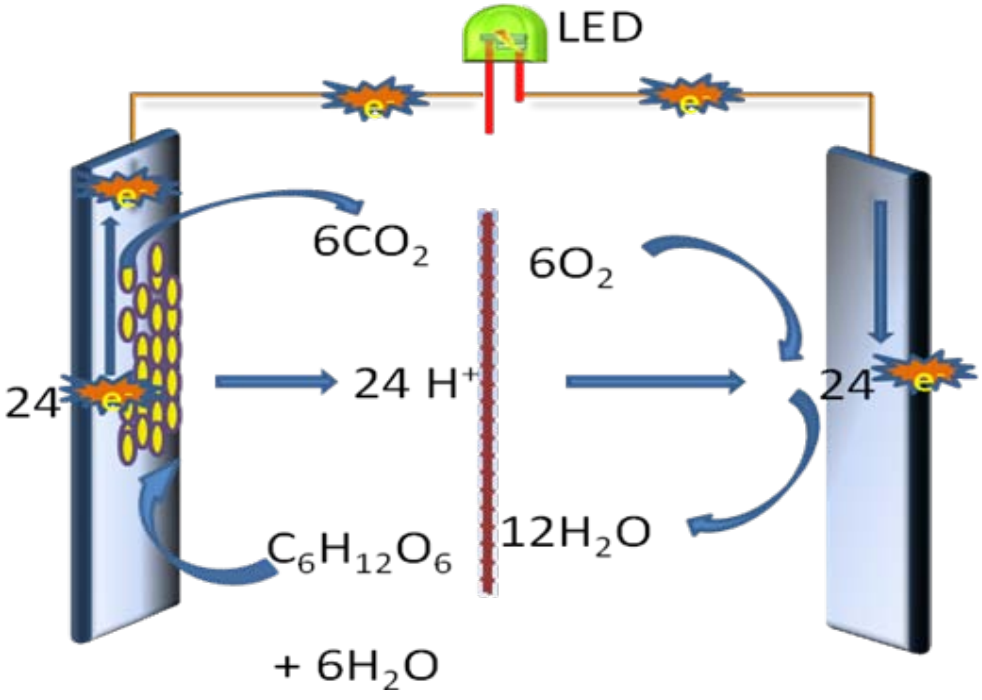

Figure 1. Microbial Fuel Cell schematic showing the biofilm-anode (left), and the cathode (right).[2]

The initial discovery of this bio-electrochemical phenomenon by James Potter took place in 1911. [3] He monitored the electrical effects associated with fermentation by constructing a galvanic cell based on platinum wires and a pure culture of yeast. He measured the potential difference and discovered the first bio-based battery. The bio-electrochemical concept was presented again in the literature in 1931 by Cohen who was able to generate 35 volts but only 2mA with his reactors.[4] The study of this phenomenon then cycled with scientific breakthroughs and technology demand. For example, advances in battery science and NASA's goal of waste to energy production for space missions spurred research during the 1960s. [5] The concept attracted some interest in the 1970s[6-7] but faded as the costs of fossil fuel based energy decreased dramatically. In the 1980's and early 90's H.P. Benetto reignited MFC research as a way to produce energy in developing countries[8-11]. Research was fairly small scale until the late 90's saw a surge in MFC research as the issues of climate change and energy came into focus. Since then there has been a major convergence of various disciplines in MFC research; namely material science, environmental engineering, electrical engineering, biophysics, microbial physiology, genetics and electrochemistry. Contributions from scientists and engineers of all backgrounds have pushed the knowledge base and made the study of MFCs a truly interdisciplinary endeavor.

1.2 TECHNOLOGY PERSPECTIVE

Oftentimes MFCs are compared to hydrogen fuel cells which are ubiquitous in the literature. And while it is easy to see that current densities for hydrogen fuel cells are 2-3 orders of magnitude greater than those produced by MFCs [12] it is also important to note that the two technologies differ greatly in operating conditions and applications [13-14]. MFCs operate at ambient temperature and pressure and utilize a variety of substrates as their fuel source. As a result, MFCs are more versatile and can better serve to convert our wastewater, which contains energy equivalent to ~2% of total US electricity demand, to electricity [1, 15] .

Recent reports suggest that creating an MFC with a consistent power output of 1 kW/m^3 (volume of the reactor) would allow the technology to be economically viable for wastewater treatment application [14, 16]. A quick comparison would show that deployed waste-to-energy technologies such as converting methane gas from an anaerobic digester to electricity via combustion, assuming 40% conversion efficiency, produces 1.5kW /m3 of reactor per kg COD removed. [16-17]. Given relatively equal power outputs the competitive advantage will be given to the technology with a lower implementation/capital costs. Therefore understanding the role that materials play in the performance of MFCs is critical for MFC development and for scaling up operations [18] that will be both economically viable and competitive.

Finally, understanding the effect of catalyst/electrode architectures on biofilm-electrode interactions will provide a framework to evaluate novel materials and or deposition methods. This fundamental research is not only essential for improving MFC performance but also has implications for the development of biotechnologies in medicine, bioremediation, and water

quality. The biofilm-electrode may also serve as a tool to enhance our understanding of fundamental phenomena in microbiology, biophysics, electronics, and bio-electrochemistry.

2.0 BACKGROUND

2.1 FUEL CELL ELECTROCHEMISTRY

2.1.1 Overpotentials

The deployment of MFCs is hindered by low power generation. These low current densities restrain the technology from being economically viable. The low current densities are due mainly to the internal resistance of the reactors. This internal resistance can be defined as the collective resistance experienced as electrons and protons travel from substrate, through the fuel cell to the terminal electron acceptor [14]. This internal resistance can be graphically explained via the polarization curve (I-V curve) in the following figure.

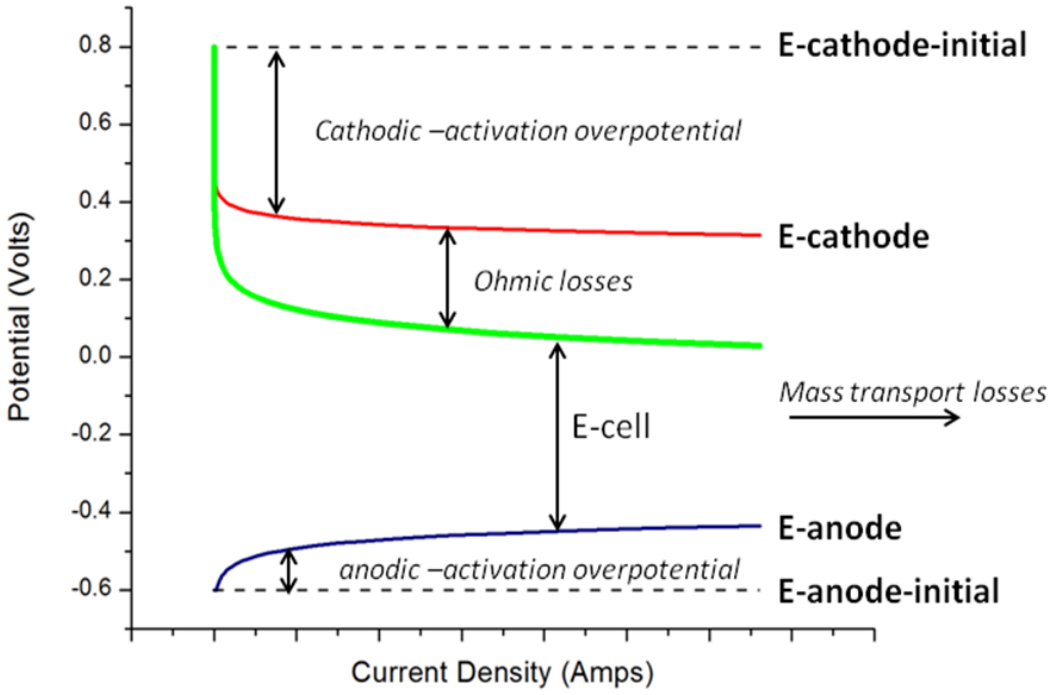

Figure 2. Polarization curve used to illustrate the typical potential losses in a fuel cell. Potential losses can be calculated by subtracting the upper (upper line) and lower (bottom line) bounds straddling each region. The three main designations given to the resistances in an electrolytic cell are activation overtpotential, ohmic losses/drop ,and mass transfer overpotential.

Potential losses in a MFC collectively make up the internal resistance.[19] In an electrolytic cell they are often described as overpotentials while in a fuel cell one can simply refer to them as resistances (i.e. the activation resistance, the ohmic resistance, and the mass transfer resistance).[20] The activation resistance describes the energy barrier encountered during an electron transfer to the electrode. This is the same activation energy barrier used to describe electron transfer in basic chemical reactions. The ohmic resistance describes the resistivity of the electrolyte and of the physical elements of the fuel cell (e.g. electrodes). Ohmic resistances are derived from the inherent properties of the fuel cell materials and their design. The mass transfer

resistance describes the resistance imposed upon the fuel cell at high current densities. As the fuel/substrate diffuses toward the electrode there is a reaction rate at which the mass transport of the fuel/substrate cannot keep up with the rate at which it is being consumed at the electrode. This resistance, derived from the concentration of the electrolyte and its diffusivity, is generally described as the mass transfer resistance.

2.1.2 The Effect of Catalysts on Electron Transfer

Catalysts, typically bound on the electrode, are used to reduce the activation resistance experienced by electrons during electron transfer to or from the electrode. Catalysts are used for both anodic and cathodic reactions. A catalyst typically reduces the activation energy barrier for electron transfer by enabling a more efficient reaction setup, electron transfer, and reaction termination (e.g. dissociation of the target molecule, increased formation of reactive species, increased coordination between donor and acceptor). Typically, catalysts increase reaction rates by addressing the rate-limiting step and increasing the availability of a catalyst may increase the reaction rate. Though catalysts are not consumed in the reaction they can undergo poisoning when its reactive sites bond with another compound and prevent it from reacting with the target substrate. Catalysts are also subject to physical stresses that may remove it from the electrode.

2.1.3 The Effect of Electrode Properties on Electrochemical Reactions

The rate of a basic electrochemical reaction on a bare electrode (i.e. without a catalyst) will be influenced by the electron transfer kinetics between the target compound and the electrode, the

total available reactive surface area of the electrode and the conductivity of the electrode. Some electrode materials are able to catalyze reactions and reduce the activation resistance for electron transfer while most increase performance by increasing the total available reactive surface area. In MFCs, carbon-based electrodes are often used and performance enhancements have been largely attributed to the increase in surface area (e.g. carbon nanotubes, graphene). As for conductivity, it is largely determined by the density of the material. The conductivity of an electrode is a function of areal wt (i.e. mass/geometric area) so that a larger areal weight will increase the conductivity of the electrode and reduce the ohmic resistance.

2.2 MICROBIAL FUEL CELL BACTERIA

2.2.1 Substrates and Strains

Understanding and determining the flow of electrons from substrate to bacterium to anode requires information about a cell's physiology and energetics. These can vary for each bacterial strain. As bacterial communities diversify, which is the case in the majority of environmental contexts, quantifying the flux of electrons is increasingly difficult because of competition amongst bacteria, electron sinks (methanogens), and poorly quantified mechanisms. The ability of bacteria to generate electricity from a variety of substrates adds to the complexity especially since researchers have generated power using fermentable and non-fermentable substrates, a variety of bacterial strains and mixed communities [21]. As a result, the community dynamics of a biofilm make it increasingly difficult to measure and model electron flux and electrochemical

reactions. Consequently, efforts to qualify the effect of community structure on MFC performance or use well-studied pure cultures in MFC experiments are becoming increasingly important [22-23] .

2.3 EXTERNAL ELECTRON TRANSFER (EET) MECHANISMS

2.3.1 Direct Electron Transfer

Direct electron transfer assumes that bacteria arrange their outer membranes to be adjacent and physically connected to the anode electrode [24]. The fundamental assumption here is that the proximity of the bacteria to the electrode is necessary for electron transfer. Some have suggested that this mechanism is impractical for describing all anode reactions because MFC biofilms were shown to sustain bacteria more than 10 μm from the electrode [25] and that this EET model could not kinetically account for the high current densities (i.e. 10A/m^2) reported by the literature. [25]

2.3.2 Mediated Electron Transfer

Mediated electron transfer, which has been documented in various papers [26-28], occurs when bacteria use chemical redox mediators to transfer electrons. In short, bacteria would reduce a mediator (i.e. thionine, methyl viologen, methyl blue, humic acid, neutral red) [29-30] which diffuses to the anode, is oxidized, and then diffuses back to the cell to be reduced. Newman and

Kolter demonstrated this for the pure culture of *Shewanella oneidensis* [31]. Another study suggested that some bacteria are able to use mediators produced by foreign bacteria to transfer electrons. [32] The key to this mechanism is that you have a soluble mediator diffusing back and forth between bacteria and electrode. Given this EET model, the main limitations for electricity production would be the concentration of the mediators and the mass transport resistance that would be experienced at high current densities. However, while it has been proven that this is a valid EET model it also does not kinetically account for the high current densities reported in the literature.

2.3.3 Conduction-based Electron Transfer

Conduction-based electron transfer implies that bacteria are able to conduct electrons to the anode via the biofilm matrix [33]. A cursory review suggests that bacteria are able to do this via a network of bionanowires [34-41] or sequestered riboflavins [27]. Technically, conduction based transfer could use the same mechanisms used in mediated transfer however the mediators would be fixed and conjugated in the biofilm. Richter *et al.* demonstrated that *Geobacter sulfurreducens* used a conductive network of non-diffusing intermediates to transfer electrons to the anode [42]. Research is currently addressing how complex bacterial networks are able to transfer electrons in biofilms that can be as thick as 80µm [25] but the more important aspect is that the conduction-based electron transfer model has thus far been the basis for understanding the biofilm-anode and that it kinetically accounts for the highest current densities reported in the literature. [25]

2.4 BIOFILM-ANODE

In an MFC the biofilm-anode provides the framework for conversion of a chemical substrate to electricity. The biofilm metabolizes the substrate and transfers the resulting electrons to the anode via a series of protein-based redox reactions. The amount of electricity actually generated from these reactions depends on the efficiency with which a bacterium's outer membrane proteins or cytochromes transfer electrons to the anode. This efficiency is affected by 1) the metabolic efficiency of the bacteria metabolism and its electron transport chain and 2) the activation resistance between the electron transport chain and the anode. Although genetic engineering may improve the metabolic efficiency of the electron transport chain, it cannot optimize the anode, the terminal electron acceptor within the biofilm-anode. However, the activation resistance experienced in the terminal electron transfer could be improved by engineering a better connection between the electron transport chain and the anode through the use of a catalyst or a modified electrode. This is supported by the fact that protein-protein interactions have evolved to be efficient but protein-electrode interactions continue to be understood and developed. [43-45].

MFC research can often focus on one aspect of the biofilm-anode (the biofilm or the electrode) leaving the other much less developed. As researchers continue to understand both the microbiological and electrochemical aspects of the biofilm-anode it is important to capitalize on these developments simultaneously. For example, in a pure culture details about the bacterial

metabolism help to evaluate the substrate conversion efficiency and the nature of its electron transport chain given a specific electron acceptor. At the same time an in-depth characterization of the electrode (i.e. catalyst and or base electrode) enables one to thoroughly evaluate electron transfer efficiency from the electron transport chain to the anode using electrochemical techniques such a cyclic voltammetry. The field would benefit a great deal by combining pure cultures that have been well-characterized in a bioelectrochemical context with well designed electrodes in experiments.

2.5 APPLICATION OF MODIFIED ELECTRODES TO IMPROVE MICROBIAL FUEL CELL PERFORMANCE

In an attempt to use modified electrodes to improve MFC performance it is useful to think of the biofilm-anode as a tri-composite material. The electrode and catalyst form the initial composite and the anode respiring biofilm, which adds the biological material, acts as the final extension of the electrode. Given this schematic, it is easy to see that the electrode/catalyst materials might significantly influence electron transfer kinetics, ohmic resistance, mass transport resistance and biofilm colonization. These all have consequences for electricity production and in the case of the biofilm-anode, the long term growth and maintenance of the biofilm.

Catalyst and electrode materials such as conductive polymers, porphyrins, and non-noble metals have been used to improve current production in MFCs. [46] Further review shows that

most of the electrodes that have been used in MFCs to date were carbon based and have enabled some of the highest current densities in the literature. While many experiments have used various electrodes of different geometry and compositions in MFCs over the past 20 years [47-50], fewer have taken advantage of new nanofabrication and characterization techniques to focus on which specific catalyst and electrode properties (e.g. location of the catalyst, amount of catalyst, surface area of the catalyst and the electrode, electrode conductivity, electrode surface morphology) to improve MFC current production. These new nano-techniques present the ability to tailor electrode properties for more focused experiments.

For example, metals, such as platinum (Pt), have been used in MFCs to increase current densities. However, it is difficult to determine whether electrode fabrication should focus on increasing surface coverage, surface area to volume ratio, Pt layer thickness or electrode conductivity. Certainly, understanding how a well known catalyst like Pt or carbon-based electrodes affects performance will provide a foundation for the development of novel and innovative MFC electrodes[48, 51-54] using the host of other materials[49, 52-59] that have been shown to influence performance.

3.0 SCOPE AND OBJECTIVES

Many articles in the literature suggest that the use of catalysts and modified electrodes would improve current density by using a catalyst to decrease the activation resistance or modifying the electrode material to increase surface area. The research conducted and described below is an attempt to optimize the use of a platinum catalyst using nanofabrication methods and to determine which carbon electrode properties (i.e. surface area, activation resistance, electrode conductivity, electrode surface morphology) most influence MFC current production. The question to be answered is how does one efficiently use a catalyst in MFC electrodes and which aspects of the bare electrode significantly influence the current output of MFCs. While the initial experiments focus on the evaluating novel nanoparticle-based deposition methods to decrease platinum loading while increasing current density, the latter experiments seek to compliment the research by designing experiments aimed at identifying which properties (i.e. surface area, activation resistance, electrode conductivity, surface morphology) of the carbon electrode enable high current production from the biofilm-anode. The scope of the dissertation research is limited to a study of a platinum catalyst and carbon-based electrodes. The two main objectives were to:

1.) Employ nanofabrication methods (e.g. e-beam deposition, co-deposition of nanoparticles) to vary platinum deposition onto electrodes and evaluate how they increase the mass specific current density (Amps/mg Pt) of platinum in MFCs.

2.) Determine which properties (i.e. surface area, activation resistance, electrode conductivity, and surface morphology) of the carbon electrodes most significantly enable high current production from a biofilm- anode using *Shewanella oneidensis* MR-1 and *Geobacter sulfurreducens*.

3.1 PRELIMINARY EVALUATION OF PLATINUM LOADING

Depositing a layer of Pt onto a surface could effectively change that material surface into Pt. Therefore, nanofabrication techniques that allow one to accurately control the thickness of deposited layers have the potential to maintain the reactivity of a surface while decreasing the amount of material used. Using electron-beam evaporation provides this option for platinum deposition and presents an opportunity to increase MFC current production while reducing capital costs. A preliminary evaluation using the materials and methods described in previous work[48] showed that as the thickness of the platinum layer decreased from 1000 Å to 500 Å and 250 Å the performance differences were negligible (see Figure 3.). This demonstrated, in the context of MFCs, that pure surface deposition and engineering the platinum thickness would not improve mass specific current density (amps/mg Pt) significantly. This was surprising given that hydrogen fuel cells use a similar range of Pt loadings (i.e. 0.05mg/cm^2 to 0.4mg/cm^2) and are able to produce current densities 2-3 orders of magnitude greater than that reported in microbial fuel cells. As a result, the focus of our work shifted toward the use of nanofabrication methods that would increase the catalyst surface area.

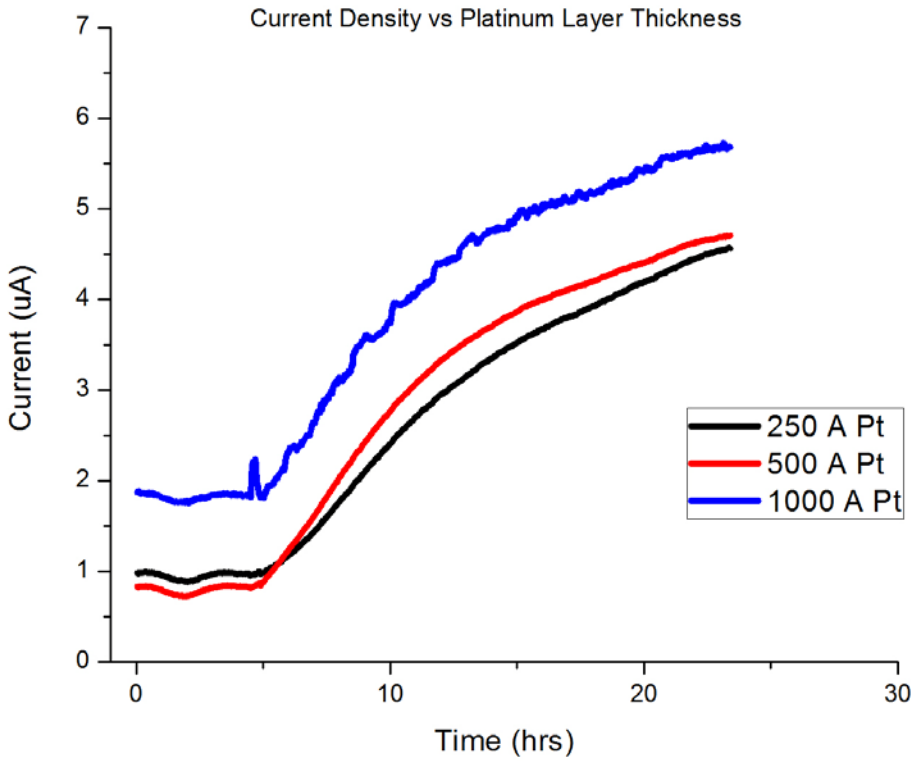

Figure 3. Preliminary evaluation of the effect of platinum thickness on current density. Platinum was deposited via electron-beam evaporation and was tested according to methods in Park et al.[48]

4.0 EVALUATING THE EFFECT OF INCREASING PLATINUM SURFACE AREA ON MFC CURRENT DENSITY BY INCOPORATING PT NANOPARTICLES INTO THE BIOFILM-ANODE AND MEASURING CURRENT PRODUCTION

Given the preliminary evaluation of Pt loadings I hypothesized that incorporating platinum nanoparticles into the electrode would increase current density because of the increase in available surface area. Collaborating with Sungkyunkwan Advanced Institute of Nanotechnology at Sungkyunkwan University in Suwon, South Korea (SKKU) we focused on efficiently fabricating an electrode with platinum nanoparticles, validating its electrochemical performance, and testing the electrode in a MFC alongside the e-beam platinum electrode (1000 Å thickness) that was evaluated in the preliminary studies.

4.1 SUMMARY

We used a simple and efficient method of synthesizing highly electrocatalytic Pt nanoparticles on a carbon nanofiber mat. Platinum acetylacetonate ($Pt(acac)_2$) molecules were adsorbed on functionalized carbon nanofibers and further reduced to Pt nanoparticles by diffusion-limited sublimation in a confined space. Pt nanoparticles were formed with sizes of 2.9 ± 0.4 nm and a loading yield of 100 %. Using electrochemical activation in the form of cyclic voltammetry we obtained high active surface area Pt nanoparticles and confirmed formation of

specific crystalline facets. The methanol oxidation current density per mg Pt of Pt-loaded carbon nanofiber sample was about 60 times as high as the commercially available (E-tek) sample and superior to other existing samples. We then used the Pt-loaded carbon nanofiber mat as the anode in a microbial fuel cell. The activated Pt nanoparticles are believed to mediate the electrons from the bacterial matrix to the carbon nanofiber mat. The electrochemically activated electrode showed a significantly higher current density (0.6 A/m^2) than the untreated sample and higher than an e-beam deposited Pt/Toray carbon paper that was previously tested showing that the increase in the reactive surface area of platinum using our methods increases MFC current density. An additional benefit to the method described here is that the long-term stability at the reported current was four times (150 hours) longer than the reported values. We believe that this method can be practically applied to load the organometallic compound-based catalyst on various carbon-based supports.

4.2 INTRODUCTION

In mediator-less microbial fuel cell systems, Pt has shown an ability to increase efficient electricity generation.[60] However, preparing a catalyst with large surface area and high activity has been a critical barrier to development.[61-62] There have been many well-known methods for loading Pt catalysts on powder supports in liquid phase such as stirring,[61] sonochemistry,[63-64] supercritical liquid,[65] and microwave treatment.[66-68] Yet these methods have not been used in three-dimensional supports. Typically, incorporation of an additional binder is required to form three-dimensionally structured supports for catalyst applications.[61-62] As a consequence, the

advantages of both high porosity and good electrical conductivity of the supports have been obscured due to the presence of the binder. The most recent approaches for designing electrodes of three-dimensional scaffolds use TiO_2/PVP fibers[62, 69] and SiO_2 nanoparticles as a glue between carbon particles.[61] However, due to the high resistivity of the support, these approaches are not practical for applications which require highly conductive supports, for instance, in fuel cells.

In another aspect, most of the methods for loading Pt nanoparticles on the support in solution-phase use linkers, protective agents, and reductants, by which the size, shape, and density of the nanoparticles can be controlled to improve the catalyst activity.[63, 70-72] In such cases, the particle surfaces are often partially deactivated due to the remaining linkers and protective agents.[63, 72] Thus, it is better to find another method that can activate the catalyst surface prior to the fabrication of the unit cell.

The purpose of this experiment was threefold: i) to design a simple and efficient method for constructing uniformly distributed Pt nanoparticles on a carbon nanofiber (CNF) mat that has high electrical conductivity and porosity, ii) to activate surfaces of Pt nanoparticles and evaluate the electrochemical activity and mass-specific current density by examining methanol oxidation on the electrode and iii) to use this electrode to evaluate whether the increased surface area of platinum nanoparticles increases current density in MFCs.

In our approach, the $Pt(acac)_2$ was absorbed on an acid-treated electrospun polyimide based-CNF mat. The Pt-loaded CNF mat was then reduced into Pt nanoparticles of ~ 3 nm by heat treatment under Ar ambient in a confined space to preserve the sublimated $Pt(acac)_2$ molecules. Unlike the previous works,[62-63, 69] no capping agent, reductant, or linker was used to control the size of Pt nanoparticles. Using a simple electrochemical cyclic scanning activation, a clean and fully activated surface of Pt nanoparticles was obtained. As a consequence, the mass-

specific current density of methanol oxidation was increased to 1,838 mA/cm^2/mg Pt from 846 mA/cm^2/mg Pt shown by the unactivated sample. We finally incorporated the Pt nanoparticle-loaded CNF mat as an anode in a MFC. The electrode produced a significantly higher current density (0.6 A/m^2) than previous experiments using platinum-based electrodes and had a long-term stability of the current (150 hours). Most importantly, the mass-specific current density of the MFC anode using the Pt-loaded CNF mat was larger than (0.6A/mg Pt) the highest reported mass specific current density for e-beam platinum (0.4A/mgPt).[48]

4.3 MATERIALS AND METHODS

4.3.1 Synthesis of Pt-loaded carbon nanofiber mat

The synthesis of poly(amic acid), electrospinning of the poly(amic acid) nanofiber mat, and the carbonization into carbon nanofiber mat were performed similar to a previous report.[73] The carbon nanofiber mat was immersed in a 5 M H_2SO_4 solution for a week to generate oxygen-related functional groups. The functionalized carbon nanofiber mat was washed with distilled water and dried in a vacuum oven at room temperature. $Pt(acac)_2$ / acetone of 0.01 M was deposited onto the acid-treated carbon nanofiber mat. The amount of Pt initially loaded was 20 wt% relative to the mass of the acid-treated carbon nanofiber mat. The Pt-loaded carbon nanofiber mat was then kept between two ceramic plates under a pressure of 4400 Pa and heated in a furnace under Ar gas ambient at 300 ^oC for 30 minutes.

4.3.2 Electrochemical activation of Pt nanoparticles

In order to activate the Pt nanoparticles, the Pt-loaded carbon nanofiber mat was directly immersed into a 0.1 M H_2SO_4 solution. A three-electrode cell with a Pt mesh counter electrode and a Ag/AgCl KCl saturated reference electrode was used to perform voltage scans. The voltage was scanned by cyclic voltammetry (Bio-Logic SA-Model VSP # 0073, France) from -0.23 to +1 V with a scan rate of 50 mV/s. This cycle was repeated 10 times.

4.3.3 Microbial fuel cell setup

The anode and cathode compartments of the microbial fuel cell were separated by a cation exchange membrane (Nafion-112; Dupont, Wilmington, DE). The anode compartment was supplied with nitrogen sparged fuel to maintain anaerobic conditions and the cathode compartment was supplied with air-saturated water. Both compartments contained an electrode (1.0×4.0 cm^2). Cathodes for all fuel cells were e-beam Pt (1000 Å thickness) deposited carbon papers; deposition was made using an e-beam evaporator (VE-180, Thermoionics Laboratory, Inc., Port Townsend, WA). The anodic biofilm was enriched from an anaerobic sludge taken from the Franklin Township Municipal Sanitary Authority in Pittsburgh. The fuel cell was inoculated using an artificial waste water containing 50 mM phosphate buffer (pH 7.0), glucose and glutamate fuel,[74] trace mineral solution,[75] and a salt solution.[76] The flow rate of the fuel supplied to the anode was adjusted from 1 to, 3 to 15 rpm (1 rpm = 2.25 ml/ min). Current density was monitored via a keithley meter connected to a personal computer.

4.3.4 Measurements

For transmission electron microscope (TEM) analysis, the prepared Pt-loaded carbon nanofiber mat was ground into small fragments. This powder was dissolved in ethanol and sonicated in a bath-type sonicator (Power Sonic 505, Hwashin) for up to a minute to get individually dispersed nanofibers. This solution was then dropped on a carbon TEM grid and dried in a vacuum furnace. The transmission electron microscope used was a field emission JEM 2010F (JEOL) operated at 200 kV. The corresponding Fourier transform patterns were obtained during TEM analysis. A scanning electron microscope (SEM, JEOL JSM6700F) was used to observe the morphology of the Pt-loaded carbon nanofibers. Thermogravimetric analysis (TGA) was used to measure the amount of Pt loading in the carbon nanofiber mat. The samples were ground and dispersed in isopropanol by sonication and then dropped on a glassy carbon electrode with a 4 mm diameter. The measurement of catalytic activity was performed in methanol 1 M/ H_2SO_4 0.5 M. The methanol / H_2SO_4 solution was bubbled with N_2 gas for 30 min to remove molecular oxygen right before the measurement. An E-tek sample of 20 wt% Pt on Vulcan XC-72 (lot #JJ121506) was used for comparison. The voltage was scanned from -0.225 V to +1.15 V vs Ag/AgCl KCl sat using differential pulse voltammetry (pulse height; 3 mV, pulse width; 1 ms, step height; 0.5 mV, step time; 100 ms) at room temperature. Scanning was conducted until the curve was saturated to a stable state.

4.4 RESULTS AND DISCUSSION

The Pt-loaded CNF mat (4 x 5 cm^2) is shown in Figure 4a. The CNF mat was closely packed, as can be seen from the cross section (Figure 4b). The CNF mat was a highly permeable porous material and its conductivity was 15 S/cm. Pt nanoparticles were uniformly distributed on the nanofiber surface (Figure 4c). The size of the Pt nanoparticles was 2.9 ± 0.4 nm, measured from X-ray diffraction. They were monodispersed on the surface of CNFs with a negligible amount of aggregation which contrasts previous reports that some of the Pt nanoparticles were embedded in bulk (Figure 4d,e).[63, 77-78] A dark field (HAADF) TEM image of Pt-loaded CNF was also taken to avoid the overlapping of Pt nanoparticles above and below the CNF surface. Excellent uniformity of Pt nanoparticles was observed in Figure 4f. It is of note that due to the high permeability of the CNF mat, the Pt nanoparticles decorated the surface of CNFs located deep in the mat, as shown in Figure 4c. Typically, the conductivity of the supports is degraded due to the use of functional groups to enhance adhesion of Pt to the supports.[63] In our case, however, the conductivity of the CNF mat was not degraded after Pt loading due to their direct adsorption on the surface of the nanofibers.

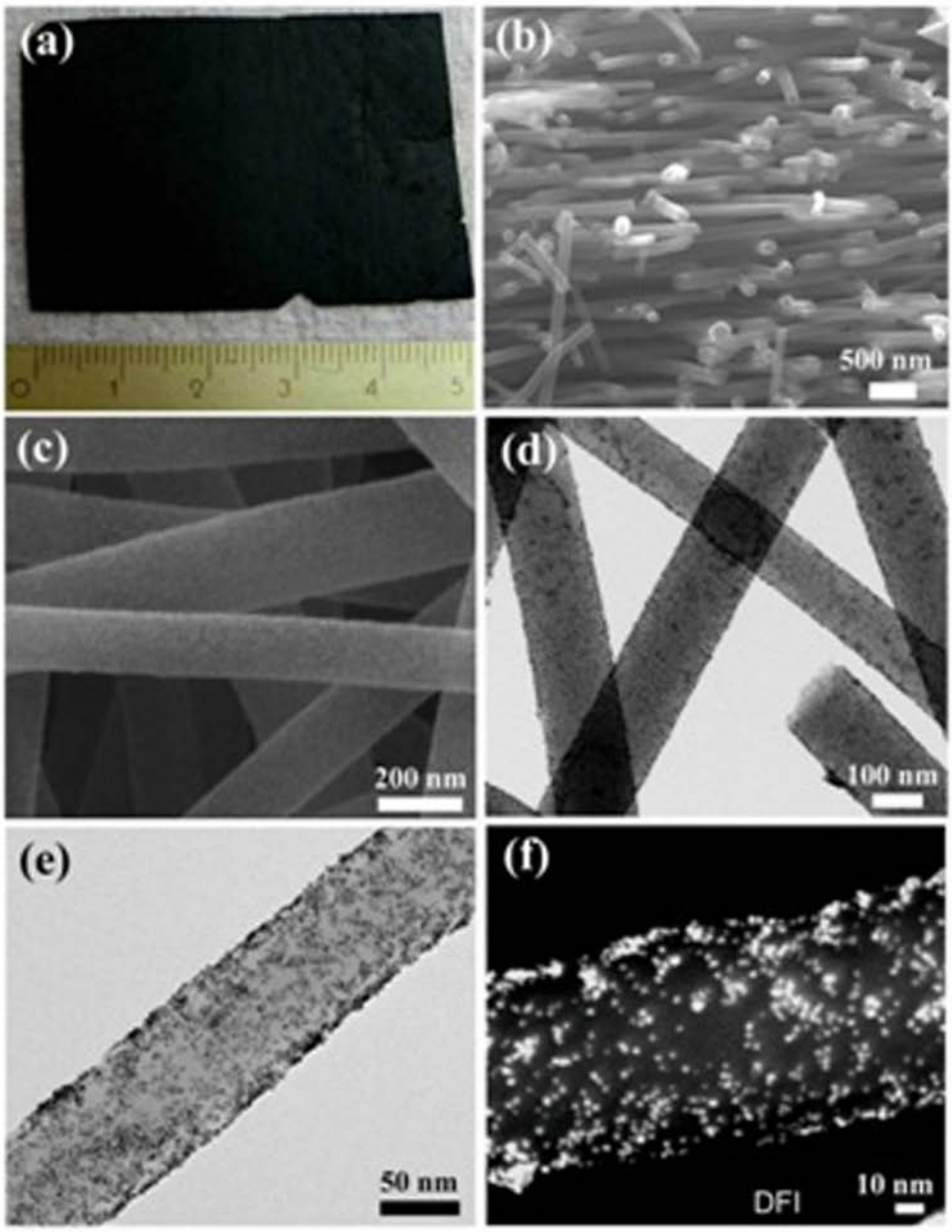

Figure 4. (a) Optical microscope image of Pt-loaded CNF mat, (b) cross section of Pt-loaded CNFs, (c) SEM image, (d)-(e) TEM image of Pt-loaded CNF mat before electrochemical activation, and (f) Dark field TEM image of Pt-loaded CNF mat before electrochemical activation. Xuyen, Sanchez et al. 2010. Diffusion-limited reduction of organometallic compound on carbon nanofiber mat for catalytic applications. Journal of Materials Chemistry 20, 5468-5473. Reproduced by permission of The Royal Society of Chemistry.

The underlying mechanism of loading Pt nanoparticles on the CNF mat is shown in Figure 5. Due to the functionalization of CNFs by acid treatment described in the experimental part, $Pt(acac)_2$ molecules adsorbed well onto the CNF surface (step I). The functional groups such as carboxylic acid, hydroxyl, and carbonyl groups act as nucleation sites for $Pt(acac)_2$ on CNFs.[78] As the temperature increases gradually up to 150 ^{o}C, $Pt(acac)_2$ molecules in the solid phase start to sublimate.[79-81] When the Pt-loaded CNF mat is pressed between two ceramic plates, the diffusion of the $Pt(acac)_2$ molecules is confined to the space among CNFs and by the gap between the mat and two ceramic plates (step II). The sublimation occurs rapidly until the partial pressure of $Pt(acac)_2$ molecules reaches the sublimation pressure, resulting in an equilibrium state.

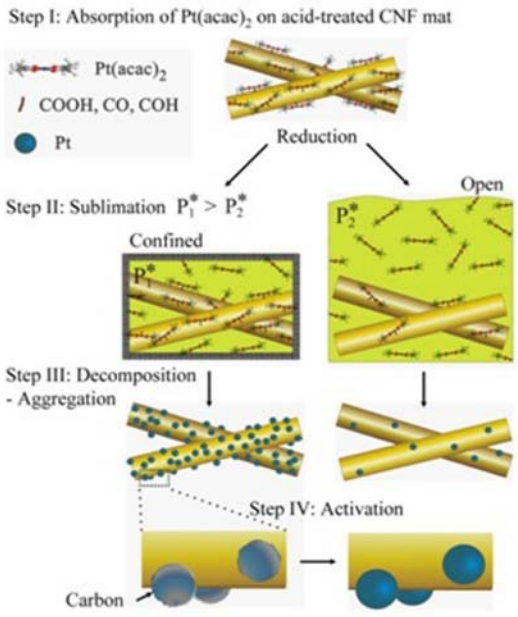

Figure 5. Schematic of the equilibrium phase of $Pt(acac)_2$ molecules on CNFs in a surrounding space at elevating temperature, when the surrounding space of CNF mat is (a) confined and (b) open. Xuyen, Sanchez et al. 2010. Diffusion-limited reduction of organometallic compound on carbon nanofiber mat for catalytic applications. Journal of Materials Chemistry 20, 5468-5473. Reproduced by permission of The Royal Society of Chemistry.

Due to the confined space, the amount of sublimated $Pt(acac)_2$ is small compared to the remaining solid phase of $Pt(acac)_2$ on the CNF mat. Although more $Pt(acac)_2$ molecules are sublimated at an elevated temperature according to the Clausius-Clapeyron relation, the increasing amount of $Pt(acac)_2$ in the gas phase is negligible. This is in contrast with the case of the open space in which the sublimated $Pt(acac)_2$ molecules diffuse away. As the temperature rises above 150 ^{o}C, the $Pt(acac)_2$ molecules decompose leaving Pt nanoparticles behind (step III).

The confined space preserves the majority of $Pt(acac)_2$ adsorbed onto the mat from sublimating. TGA revealed that the nominal amount of Pt loaded (20 wt%) was reduced to 19.55 wt% after reduction, demonstrating the efficiency of reducing the adsorbed $Pt(acac)_2$ molecules in a confined space. This is excellent when contrasted with the case of the open space, where the amount of Pt nanoparticles was only about 4.5 wt%. Ultimately, controlling the kinetics of Pt precursors by diffusion-limited reduction not only minimizes the complication of procedures such as the use various agents or time consuming tasks,[62] but also produces a uniform distribution of Pt nanoparticles through the porous mat. This is because the $Pt(acac)_2$ molecules were immobilized by the functional groups uniformly over the mat and then subsequently reduced into nanoparticles.

We note that the geometry of the CNF mat was perfectly preserved during acid and heat treatment, and the conductivity of the CNF mat was not degraded. These observations are characteristic of methods that control the kinetics of Pt precursors, while keeping the support in a static state. One such method was previously demonstrated for growing a catalyst on a polymer membrane.[62]

The sample was then activated electrochemically as described in the experimental section (step IV). The effect of electrochemical activation on the Pt-loaded CNFs in acid solution can be observed in the high-resolution TEM images (Fig. 2). The Pt nanoparticles were formed by heat treatment under Ar ambient when the (acac) ligands decomposed and evolved into either the gas phase or adsorbed fragments.[80] The adsorption of these fragments onto the surface of Pt nanoparticles cannot be avoided due to the high surface energy of Pt nanoparticles.[82] This may result in the outer layer of the Pt nanoparticles being covered by a form of hydrocarbon groups or oxygen-containing species. This was confirmed in the high-resolution TEM images shown in Fig. 2a. The inset clearly shows the presence of a thin film on the Pt nanoparticle. In order to remove these contaminants, we chose a method of electrochemical cyclic scanning activation. It has been shown that an applied potential is required to remove the hydrocarbon and oxygen-containing species on Pt surfaces in acid solution.[82-84]

A wide range of applied potential from -0.23 V to +1 V was chosen to remove all of these complexes and/or convert neutral Pt atoms. After a cyclic scanning process of ten cycles from -0.23 to +1 V in H_2SO_4 solution, the surfaces of the Pt particles were cleaned completely as shown in the inset of Figure 6b. The related fast-Fourier transformed (FFT) pattern of the selected Pt nanoparticle in the inset is also shown in the inset. The hexagonal spots indicated by the numbers of the FFT pattern are indicative of the different facets, as shown in the figure caption. This is congruent with a previous report that the electrochemical treatment of Pt surfaces can generate various facets of Pt surfaces to enhance the catalyst efficiency.

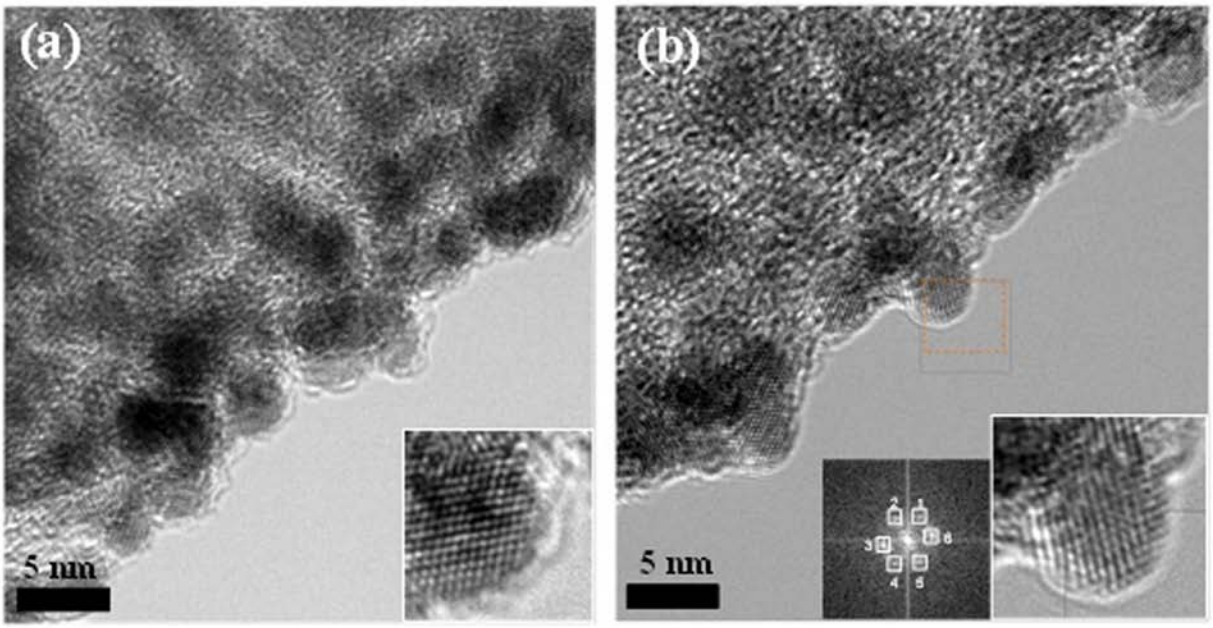

Figure 6. TEM images of Pt surface (a) before and (b) after electrochemical activation and the amplified particle surface in the inset. FFT pattern is in the inset. The crystal facet of point 1 is (1,-1,-1), 2 is (2,0,0), 3 (1,1,1), 4 (-1,1,1), 5 (-2,0,0), 6 (-1,-1,-1) and the zone X is (0,-1,1). Zone X is the observed plane. Xuyen, Sanchez et al. 2010. Diffusion-limited reduction of organometallic compound on carbon nanofiber mat for catalytic applications. Journal of Materials Chemistry 20, 5468-5473. Reproduced by permission of The Royal Society of Chemistry.

The oxidation of Pt nanoparticle surfaces in H_2SO_4 solution was observed in the CV curve, in Figure 7a. The current increase above 0.78 V was assumed to be attributed to Pt oxidation. The oxidative peak current in the first cycle revealed the presence of Pt oxide substances on the Pt nanoparticles in the early stage of the activation process. By the tenth cycle, the oxidation peak was collapsed indicating the removal of oxide substances from the Pt nanoparticle surfaces. Additionally, the H adsorption/desorption peaks significantly increased in the tenth cycle. In the first cycle, a broad H_{ads} peak stems from the facets of the Pt nanoparticles being polycrystalline. In the latter cycles, the H_{ads} peaks were split into three individual peaks. Each peak can be assigned to the single crystalline facets of Pt nanoparticles. These single facets in the Pt nanoparticles were not visible from the TEM image in Figure 6b. No appreciable differences in the peak currents were observed after the tenth cycle. With further cyclic scanning activation, the peaks became sharper, which was caused by the facet-selective etching. The H adsorption peak was used to calculate the active surface area of Pt nanoparticle.[85] The active surface area of the activated Pt/CNFs significantly increased from 846 to 1,854 cm^2/mg Pt (Table 1). The removal of oxygen-related substances and formation of single crystalline facets contributed significantly in enhancing the active surface area of Pt nanoparticles.

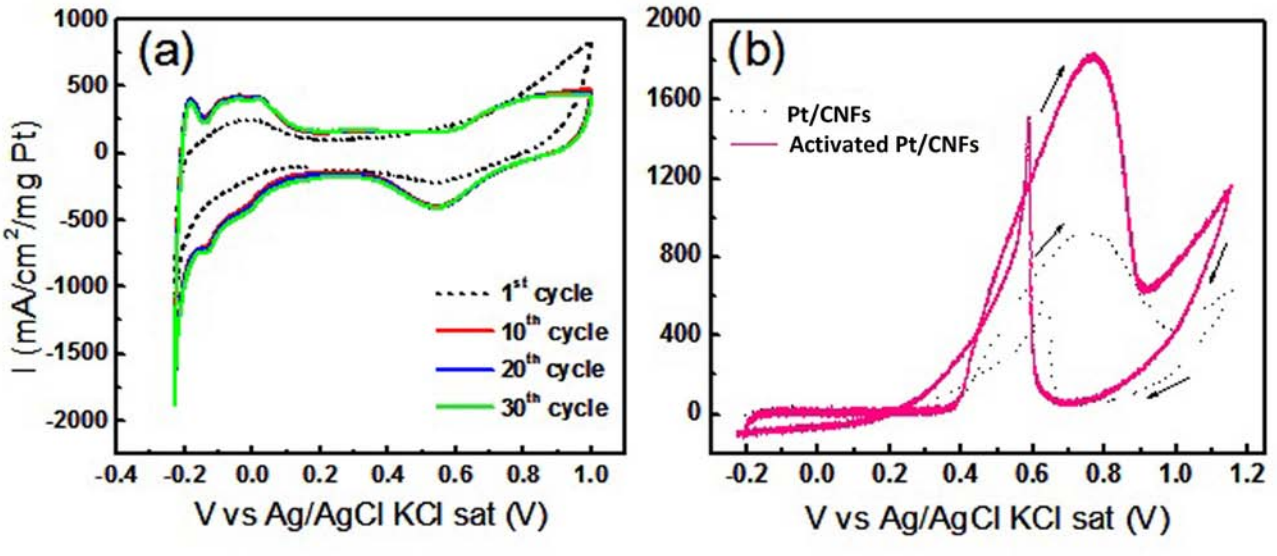

Figure 7. (a) Cycle voltammetry of Pt/CNFs in 0.1 M H_2SO_4 at RT. Potential sweep rate is 50 mV/s. (b) Differential pulse voltammetry of Pt-loaded CNFs in 1 M methanol and 0.5 M H_2SO_4 before (dotted line) and after (solid line) electrochemical activation. Xuyen, Sanchez et al. 2010. Diffusion-limited reduction of organometallic compound on carbon nanofiber mat for catalytic applications. Journal of Materials Chemistry 20, 5468-5473. Reproduced by permission of The Royal Society of Chemistry.

Differential pulse voltammetry was used to investigate the catalytic activity of the Pt nanoparticles for methanol oxidation. In order to see the catalytic effects from the Pt nanoparticles exclusively, the current contribution from the CNF support was subtracted. Figure 7b shows the cyclic-voltammetry curves of Pt-loaded CNFs before and after electrochemical activation. The curves describe the current contributed exclusively from methanol oxidation from the Pt nanoparticles.

Table 1. Active surface area calculated from Hads peak in 0.1 M H2SO4, the maximum current density, and ratio of area forward peak to backward peak of Pt/CNFs in methanol oxidation before and after electrochemical activation. **Xuyen, Sanchez et al. 2010. Diffusion-limited reduction of organometallic compound on carbon nanofiber mat for catalytic applications. Journal of Materials Chemistry 20, 5468-5473.** **Reproduced by permission of The Royal Society of Chemistry.**

Samples	H_{ads} peak	Methanol oxidation	
	Active surface area (cm^2/mg Pt)	I_m (mA/cm^2/mgPt)	A_f/A_b
Pt/CNFs	846	926	3.4
Activated Pt/CNFs	1,854	1,838	3.7

The pristine Pt-loaded CNF sample exhibited an oxidation current of 926 mA/cm^2/mg Pt in Figure 7b (dotted line). The advantages of a monodispersed size of 2.9 nm nanoparticles, a high loading of Pt, the uniform distribution without embedment of the Pt nanoparticles, and the high electrical conductivity of the support all contributed to the high performance of the electrode. However, after electrochemical activation, the peak current and thus mass-specific current density was significantly improved to 1,838 mA/cm^2/mg Pt from 926 mA/cm^2/mg Pt. The increased active surface area of Pt nanoparticles, as evidenced from the ratios of active surface area (see Table 1.), produced this higher methanol oxidation current. The peak position of the forward scan was 0.76 V vs Ag/AgCl KCl sat for both samples. In both cases, the forward current showed a rather broad peak, whereas the backward current showed a sharp peak. The broad peak of the forward scan was due to several intermediate steps of oxidation of methanol.[86-88] With the backward scan, some of the un-reacted intermediate methanol derivatives produced during the forward scan continued further reactions to generate CO_2 which is the final product.[89] In our case, a sharp peak in the backward scan was observed. The peak area ratio (A_f/A_b) was enhanced from 3.4 to 3.7 after electrochemical activation. We conclude here that electrochemical cyclic scanning activation of the Pt-loaded CNFs offers a higher catalytic activity than the pristine sample.

To test the catalytic activity of Pt nanoparticles on CNF mats and its effect on anode performance, we tested them in a MFC (Figure 8a). In MFCs, catalysts are typically used to decrease the internal resistance. In particular they are used to address overpotentials and improve the performance of the biofim-anode.[52, 90-91] The innoculant used was anaerobic sludge from Franklin Township Municipal Wastewater Treatment plant.

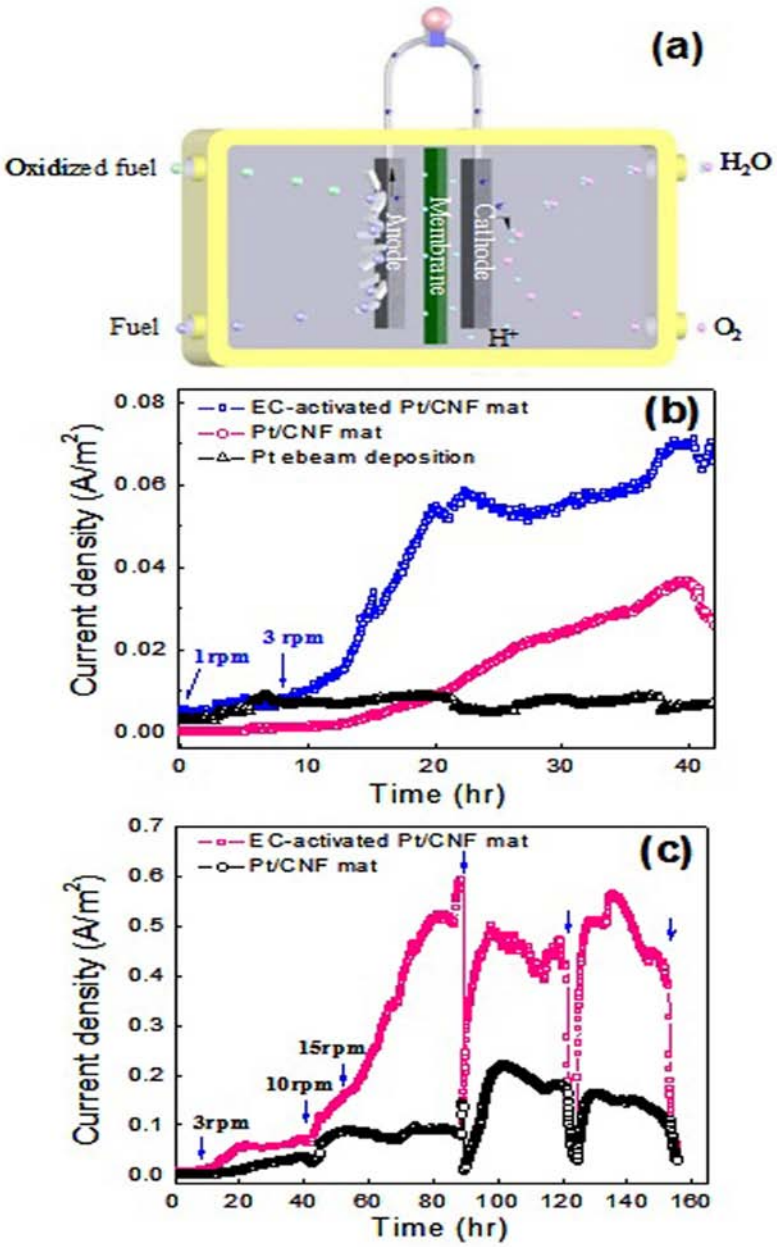

Figure 8. (a) The principle of the mediator-less microbial fuel cell. (b) Current density of the Pt-loaded CNF mat, the electrochemical (EC) activated Pt-loaded CNFs mat, and the e-beam deposited-Pt/carbon microfiber paper electrode on the anode compartments at a fuel flow rate of 3 rpm. (c) Current density of the Pt-loaded CNFs and the electrochemical activated Pt-loaded CNF electrode on the anode compartments at a fuel flow rate of 3 rpm, 10 rpm, and 15 rpm. Xuyen, Sanchez et al. 2010. Diffusion-limited reduction of organometallic compound on carbon nanofiber mat for catalytic applications. Journal of Materials Chemistry 20, 5468-5473. Reproduced by permission of The Royal Society of Chemistry.

Figure 8b shows the current densities of the Pt-loaded CNF mat, an electrochemically activated Pt-loaded CNF mat, and an e-beam deposited Pt/carbon paper electrode in a microbial fuel cell at a fuel flow rate of 3 rpm. For 40 hours, the current densities of both the unactivated and activated Pt-loaded CNF mat continuously increased while the e-beam deposited Pt/carbon microfiber paper sample exhibited smaller current densities. Specifically, the current densities of the unactived and activated Pt-loaded CNF mat at 40 hours were 4 times and 10 times higher than that of the e-beam deposited Pt/carbon carbon paper, respectively. The difference in catalytic activity can be attributed to the high surface area and activity of Pt nanoparticles. The electrochemical activation of the Pt nanoparticles increased the current density twice compared to the untreated sample. The Pt nanoparticles are likely promoting electron transfer between the bacteria and the carbon support by decreasing the activation overpotential. As the fuel flow rate was elevated, the slope of the current density curve increased. The flow rate increases and current measurements were performed for 160 hours, as shown in Figure 8c. The fiber mat allowed the fuel flow rate to reach as high as 15 rpm. From about 90 to 155 hours, the current density of Pt-loaded CNF mat and the current density of the electrochemically activated Pt-loaded CNF mat were saturated at 0.17 and 0.6 A/m^2, respectively. Similar current densities were previously reported for continous flow reactors.[18, 92] Although the media was changed at several steps, marked by arrows in the figure, the current rapidly recovered and maintained the saturated value for both samples. In addition, the electrochemically activated Pt-loaded CNF mat was tested further after being exposed to air for ten days. It still showed the high current density of about 0.57 A/m^2. This trend proves that the clean Pt nanoparticles play an important role in harvesting electrons from bacteria metabolic reactions. Finally the mass-specific current density of the activated Pt-loaded CNF mat (0.6A/mgPt) in the MFC was larger than the highest reported

mass-specific current density for e-beam evaporated Pt electrodes (0.4A/mgPt)[48] confirming that an increasing catalyst surface area is necessary for increasing MFC current density.

4.5 CONCLUSIONS

In conclusion, the diffusion-limited reduction process preserved $Pt(acac)_2$ molecules on the CNF mat until $Pt(acac)_2$ molecules were decomposed into Pt nanoparticles. A high loading yield, uniform distribution, and a uniform size of Pt nanoparticles were obtained. The subsequent electrochemical activation of Pt nanoparticles removed the contaminants (e.g. residual (acac) ligands) and generated specific facets to enhance the active surface area of Pt nanoparticles. This was observed via TEM, H_{ads} measurements and methanol oxidation tests. The effect of the new electrode on MFC current density was then evaluated.

Using the new electrode MFC current density was increased relative to the e-beam Pt electrode, with the device producing a current of up to 0.6 A/m^2 with a long-term stability of up to 150 hours. The recorded mass-specific current density was (0.6A/mgPt) and was larger than the highest reported mass-specific current density reported for e-beam evaporated Pt electrodes (0.4A/mg Pt)[48] showing an increase by a factor of 1.5. This confirms that increasing the active surface area of the Pt catalyst using nanoparticles is more efficient at increasing MFC current density than mere Pt surface deposition. More importantly, the results suggest that increasing active surface area of the Pt catalyst is necessary for increasing current production despite the fact that Pt loadings for MFCs are comparable to hydrogen fuel cells yet MFC current densities are significantly smaller. Finally, this research demonstrates a practical nanoparticles-based

deposition method that can be applied to load various organometallic compound-based catalysts on various carbon-based supports for future MFC research.

5.0 EVALUATING THE EFFECT OF INCREASED PLATINUM SURFACE AREA ON THE CATHODE REACTION BY INCOPORATING PT NANOPARTICLES INTO THE CATHODE AND MEASURING MASS-SPECIFIC CURRENT DENSITY

After demonstrating that incorporating Pt nanoparticles into the anode increases MFC current density we focused on whether the increased surface area of Pt nanoparticles could improve the cathodic oxygen reduction rate. The oxygen reduction reaction has a high activation overpotential and previous MFC experiments [48, 93] have shown that incorporating platinum onto the cathode electrode improved performance. The difference is that while we sought to efficiently increase the Pt catalyst surface area to increase MFC current density we also did so trying to eliminate the use of binders and mediators that would increase costs and potentially contaminate the catalyst.[50]

5.1 SUMMARY

This section of the dissertation describes the characterization and evaluation of a single wall carbon nanotube (SWNT) sheet electrode with infused platinum nanoparticles (nPts) as a cathode in a microbial fuel cell. The design is intended to increase electrode efficiency by increasing the surface area to volume ratio of Pt and thus the available surface area of the catalyst. The electrode fabrication procedure is an extension of the conventional bucky-paper like fabrication

technique to a two-component system and incorporates nPt throughout the thickness of the sample. The electrodes were characterized via scanning electron microscopy (SEM), Raman spectroscopy, transmission electron microscopy (TEM), and cyclic voltammetry (CV). Our characterizations confirmed the architecture of the electrodes and the current density from our MFC increased significantly, approximately an order of magnitude, when an e-beam evaporated platinum cathode was replaced with this SWNT-nPt sheet electrode. The enhancement of catalytic activity can be associated with the increase of Pt surface area in the active cathode layer as shown by the increase in mass-specific current density of Pt by a factor of 4. Our data clearly suggest that nanoparticles co-deposited into layers of nanotubes can more efficiently catalyze the cathodic reaction than electrodes that efficiently deposit Pt on its surface.

5.2 INTRODUCTION

In order to become a viable source of renewable energy, MFCs require an increase of current densities relative to their abiotic counterparts.[12, 94] The increase of current density requires a decrease of the internal resistance (often characterized by ohmic losses), an improvement of proton transport out of the biofilm, and a reduction of overpotentials for both anodic[95] and cathodic reactions.[90, 96]

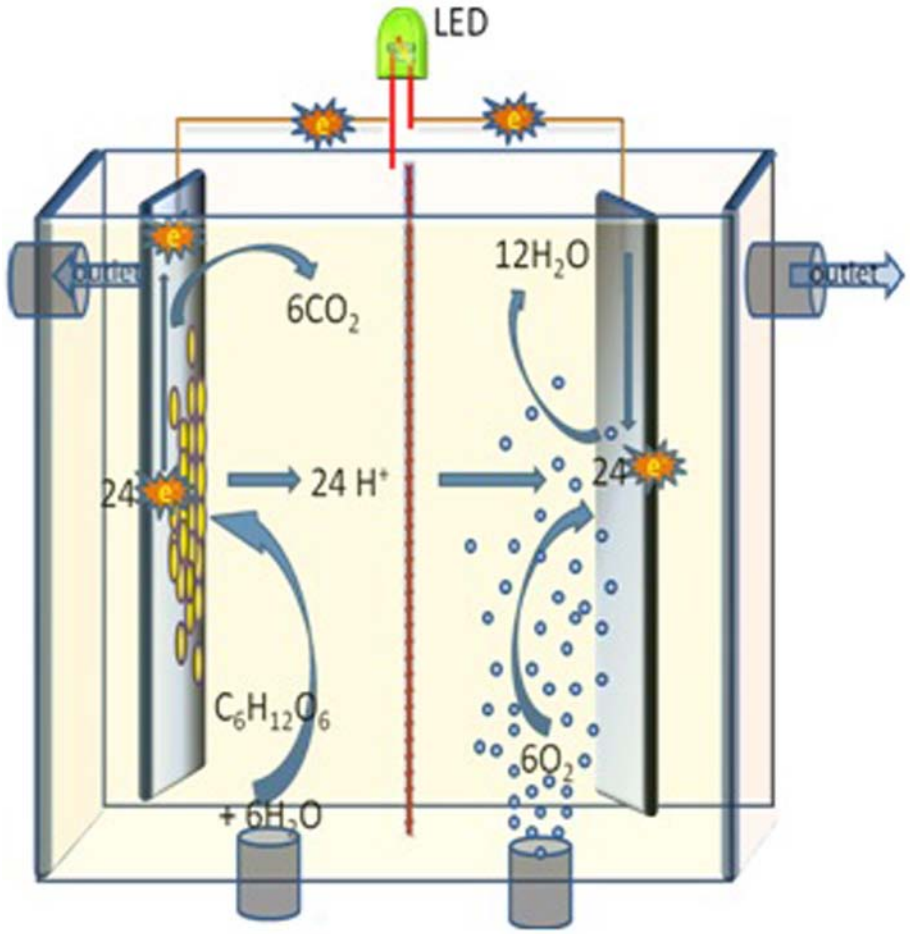

Figure 9. Schematic diagram of a microbial fuel cell (MFC) system. As bacteria (yellow rods) consume glucose, the produced free electrons flow from the anode to cathode via the electrical circuit while protons are transferred from anode to cathode through a proton exchange membrane (Nafion). Reprinted with permission from Sanchez et al. 2010. Carbon Nanotube/Platinum (Pt) Sheet as an Improved Cathode for Microbial Fuel Cells. Energy & Fuels 24, 5897-5902. Copyright 2010 American Chemical Society.

Addressing the issues for both anode respiration and the oxygen reduction reactions can significantly affect MFC performance. For example, cathodic performance was shown to improve greatly by augmenting proton transport with buffers, using low pH catholyte solutions, and incorporating platinum (Pt) or other catalysts into cathodes.[54] However, to attain high current densities platinized MFC electrodes have typically used high Pt surface loading (>0.4mg/cm^2),[12] expensive binders (i.e. Nafion)[55] and artificial mediators (i.e. FeCN). Increasing current densities by loading Pt efficiently, increasing the available surface area of Pt and eliminating binders and artificial mediators are the steps needed to make MFCs an industrially viable technology.

5.2.1 Mass transfer limitations and oxygen reduction kinetics

The high overpotentials of cathodic reactions in oxygen-based microbial fuel cells[12] originate from i) the concentration overpotential caused by inadequate proton transport to the cathode and ii) the surface overpotential, a consequence of the 4- electron transfer needed for oxygen reduction (see Equation 1). [93]

$$(1) \qquad O_2 + 4H^+ + 4e^- \rightarrow 2H_2O$$

The rate-determining reaction on a modified cathode was shown to change from 4e-/4H+ to 4e-/2H+ with a variation of pH. As pH increased the oxygen reduction potential decreased. Negative slopes of 59mV/pH and 29mV/pH for pH below and above[97] respectively, were demonstrated for cathodes with surface catalysts.[93] As a quick illustration, open-circuit potentials of ~0.6V, ~0.33V, and ~0.27V were shown for a carbon foil electrode with a CoTMPP (cobalt tetramethoxyphenylporphyrin) catalyst at pHs of ~1,~7, ~9.3 respectively.[93]

Additionally, the rate determining reactions (i.e. four electron and two electron transfers for oxygen reduction) have been studied in alkaline media using bulk platinum and are shown in Equations 2 and 3 respectively[98] :

$$(2)\ O_2 + 2H_2O + 4e^- \rightarrow 4OH^-$$

$$(3)\ O_2 + H_2O + 2e^- \rightarrow HO^-_2 + OH^-$$

Since the concentration of protons at neutral pH is about 3 orders of magnitude lower than the concentration of oxygen in air saturated water (~9mg/L) and 4 protons per oxygen molecule are needed for the cathodic reaction to occur (Equation 1), a proton mass transfer limitation can typically be expected in MFCs. Torres et al. and Zhao et al. defined proton mass transfer limitations for both bio-anodic (proton generating) and cathodic (proton consuming) reactions.[93, 95] These mass transfer limitations can be reduced by the addition of concentrated phosphate buffer to the anolyte or acid to the catholyte. Only when proton mass transfer limitations are removed are oxygen mass transfer limitations realized. For example, under acidic conditions and a high catalyst loading of (1 mg/cm^2) Zhao et al. demonstrated a mass transfer limitation for oxygen. Ultimately, cathode performance primarily depends on the proton concentration so that the oxygen reduction rate increases with a decreasing pH and or an increasing buffer concentration.

Enhancing the reactivity at the cathode is important since oxygen reduction requires a 4 electron transfer. Fortunately, the reactivity can be improved via the addition of catalysts such as Pt. For neutral pH solutions, which are preferred for MFCs, a higher catalyst loading correlates with an increased rate of oxygen reduction and higher current densities,[93] To demonstrate the

trade-off between maintaining a neutral pH and adding a catalyst it was shown that as the Pt loading increased from 0.5 mg/cm^2 to 2 mg/ cm^2 the current density in a pH neutral solution with a phosphate buffer concentration of 0.1M increased from 45% to 74% of the value recorded for a solution at pH 3 with 0.5M phosphate buffer.[93]

5.2.2 Nanostructured Electrodes

Nanostructured carbon-based materials, nanotubes in particular, can have high surface area to volume ratio, mechanical strength, high electrical conductivity, and catalytic properties. As a result, nanomaterials can be beneficial to MFC performance if they are used for electrodes instead of conventional bulk graphite.[99-100] Considering that carbon nanotubes can be assembled into highly porous macroscopic paper-like sheets similar to carbon microfiber mats from Toray Industries[48] the scalability issues for nanotube sheet fabrication can be similar. In fact, carbon nanotube sheets can presently be manufactured from liquid-dispersed carbon nanotubes, using a process similar to that used for making ordinary paper.

MFCs utilizing nanostructured electrodes have yielded promising results. Park et al. showed that electron beam (e-beam) Pt deposition improves the performance of plain carbon paper from Toray Industries,[48] Sharma et al. reported the impact of noble nanoparticles and artificial mediators on improving current density,[91] and Zou et al. improved MFC performance using polypyrrole coated nanocomposites.[59] These and other examples demonstrate the ability of catalysts to decrease activation overpotentials, and the utility of high surface-to-volume ratio electrode structures for improving MFC performance.

The concept of incorporating nPt into the cathode is motivated by the fact that reducing oxygen at the cathode in fuel cells is a relatively slow reaction that can be improved with a

catalyst. At the same time, it is important to note that the crossover of substrate from anode to cathode can cause side reactions that decrease oxygen reduction efficiency on Pt electrodes;[51, 101] illustrating yet again the importance of increasing the available Pt surface area on the cathode and the promise of using nPts.

In this experiment, we inoculated a MFC using activated sludge and a buffered electrolyte with an e-beam Pt deposited cathode. We then substituted the cathode with a SWNT-nPt electrode and evaluated resulting energy generation. We focused on the characterization of the cathode fabricated from single-walled carbon nanotubes (SWNTs) embedded with nPt and the evaluation of its performance in a two compartment MFC by measuring current density and evaluating the mass-specific current density of Pt.

5.3 MATERIALS AND METHODS

5.3.1 Electrode Fabrication Procedure

Single-walled carbon nanotubes (SWNT) made by the high pressure carbon monoxide (HiPco) process were purchased from Unidym Inc. (Sunnyvale, CA). About 15 mg of SWNT were placed in an aqueous surfactant solution and subjected to probe sonication (Fisher Scientific Model 500) for about 25 minutes in 5 min cycles. The dispersion was kept in an ice bath to avoid heating. Two types of surfactants, Triton-X-100 and Pluronic X (Aldrich), were used in this study.

Approximately 0.1g Triton-X-100 in 50 mL of water was added to the SWNT dispersions. Sonication continued for ~5-10 minutes until a good dispersion was achieved, thus allowing for the uniform addition of ~15 mg nPt (Aldrich Platinum black HiSPEC 1000) . The solution was diluted with one liter of water and a decanting-method was used to repeat the process. The whole solution was then filtered through a vacuum filter apparatus with a 47mm diameter filter (Millipore, 10-micron MITEX PTFE membrane filters). After filtration, 1000 mL of water was passed through the filter until all foam disappeared. A second 1000 ml solution of 30% methanol was passed through the filter. The methanol solutions were diluted to ensure that methanol would not react directly with oxygen in the air using Pt in the carbon nanotube paper as a catalyst. The vacuum was released and the vacuum filtration apparatus was disassembled. Immediately, another 10-micron MITEX PTFE membrane filter was placed on top of the carbon nanotube sheet forming a "sandwich". The whole vacuum filtration apparatus was reassembled and the vacuum was continually applied for one hour. The purpose of enclosing carbon nanotube paper between two membranes was to maintain a flat and uncurled sheet. After air-drying for an additional hour, the membrane filter was peeled off. The process was also conducted using Pluronic-X in place of Triton–X-100. The carbon nanotube paper with nPt was then used as the anode and or cathode of the MFC. It is important to note that the size and shape of the SWNT-nPt sheet prepared in this way is limited only by the size and shape of the membrane filter used.

5.3.2 Characterization of SWNT-nPt electrode

In this study SWNT-nPt electrodes were characterized using three different methods: scanning electron microscopy (SEM), Raman spectroscopy, and transmission electron microscopy (TEM).

5.3.2.1 SEM

In order to ensure that the nPt had not completely agglomerated throughout the sample or on the surface of the SWNT-nPt sheet, SEM images were taken of the electrode surface and from fractured sample using a LEO 1530VP field emission microscope. Electrode samples were cut at random positions and viewed in a scanning electron microscope at different magnifications for the surface analysis.

5.3.2.2 Raman Spectroscopy

Raman spectroscopy provides spectra between 100 cm^{-1} and 3500cm^{-1} for 633nm laser excitation which was used to characterize the SWNTs in the electrodes and to detect the presence of contaminants, such as surfactants or organic residue from the production of carbon nanotubes, in the electrodes. A Jobin Yvon LabRam HR800 Raman Microscope was used.

5.3.2.3 TEM

To confirm the distribution and sizes of nPt in the SWNT-nPt matrix, a small sample (~0.25 cm^2) was sonicated in isopropyl alcohol for a total of 35 minutes. Water in the sonication bath was exchanged every 7 minutes to avoid temperature increase in the solution. A sample of the isopropyl alcohol solution containing SWNT-nPT was deposited on a lacey carbon TEM grid and dried. Images were taken at several magnifications using JEOL 2100F TEM/STEM machine at 200kV. The images were used to determine the size of the nPt and the relative dispersion.

5.3.3 Microbial fuel cell (MFC) System

A dual compartment MFC, separated by a Nafion proton exchange membrane (Nafion-112; Dupont, Wilmington, DE)[102] was used with each compartment holding a 4 cm x 1cm electrode. An external resistor (10 Ω) was used as a fixed load and the potential across the resistor was measured with a Keithley meter (Model 2701 DMM, Keithley Instruments, Inc. Cleveland, OH) and collected via a personal computer.[48] Influent was pumped into the reactor using a peristaltic pump (Watson-Marlow 323S Bredel, Watson-Marlow Inc. Wilmington, MA) and attached cassette (Watson Marlow 314MC cassette) at a rate of 3 rpm using marprene tubing with a 2.79 mm bore. The anode compartment was continuously sparged with nitrogen throughout the experiment.

5.3.3.1 Anode

Glucose(50ppm), glutamic acid (50ppm), and phosphate buffer (100mM, pH 7.5) were added to a media consisting of a trace element and salt solution described previously.[103] Each reactor was inoculated with activated sludge (biomass taken from the aeration tank in a wastewater treatment plant) from ALCOSAN wastewater treatment plant (Pittsburgh, PA) and was recycled through the reactors until current was generated. Substrate was then fed in continuously until a significant amount of current was produced. The start-up procedure lasted about 1 week after which cathode testing commenced. After testing in the MFC was complete, anodes were extracted and imaged using SEM (SEM; e-LiNE, Raith GmbH, Germany) to ensure the accumulation of a biofilm.

5.3.3.2 Cathode

The cathode was fed with air-saturated water containing phosphate buffer and the same salt solution as in the anolyte. The influent was pumped using the same setup described above. For the first part of the experiment,1000Å Pt was deposited on plain Toray carbon paper (TGPH-120, E-tek, Somerset, NJ) using an e-beam evaporator (VE-180, Thermionics Laboratory). This electrode containing e-beam deposited Pt was inserted as the cathode. E-beam deposited Pt electrodes were used as a base for comparison because they were previously tested in MFCs.[48] It is also important to note that e-beam evaporation does not deposit Pt throughout the thickness of the sample. The e-beam Pt deposited electrodes (1000 Å) in the cathode compartment were used in operation for 2 days and were then replaced by a SWNT-nPt sheet electrode in order to evaluate relative performance. The MFC was again operated for a day after the replacement. Samples of both SWNT-nPt and e-beam Pt (1000 Å) electrodes, 1cm^2 in size, were placed in a 100mM phosphate buffer solution, an Ag/AgCl reference electrode, and a 2cm^2 e-beam Pt counter electrode. The solution was continuously sparged with air. Cyclic voltammetry was performed on each cathode individually using a CH Instruments 1040A potentiostat at a scan rate of 2$mV*s^{-1}$ in the range of -0.2V to 1.2V (vs Ag/AgCl).

5.4 RESULTS AND DISCUSSION

The SEM image in Figure 10A shows the uniform architecture of the SWNT-nPt matrix at the micro scale. Assemblies of SWNT bundles were seen throughout the thickness of the sample. Figure 10B at higher magnification shows the uneven topography and high surface area that we expected.

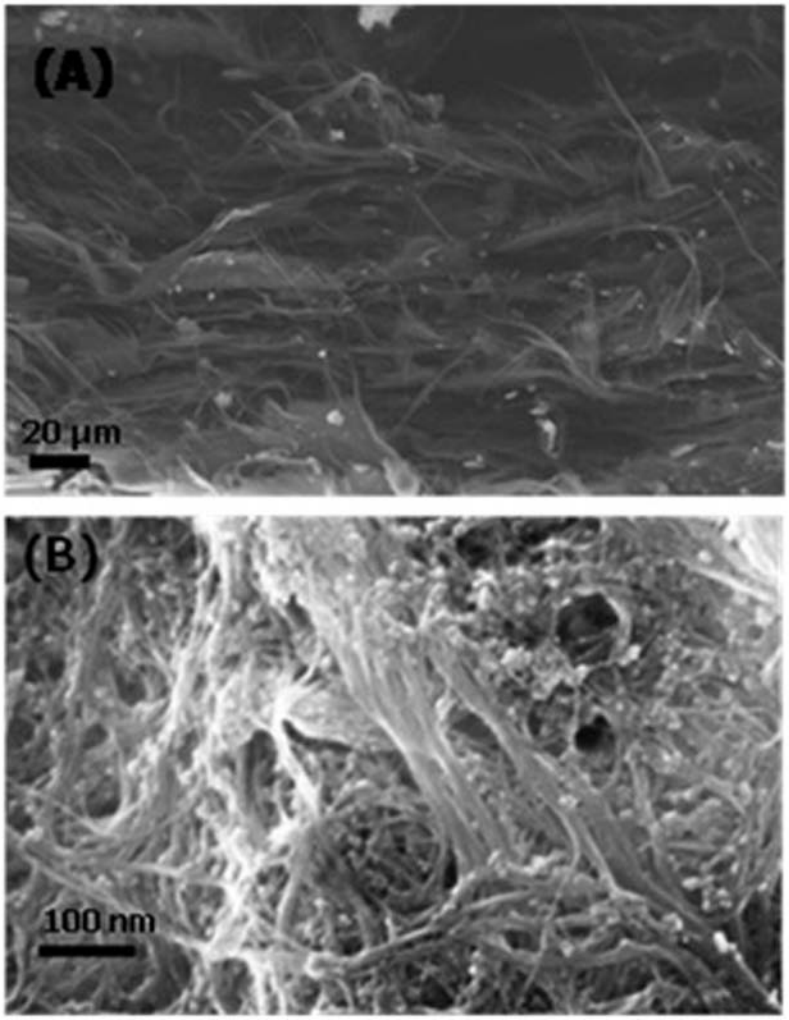

Figure 10. SEM images of a fractured surface of SWNT-nPt matrix at low (A) and high magnifications. The images illustrate the fibrous nature of the electrode and that the platinum nanoparticles are not highly agglomerated. Reprinted with permission from Sanchez et al. 2010. Carbon Nanotube/Platinum (Pt) Sheet as an Improved Cathode for Microbial Fuel Cells. Energy & Fuels 24, 5897-5902. Copyright 2010 American Chemical Society.

The Raman spectra of SWNT samples with and without nPt showed identical Raman features (Figure 11). The G, G' and D bands were at the usual positions for SWNT spectra.[104] The spectra showed about the same intensity for SWNT and SWNT-nPt and revealed no

significant shifting or broadening of the peaks. The dominant peak near 1580cm^{-1} is characteristic of SWNT and typically relates to the phonon modes.[104] These spectra indicate a consistency in the process of electrode fabrication. Most importantly, the material did not change during the process and no contaminant, such as surfactant used to disperse SWNTs or organic material from source carbon nanotubes, was found.

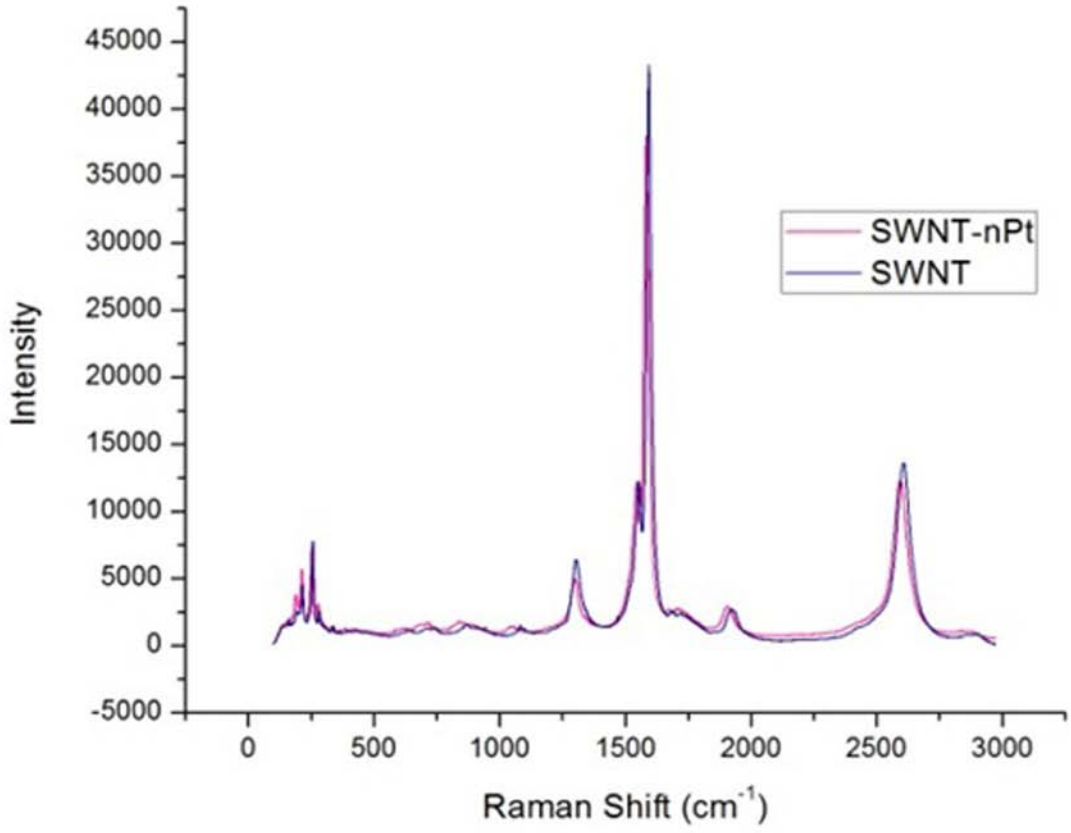

Figure 11. Raman spectra of SWNT samples with and without platinum nanoparticles. The samples were measured using 633nm laser excitation. This image shows that there is no notable shift in the G,G', and D bands between SWNTs with and without platinum nanoparticles. Reprinted with permission from Sanchez et al. 2010. Carbon Nanotube/Platinum (Pt) Sheet as an Improved Cathode for Microbial Fuel Cells. Energy & Fuels 24, 5897-5902. Copyright 2010 American Chemical Society.

The TEM images in Figure 12 illustrate the size and distribution of nPt throughout the SWNT sheet. Relatively complete coverage of the SWNTs with nPt can be seen in Figure 12A. The distribution of these nPt throughout the SWNT matrix was such that nPts were clearly separated and well distributed with rare occurrences of agglomeration. Sizes of nPt were between 4-10nm and were confirmed with images of increasing magnification shown in Figure 12B,C and D.

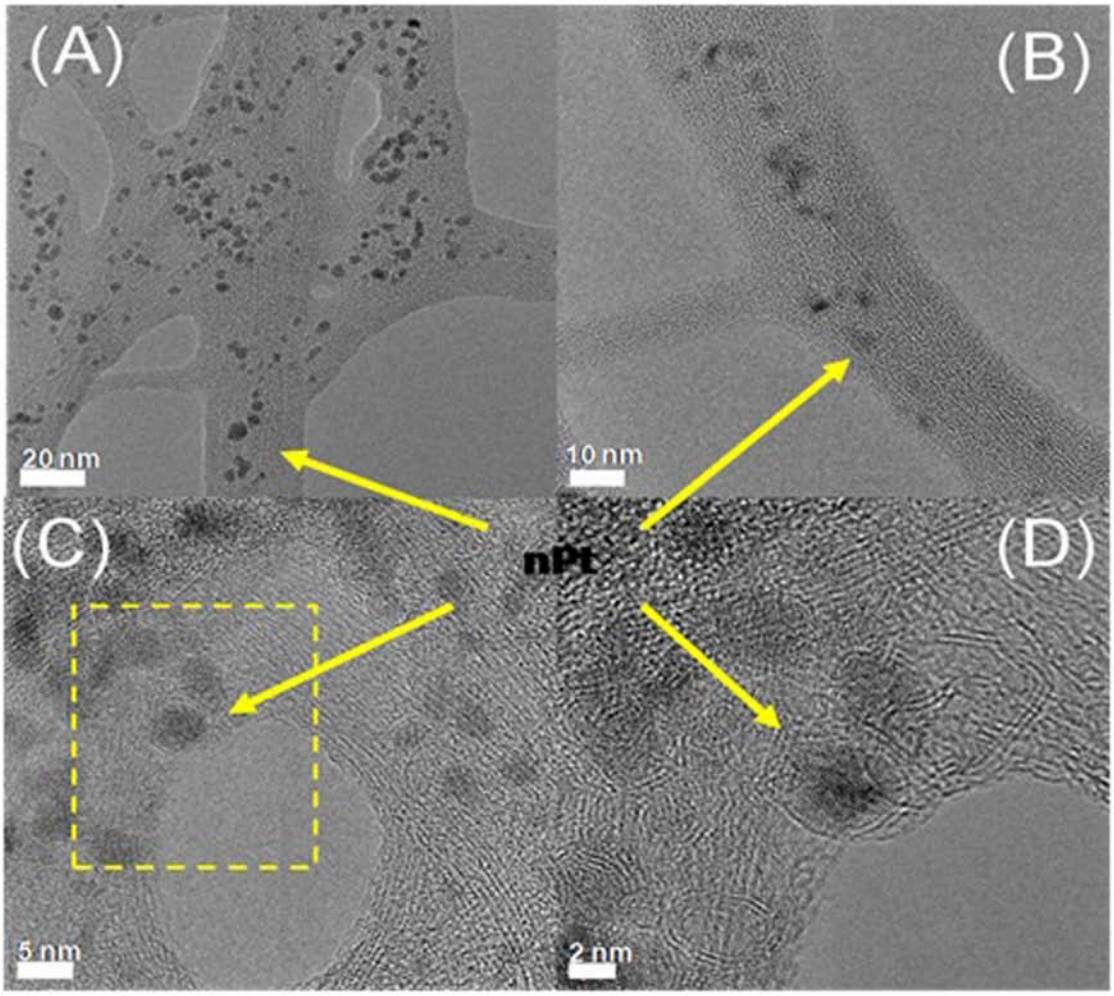

Figure 12. TEM images of SWNT-nPt samples at (A) low magnification, (B) medium magnification, (C) high magnification, and (D) magnification of inset in B. The images show 4-10nm platinum nanoparticles evenly dispersed in the SWNT matrix. Reprinted with permission from Sanchez et al. 2010. Carbon Nanotube/Platinum (Pt) Sheet as an Improved Cathode for Microbial Fuel Cells. Energy & Fuels 24, 5897-5902. Copyright 2010 American Chemical Society.

Figure 13A shows the difference in anodic performance for the SWNT with embedded nPt made with different surfactants; e-beam Pt (1000Å) electrodes were used as cathodes. It is important to note that e-beam Pt (1000Å) cathodes were previously shown to increase current density (~0.2 A/m^2) when substituted for plain carbon cathodes. This serves as our performance reference for improving the cathode electrode with nPts. The shapes of the current density profiles in Figure 13A were similar to each other and the difference in performance of the two electrodes was small. The shape of the current densities/voltage discharge seen in Figure 13A and B are similar to those reported previously.[59] The initial discharge is typically followed by a plateau of the current density which could be due to activation overpotentials of the biofilm anode and/or slow diffusion of reduced mediators that may be in the biofilm. To test the reactivity of the cathode the influent pump for the cathode was shut off for 5 hours to decrease the oxygen reduction rate but allow charge (i.e. reduced mediators and or proteins) to accumulate within the biofilm anode as bacteria continued to consume the substrate. The shut-off period occurred from hours 22 to 27 in Figure 13A, which resulted in the increase in charge in the biofilm anode. As the influent pump for the cathode was re-started at the 27th hour to increase the oxygen concentration in the cathode a second peak discharge occurred (Figure 13A). This peak discharge confirms the accumulation of charge in the biofilm anode and characterizes the reactivity of the cathode.

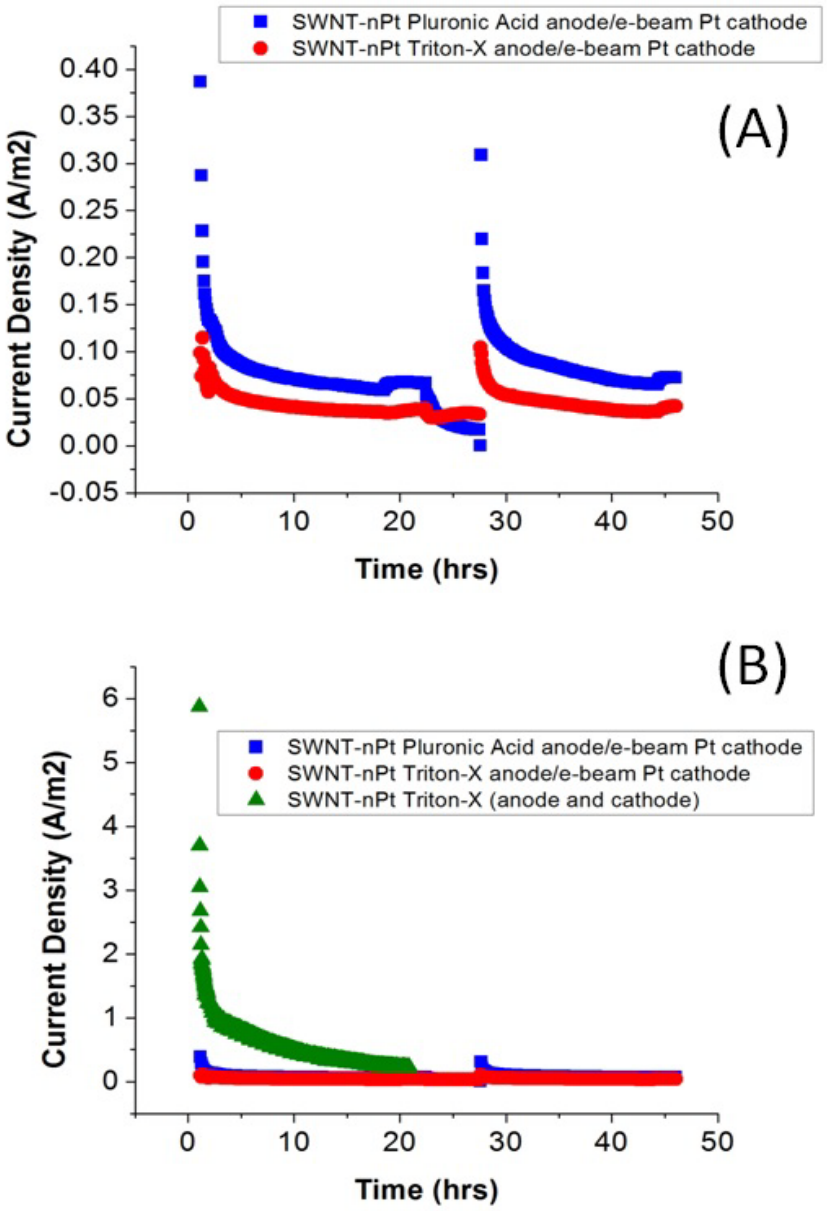

Figure 13. Current density profiles from a Microbial Fuel Cell employing (A) SWNT-nPt pluronic acid (■) and SWNT-nPt Triton-X (●)anodes with e-beam Pt (1000 Å) cathodes and (B) SWNT-nPt Triton X electrodes loaded with Pt (0.5mg/cm^2) (▲) as the anode and cathode. The results are superimposed on each other in Figure 6B. Note that changing the cathode from an e-beam Pt electode (1000 Å) to a SWNT-nPt electrode improved the current density ~an order of magnitude. Reprinted with permission from Sanchez et al. 2010. Carbon Nanotube/Platinum (Pt) Sheet as an Improved Cathode for Microbial Fuel Cells. Energy & Fuels 24, 5897-5902. Copyright 2010 American Chemical Society.

In Figure 13B the e-beam Pt cathode that is coupled with the lower performing anode (SWNT-nPt-Triton X) is swapped for a SWNT-nPt- Triton X cathode. The discharge peak and current density plateau are then increased by almost an order of magnitude. This is most interesting when we examine the Pt loading for each electrode. The loading for an e-beam evaporated Pt electrode at 1000Å thickness is 0.215mg/cm^2 and the Pt loading for the SWNT-nPt electrode is more than double that amount (0.576mg/cm^2). However, when we conservatively compare the mass-specific current densities (Amps/ mg Pt) the SWNT-nPt-Triton-X electrode (0.1A/m^2 / 0.576mg) outperforms the e-beam Pt cathode (0.01A/m^2 /0.215mg) by a ratio of 4:1.

Cyclic voltammograms (CVs) for both SWNT-nPt and e-beam evaporated Pt (1000Å) electrodes are provided in Figure 14. The reaction rate for oxygen reduction on SWNT-nPt when compared to the e-beam Pt electrode is significantly higher than for the e-beam evaporated Pt (1000Å) electrode. The results are consistent over the 4 cycles.

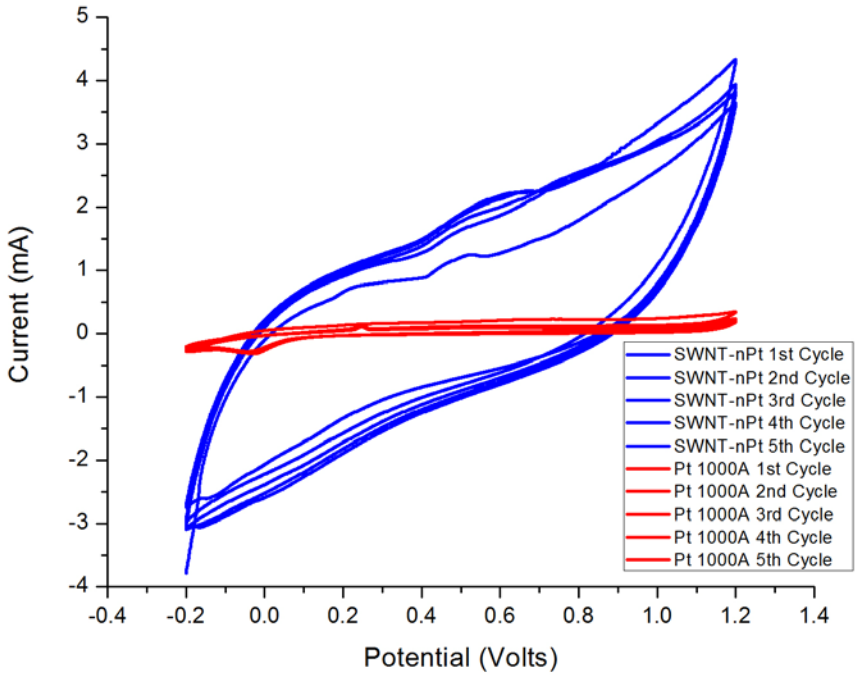

Figure 14. Cyclic scans of SWNT-nPt and e-beam Pt (1000 Å) electrodes illustrating effect of each electrode on the oxygen reduction reaction. At a scan rate of 2mV/s in a range of -0.2V to 1.2V (vs Ag/AgCl) the SWNT-nPt demonstrated superior performance. Reprinted with permission from Sanchez et al. 2010. Carbon Nanotube/Platinum (Pt) Sheet as an Improved Cathode for Microbial Fuel Cells. Energy & Fuels 24, 5897-5902. Copyright 2010 American Chemical Society.

The SEM image in Figure 15 confirms the accumulation of a biofilm on the anode. The bacteria are rod-shaped and seen throughout the sample. The top left of the image shows a putative bionanowire traversing the biofilm[105] which were scattered throughout the sample.

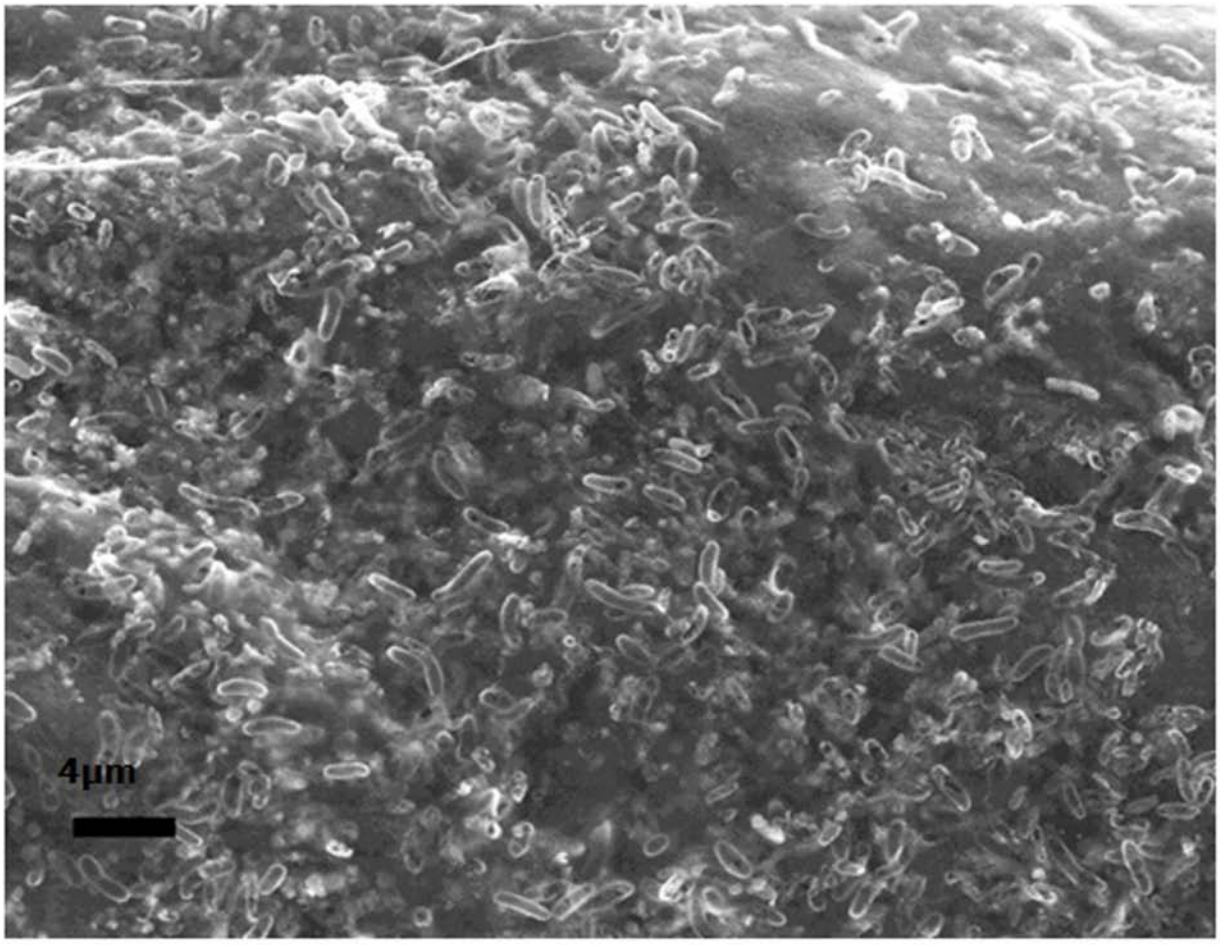

Figure 15. SEM image of the biofilm accumulated on the SWNT-nPt anode surface in a microbial fuel cell. Most of the bacteria are rod shaped which was consistent throughout the sample. Reprinted with permission from Sanchez et al. 2010. Carbon Nanotube/Platinum (Pt) Sheet as an Improved Cathode for Microbial Fuel Cells. Energy & Fuels 24, 5897-5902. Copyright 2010 American Chemical Society.

5.5 CONCLUSIONS

In this chapter, I present the preparation of MFC cathodes using SWNT-nPt dispersions and their characterizations. The fabrication method used for this SWNT-nPt cathode is an extension of the conventional bucky-paper fabrication technique for a multi-component system and it combines nPts and SWNTs into filter sheets. The electrodes were characterized with SEM, Raman spectroscopy, and TEM confirming nPt size, the even dispersion of nPt and the composition and structure of our electrode. These characterizations confirmed a successful integration of the two components; SWNT and nPt.

More importantly, the novel electrode improved the cathodic reaction rate in MFCs by increasing the current density by approximately an order of magnitude when used to replace an e-beam Pt (1000Å) cathode. These findings suggest that when the cathode is under kinetic control (i.e. mass transfer is not limiting) the oxygen reduction reaction can be effectively and more efficiently catalyzed by smaller Pt constituents (nPt) that are deposited throughout the electrode as opposed to solely on the surface. Increasing the surface area of platinum by using nanoparticles and maintaining an even distribution of those nanoparticles within an SWNT matrix increases MFC current density and the mass-specific current density of Pt 4-fold.

Finally, the electrode fabrication and catalyst deposition method determine the catalyst surface area available for the oxygen reduction reaction and are paramount to improving the oxygen reduction rates in MFC cathodes and ultimately MFC current density. Nanoparticles intermixed with SWNTs hold great potential to improve the cathodic reaction in MFCs. As a

result future research directions include decreasing the nPt loading, using non-noble metal nanoparticles, and long term feasibility studies.

In the previous two sections, the incorporation of platinum nanoparticles as a catalyst onto CNF mats and SWNTs demonstrated the significance of increasing MFC current density by using nanofabrication methods to increase Pt surface area in MFC electrodes. This is surprising when we extrapolate from the mass-specific current densities of hydrogen fuel cells (2000mA/cm^2/ mg Pt) the amount of Pt that would be necessary to maintain high current densities in MFCs (i.e. 0.5μg Pt for 1 mA/cm^2). In other words, when we consider the fact that MFC Pt catalyst loadings are similar to those used to produce current densities 2-3 orders of magnitude greater via hydrogen fuel cells, it is surprising that increasing Pt surface area is still a an effective method to significantly increasing MFC current density.

6.0 THE EFFECTS OF CARBON ELECTRODE SURFACE MORPHOLOGY ON BIOFILM-ANODE PERFORMANCE (BY *SHEWANELLA ONEIDENSIS* MR-1) USING A TUBULAR ELECTRODE CONSTITUENT MATERIAL

The previous two chapters determined that increasing catalyst surface area, by way of incorporating platinum nanoparticles, increases both anodic and cathodic contributions to MFC current density. In wanting to determine how the whole electrode (catalyst/electrode) influences the bio-electrochemical reaction it is then essential that the influence of the bare electrode on the bioelectrochemical reaction in MFCs also be investigated. In the following experiment I examine the effect of carbon fiber properties on anode-respiration by *Shewanella oneidensis* MR-1. A pure culture is chosen to reduce the complexity of the biofilm-anode's physiological profile (e.g. elimination of methanogenesis, bacterial competition, and additional electron sinks). This particular strain is chosen since its bioelectrochemical physiology is well documented in the literature. For example, both its mediated and direct electron transfer mechanisms to an electrode have been determined and electrochemically evaluated (e.g. it uses riboflavin as a mediator and it is oxidized at -0.41V vs Ag/AgCl)[27] thus enabling one to electrochemically determine how the bacteria are interacting with the electrode.

6.1 SUMMARY

The formation of biofilm-electrodes is crucial for microbial fuel cell current production because optimal performance is often associated with thick biofilms. However, the influence of the electrode structure and morphology on biofilm formation is only beginning to be investigated. This study provides an analysis of the effects of electrode morphologies on a pure culture of anode-respiring bacteria. Specifically, the effects of carbon electrode materials (i.e. carbon microfibers and nanofibers) with drastically different morphologies on biofilm anode respiration by a pure culture (*Shewanella oneidensis* MR-1) were examined. Results showed that carbon nanofiber mats had ~10 fold higher current than carbon microfiber paper and that the increase was not due to an increase in electrode reactive surface area, conductivity, or a decrease in the activation resistance stemming from the reduction in the size of the constituent material. Cyclic voltammograms reveal that electron transfer from the carbon nanofiber mats was biofilm-based which suggests that decreasing the diameter of the constituent carbon material from a few microns to a few hundred nanometers is beneficial for electricity production solely because the electrode surface of carbon nanofibers is more amenable to biofilm formation by *Shewanella oneidensis* MR-1.

6.2 INTRODUCTION

The bare anode of a microbial fuel cell (MFC) receives electrons from bacteria, serves as the substratum for bacteria to attach and initiate biofilm formation and provides the scaffold on which it grows.[106-107] In many cases, the formation and size of the biofilm are directly correlated

to high current production by a MFC.[25, 107-108] Therefore, understanding how the electrode structure and morphology might influence the formation and size of a biofilm in a biofilm-anode is paramount for the development of any biofilm-electrode based technology.

Several studies have reported that changing the structure (e.g. graphite rod, graphite foam, woven graphite) of the anode resulted in an increase in current production.[47, 109-112] These studies focused on how the electrodes influenced the electrochemical reaction or increased the available/reactive surface area thus providing a foundation for later investigation into how electrodes effected biofilm formation and growth.[14, 19, 90] Observations from these studies led to the modification of anodes in order to further increase reactive surface area[47, 49, 58-59, 113-114] and or decrease overpotentials, a conventional approach borrowed from catalytic fuel cell research.[52-53, 56, 101, 115-118] For example, Logan et al.[113] showed that increasing the overall surface area by employing a graphite electrode brush increased current density by ~2.5 times compared to a carbon cloth anode. At the same time however, Dewan et al.[119] found that current densities for electrodes with a larger surface area cannot always be directly extrapolated using the current densities generated by smaller electrodes. Additionally, Dewan et al. found that power densities scale with the logarithm of the projected surface area. As a result, anodes that serve as the substratum for electricity-producing biofilms may need to incorporate more than just a higher surface area or decreased activation overpotential. Perhaps anode selection should also account for factors that may influence the bio-electrochemical reaction indirectly, such as an anode surface morphology that impacts the onset and growth of the biofilm.

Given the size of a typical bacterium (1-3μm), increasing the surface area to volume ratio of the material does not necessarily increase the surface area available for bacterial respiration after some threshold.[47] However, changes at the micro and nanometer scale affect the surface morphology of the electrode that bacteria and their biofilms attach to and grow on. Changes in surface morphology have already been shown to affect biofilm growth[120-122] and several studies have correlated changes in electrode structure and biofilm-anode performance of mixed cultures.[123-124] In order to build upon these findings, and to eliminate the possibility that differences in performance were due to differences in the physiological profile of the mixed culture it is important to investigate whether changes in electrode surface morphology influence the ability of an electrode to spur biofilm formation in a pure culture and thus increase biofilm-anode current production.

The interface between a biofilm and an anode cannot be understood by evaluating the individual components (i.e. a bacterial species or electrode material). As a result, determining an electrode's effect on biofilm formation requires simultaneous evaluation of the electrode's properties and an understanding of the physiology of the bacteria in an electrochemical context. While one can easily measure the conductivity of an electrode and subjectively evaluate its surface morphology, accounting for the physiology of the bacteria is more challenging since a change in the environmental conditions can trigger different mechanisms of extra-cellular electron transfer (EET) in the bacteria.[27, 125]

Studies on EET in a pure culture like *Shewanella oneidensis* MR-1 facilitate the determination of which EET mechanism is being used. For example, Marsili et al.[27] revealed that

riboflavin is the shuttle being used by *S. oneidensis* during mediated electron transfer and showed that it is oxidized at a specific potential. This helps to explain its ability to respire the electrode as a planktonic biomass.[26] Additionally, Baron et al.[125] showed that *S. oneidensis* employs direct electron transfer at a distinctly different potential. Their use of cyclic voltammograms (CVs) of the anodes provide a way to reasonably identify, based on the reduction potential, which EET mechanism (mediated or direct electron transfer from a biofilm) is being used and to what extent. While the shape of cyclic voltammograms for reversible electron transfer for soluble mediators (i.e. riboflavin) is widely established,[20] the presence of direct electron transfer from a biofilm and how it manifests itself in CVs for microbial fuel cells is a more recent discovery.[33, 126]

Engineering electrodes for optimal biofilm-anodes can be improved by examining the effects of electrode properties on biofilm-anode formation and by devising experiments that incorporate the fundamental physiological findings in the literature,[27, 125] biofilm kinetics,[95, 127] and bioelectrochemistry. Given that several engineering or modification studies have shown significant changes in biofilm colonization and formation when surface morphologies were changed for mixed cultures,[122-124, 128-129] it is only appropriate to examine how this might affect the biofilm-electrode interface of a pure culture in which the electrode surface uniquely serves as both the substratum and the terminal electron acceptor. Using a pure culture removes any inconsistencies regarding the physiological profile of the community, the presence of scavengers, metabolic pathways that serve as electron sinks (e.g. methanogenesis), and the community dynamics associated with bacterial competition.

Here the effect of changing the morphology of the anode surface (i.e. decreasing the diameter of the electrode's constituent material) on anode respiration/current production by *S. oneidensis* MR-1 is studied. Experiments were repeated twice however, only two sets of electrodes are described below. Amperometry was used to monitor current production over time, CVs were used to account for its electron transfer mechanisms and, the differences between electrode materials were qualified using scanning electron microscopy (SEM), conductivity measurements and, areal weight measurements.

6.3 MATERIALS AND METHODS

6.3.1 Electrode characterization

Plain Toray carbon paper (PTCP), (TGPH-120, E-tek, USA), or carbon microfiber paper (CMF) and carbon nanofiber (CNF) mats (Applied Sciences, PR-19-XT-HHT) were used as anodes in this study. $1cm^2$ electrodes were cut from each sample and weighed to determine areal weight. Electrode conductivity was measured using a standard 4-point probe measurement.[130] Electrodes were soaked in 1M sulfuric acid for at least 1 hr prior to installing in the reactor.

6.3.2 Cell cultures

Shewanella oneidensis MR-1 (ATCC 70050) was cultured aerobically in Luria-Bertani (LB) broth from a frozen stock and transferred to a medium with 20mM D-L lactic acid as the electron

donor. The medium also contained (per liter): 1.5g of NH_4Cl, 0.92 $(NH_4)2SO_4$, 10ml vitamin solution, 10ml trace element solution, and 100mM phosphate buffer (pH 7.5). Phosphate buffer was made using sodium phosphate dibasic (Na_2HPO_4) and monopotassium phosphate (KH_2PO_4). The media was autoclaved and made anoxic by sparging with N_2 gas. Vitamin solution contained (per liter): 2.1g biotin, 2.2g folic acid, 11g pyridoxine hydrochloride, 8g thiamine HCl, 5g riboflavin, 7g nicotinic acid, 7g calcium D-(+)-pantothenate, 0.7g vitamin B12, 5g p-aminobenzoic acid, and 5g thioctic acid. Trace element solution contained (per liter): 0.018g Na_2SeO_3, 0.11g $NiSO_4$-$6H_2O$, 0.2g Na_2WO_4-$2H_2O$, 2.14g nitrilotriacetic acid, 0.1g $MgSO_4$-$7H_2O$, 0.1g $MnSO_4$-H_2O, 0.36 NaCl, 0.01g $FeSO_4$-$7H_2O$, 0.179g $CoCl_2$-$6H_2O$, 0.53g CaCl-$2H_2O$, 0.2g $ZnSO_4$-$7H_2O$, 0.2g $CuSO_4$-$5H_2O$, 0.01g $AlK(SO_4)_2$-$12H_2O$, 0.009g H_3BO_3, and 0.098g Na_2MoO_4.

6.3.3 Micro-Electrolysis Cell (MEC) Operation

The single-chamber 1-L reactor contained three working electrodes (each $1cm^2$) positioned equidistant from a single Ag/AgCl reference electrode and a counter electrode ($6cm^2$). The counter electrode was made of PTCP with a 1000 Å thick layer of platinum deposited onto its surface via electron beam evaporation.[48] A CH Instruments 1040A multi-channel potentiostat was used to maintain a potential of +0.043V vs. Ag/AgCl for each working electrode. Current was measured and recorded every 100 seconds (amperometric measurements). CV scans were conducted on a range from -0.7 to 0.3V at a rate of 2mV/s. The reactor was sparged with N_2 gas and wrapped in aluminum foil during operation. The addition of fuel included injecting 10 ml of 100mM lactic acid with 10ml trace element solution and 10ml vitamin solution. The reactor was stirred with a magnetic stir bar at 60rpm.

The experiments were initiated using sterile medium described above. After 2 days of abiotic operation, 10ml of LB media containing *Shewanella oneidensis* MR-1 was inoculated into the reactor. After two weeks of operation the anodes in the reactor were sacrificed for SEM images. The anodes were removed from the MEC, rinsed with phosphate buffer, and placed in a 4% paraformaldehyde solution for ~15min, rinsed with de-ionized water and placed in a petri dish. These fixed electrodes were then set aside for imaging. The paraformaldehyde solution was made by adding 4g of paraformaldehyde to 70 ml of de-ionized water, heating the solution to 70˚C, adding drops of 1N NaOH until the solution cleared, adding 9 ml of 1M phosphate buffer after the solution cooled and refrigerating it overnight.

6.3.4 SEM

Prior to examination, the fixed electrodes were sputtered with palladium using a Cressington Sputter Coater (108 Auto) for 30 seconds. Images of the anodes were taken before and after MEC operation for comparison. Images were taken using a JSM-6510LV SEM set at 20kV.

6.4 RESULTS

6.4.1 Current production

The differences in current production between CNF and CMF working electrodes were monitored amperometrically (Figure 16). The CNF electrode generated several times more

current than CMF throughout the experiment and is comparable to current generation from previous experiments. (29) The superior performance by CNF is confirmed by the fact that it exhibited a ~10-fold increase in current over that of CMF and that after the substitution of new electrodes into the MEC on day 15, current production by both CNF and CMF returned to the same levels exhibited prior to electrode replacement. Again, current production by CNF was substantially higher.

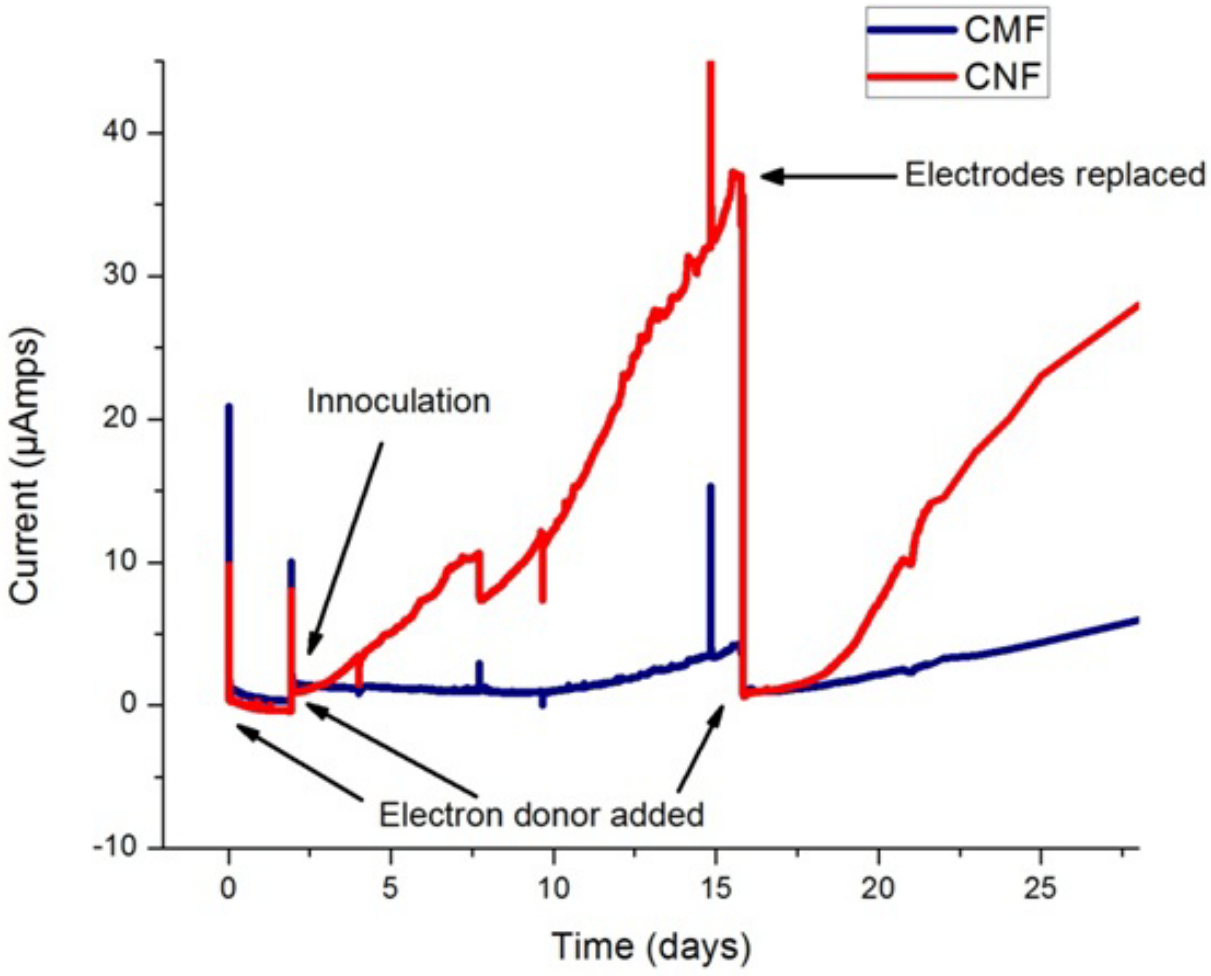

Figure 16. Amperometric data from a MEC inoculated with *Shewanella oneidensis* MR-1. Current production by carbon nanofiber mats/CNF (red) and carbon microfiber paper/CMF (blue) was monitored over a 4 week period.

6.4.2 Cyclic voltammograms

Cyclic voltammetry was performed on both electrodes on day 2 and on day 15. On day 2, the voltammograms for CMF and CNF are similar in amplitude and shape (Figure 17). However, the voltammograms taken on day 15 (Figure 17B) show that CNF is trending more towards a Nernst-Monod sigmoidal curve[33, 126] while CMF maintains a similar shape to that exhibited on day 2. After fitting the CV data taken on day 15 to the Nernst Monod Model (Figure 17B) it is easy to see that the CV for CNF correlates better to the Nernst-Monod sigmoidal shape than the CV for CMF.

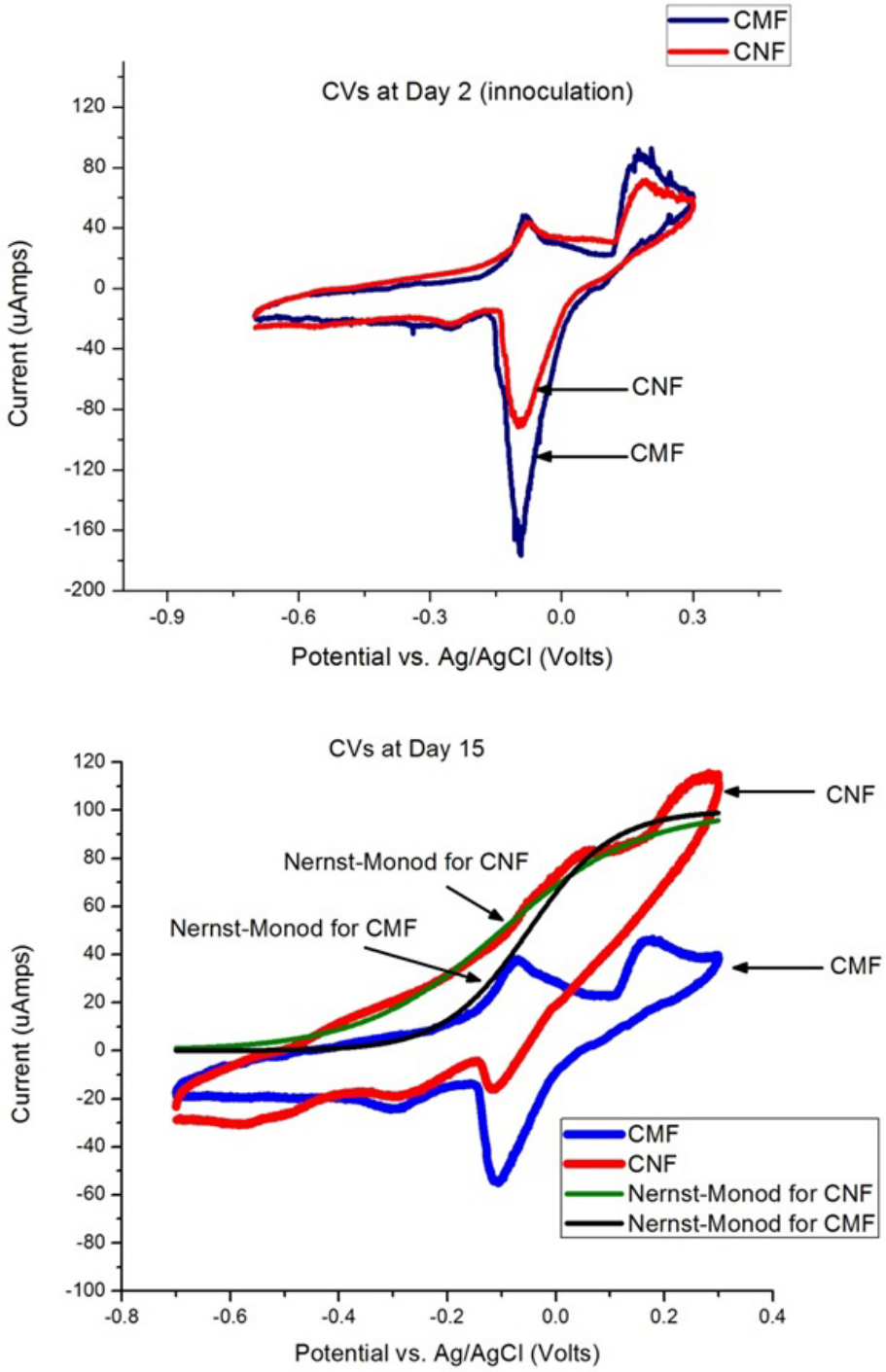

Figure 17. Cyclic voltammograms for carbon nanofiber mats/CNF (red) and carbon microfiber paper/CMF (blue) at Day 2 (top) and Day 15 (bottom) of the experiment. Day 15 was chosen because of the difference in current production. Electrode replacement took place after the CV. CVs were scanned from -0.7V to +0.3V vs Ag/AgCl at 2mV/s.

6.4.3 SEM -images for biofilm colonization

SEM images were used to demonstrate biofilm colonization on electrodes. Images in Figure 18 show a distinct qualitative difference in the amount of biofilm formed on CNF mats versus CMF. Micrographs of the CNF electrode reveal a biofilm as well as outlines of individual cells (Figure 18A and B) and are similar to other micrographs of *S. oneidensis* MR-1 biofilms on electrodes.[131] On the other hand very little cell colonization or growth was observed on the CMF electrodes (Figure 18C and D). Figure 18E is a magnification of a single bacterium found on the CNF biofilm-electrode.

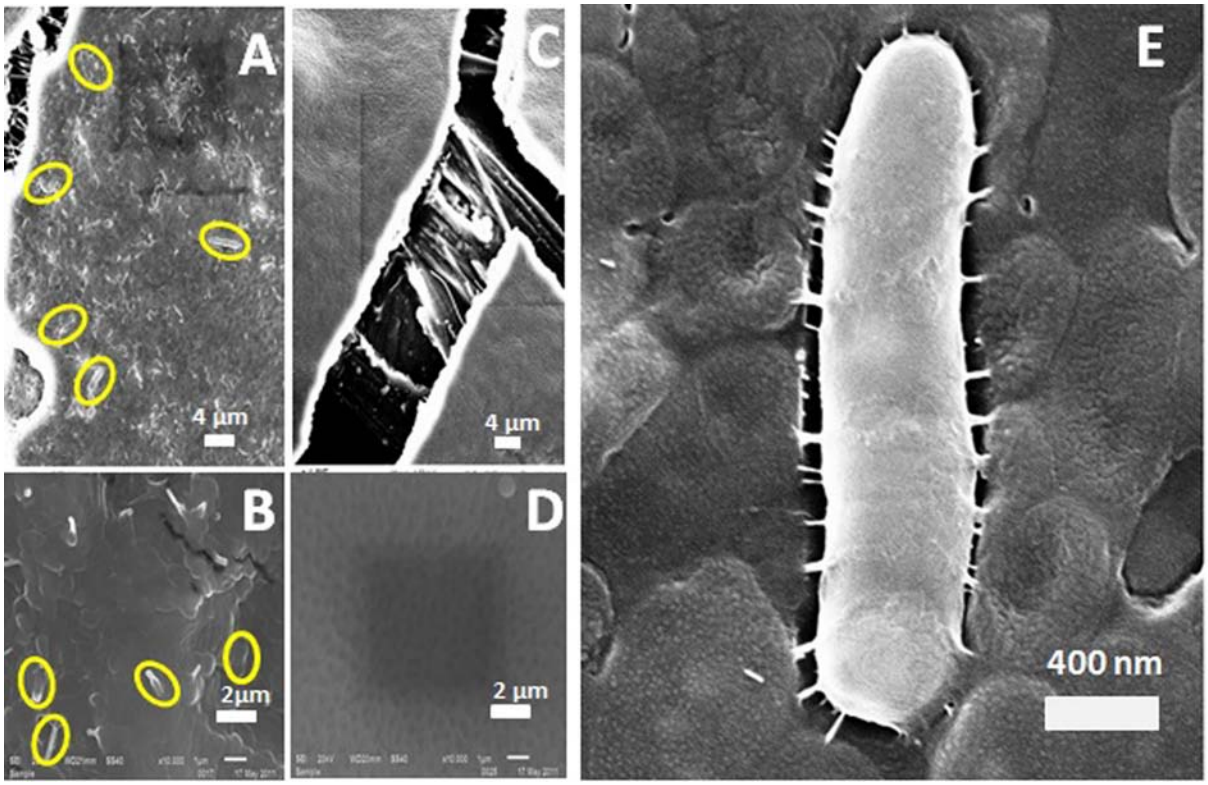

Figure 18. SEM images of increasing magnification of anodes evaluated in an MEC for 2 weeks and inoculated with *Shewanella oneidensis* MR-1. Images of both carbon nanofiber mat/CNF images (A and B) and carbon microfiber paper/CMF (C and D) were taken after elect rodes were fixed in paraformadelhyde solution. Images indicate the presence of a biofilm on the CNF electrodes. Bacteria are highlighted in (A and B). A magnified image of a single bacterium found on the CNF biofilm electrode is also shown (E).

6.4.4 Morphology of sterile electrodes

The electrode features revealed in the micrographs in Figure 19 highlight the morphological differences between CNF and CMF. The CNF mat shows a woven matrix of carbon nanofibers set upon a carbon scaffolding (Figure 19A) while CMF exhibits more of a rigid interlinked structure (Figure 19B). The typical diameter of the carbon fibers used in CMF are ~10μm while the carbon nanofibers are ~200nm in diameter (Figure 19D and E). Carbon nanofibers are more flexible and the carbon microfibers are linear and rigid. It is important to note the difference in morphology at the scale of a single bacterium when comparing electrodes in Figure 19 because the electrode features, relative to the size of the bacteria (i.e. 1-3 μm), are orders of magnitude different. CMF exhibits a constituent material (microfiber) with a serrated surface that is much larger (i.e. 10 μm) than a single bacterium. On the other hand, CNF exhibits a constituent material much smaller (i.e. 200 nm) than a single bacterium. In addition to these characterizations, physical and electrical properties of both electrodes are listed in the Table 2.

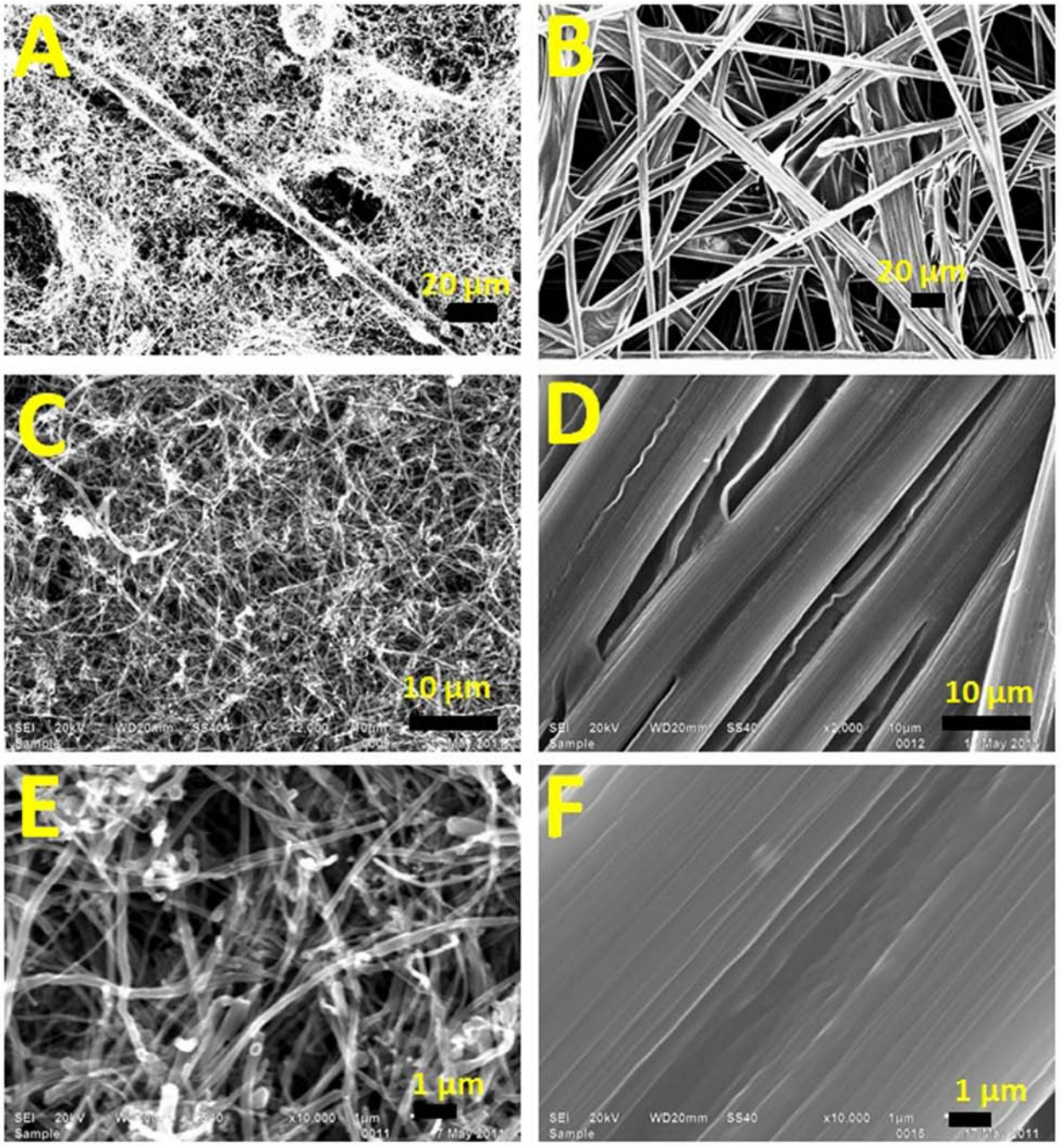

Figure 19. SEM images of increasing magnification of pristine carbon nanofiber mats (Images A, C, and E) and carbon microfiber paper (Images B, D, and F).

6.5 DISCUSSION

6.5.1 Differences in current production

The shapes of the I-t (current vs. time) curves throughout the experiment are identical and differ primarily in magnitude, with CNF producing current up to a factor of 10 more. The length of time given to the bacteria to colonize the electrode and generate current is well beyond times allotted in various experiments for biofilm formation suggesting that the time allowed for bacteria to agglomerate on the surface is not an issue. [125, 131] However, determining whether the current was generated by a biofilm or a planktonic mass is important and can be elucidated using CV.

6.5.2 Biofilm-based electron transfer

CVs for an anode-respiring biofilm will exhibit different shapes than CVs for a planktonic biomass using mediators. Biofilms using conduction based electron transfer will have a voltammogram with a sigmoidal profile [33, 126] while mediated electron transfer (planktonic biomass) will often show simple oxidation and reduction peaks.[19]

The shapes of the voltammograms taken on day 15 (Figure 17) show that CNF is trending toward a sigmoidal curve, like that of the Nernst-Monod model, while the shape of the voltammogram for CMF shows no significant changes from day 2. The fact that CNF correlates better with its Nernst-Monod model fit suggests that it formed a more complete conducting biofilm-electrode than CMF. Specifically, the sigmoidal profile generated by CNF on the

forward scan and the decrease of the reduction peak on the reverse scan support this trend in the CNF voltammogram. The fact that most of the current for CNF is generated above the redox potential of riboflavin (-0.41V vs Ag/AgCl) also supports the idea that mediated transfer was not responsible for the increase in current production. This suggests that electricity from the CNF electrode is being produced by electron transfer from a biofilm. The SEM images in Figure 18 confirm that CNF has formed a substantial biofilm on its surface relative to CMF.

6.5.3 Comparison of electroactive surface area and kinetics using CVs

There is no indication in the CVs (Figure 17) that CNF has a significant advantage because it has more electroactive surface area. If the increased current production by the CNF electrode were merely a function of surface area, the shape of the voltammogram for both electrodes would be identical differing only in the magnitude of current production. In other words, the shapes of the voltammograms would look the same, but the voltammogram for CNF would be shifted up vertically because of higher current production.

Since a kinetic advantage is often obtained from electron transfer for materials that are similar in size with its reductant (i.e. cytochromes or mediators)[132] it is important to account for the size disparity between the constituent materials for the electrodes (i.e. the size difference between carbon nanofibers and carbon microfibers). If the voltammogram for the CNF electrode is shifted horizontally to the left, relative to the voltammogram of the CMF electrode, this would indicate that CNF is more efficient than CMF at catalyzing the reaction. In the voltammograms of Figure 17 (top), the horizontal positions for the onset of current are identical; neither electrode displayed a kinetic advantage (i.e. no large decrease in the activation overpotential). In other

words, the similarity between the voltammograms taken on day 2 (Figure 17 (top)) suggests that neither electrode possessed improved catalytic properties.

As a result, the advantage of using CNF is not due to higher specific surface areas (i.e. higher concentration of active sites) or faster kinetics. This may mean that other factors (i.e. electrode conductivity and electrode morphology) contributed to the increased current production and biofilm formation on CNF.

6.5.4 Differences in electrode conductivity

Electrode conductivity is a function of areal weight (mass/geometric surface area). A more densely packed material (i.e. higher areal weight) translates into a smaller resistance to current (i.e. high conductivity). CMF has a larger areal weight and a higher conductivity yet it is CNF that produces more biofilm and more current. It seems that the smaller conductivity of CNF does not affect the formation and performance of its biofilm-electrode.

A recent study by Malvankar et al.[133] showed, for *Geobacter sulfurreducens*, that there is a direct correlation between conductivity of the biofilm and current production. They observed biofilm conductivities as high as 0.5 S/m. In our studies, CNF showed a conductivity of 1,300 S/m while CMF had a conductivity of ~15,500 S/m (see Table 2.) The differences in these values support the idea that the conductivities for CNF and CMF have no significant effect on differences in current production because both conductivities were substantially greater than the highest reported biofilm conductivities and because the electrode that performed better, CNF, had the lower conductivity. Additionally, even with electrode materials with higher resistivities Chen et al.[123] was able to generate much higher current densities with mixed cultures suggesting

that for general electrode materials there is not a strong correlation between resistivity/conductivity and current density.

Table 2. Electrode Properties for Carbon Microfiber Paper and Carbon Nanofiber Mats

	Carbon Microfiber Paper	Carbon Nanofiber Mats
Area Wt (g/m^2)	161	40
Thickness (cm)	0.038	0.015
Bulk Resistivity (Ohm-cm)	0.006	0.075
Measured Sheet Resistivity (Ohm/Square)	0.17	5
Avg. diameter of constituent material	10μm	0.2μm
Bonding	sp^2	sp^2
Surface Modifications	None	None

6.5.5 Toxicity

Since both CNF and CMF were sourced from different manufacturers there is the potential that CMF did not produce a substantial biofilm because toxins (e.g. metals) were present in the electrode. To address this issue I took samples of both CNF and CMF and examined them using energy dispersive x-ray (EDX) spectroscopy. $1cm^2$ samples were placed in a SEM (JEOL JSM-6510LV/LGS) equipped with an Oxford X-Max large area Silicon Drift Detector with an INCA microanalysis system (INCA Energy). The spectra and the quantitative results can be seen in Figure 20**Error! Reference source not found.**.

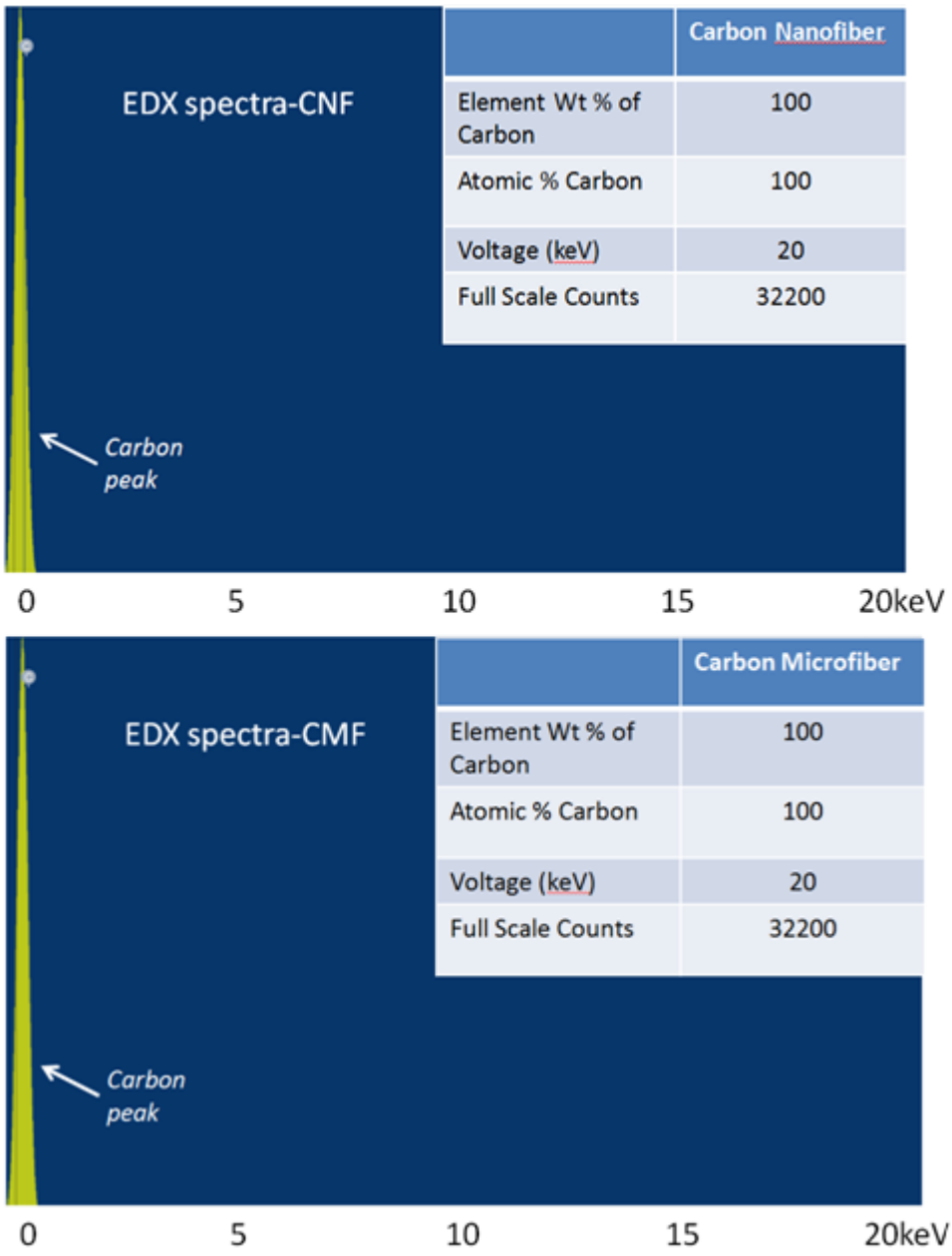

Figure 20. Energy Dispersive X-ray (EDX) Spectra of both carbon nanofiber mats and carbon microfiber paper. The quantitative results are in the right hand column. Both samples recorded spectra indicating that there was no presence of any trace metals or known bacterial toxins.

The spectra shown for both CMF and CNF illustrate that the samples were made of carbon. Both the elemental weight percentage and the atomic percentage of the samples were 100% carbon and there were no trace elements or stray peaks, particularly from metals such as Fe(III), Co(III), U(VI), Tc(VII), V(V), Ag(I) all of which can serve as electron acceptors for *Shewanella oneidensis* MR-1 [134-135] and some of which have been shown to be toxic to *Shewanella oneidensis* MR-1 in high concentrations (175μM for Cr(IV), 100μM for Ag(I), and 0.5-20mM Co).[136-138] However, it is important to note that the sensitivity of EDX is approximately 0.1% suggesting that the presence of additives may be present below this concentration.[139]

An examination of the manufacturing process showed that CNF was grown via chemical vapor deposition (CVD) using an iron (Fe) catalyst. Technical data on CNF (www.apsci.com) showed that the electrodes are made of pure carbon and the amount of iron catalyst present in the carbon nanofibers, after they are graphitized (i.e. heated to 3000˚C), is less than 100ppm or 0.01%.

On the other hand, CMF paper is a carbon-carbon composite and its manufacturing process does not use a catalyst or known toxins and any resins used are carbonized by the process. The fibers are made by the carbonization and graphitization of carbon precursors (i.e. polyacrylonitrile)[140-141] through which non-carbon atoms are excluded (~1600°C) and the orientation of the basal planes and stiffness of the fibers improved (> 2000°C).[142] In other words the carbon is distilled via pyrolysis and reordered using heat as opposed to grown using CVD. Technical information on the manufacturer's website (www.toray.com) lists that fibers can have a combined sodium (Na) and potassium (K) concentration of up to 50ppm. Additional inquiries to both the suppliers and Toray Industries revealed that that an elemental analysis of the carbon paper showed 0.2μg/g of barium (Ba). The presence of Ba is assumed to originate from the water-intensive papermaking process since Ba is commonly found in finished waters.[143] All other elements tested

for (i.e. Cd, Cr, Pb, Ar, Se, Hg) were below the detection limits. (Toray Industries Tacoma, WA, personal communication).

Given the Ba concentration of 0.2μg/g , the size of the electrodes (1cm^2) and that the areal wt. of CMF (161g/m^2, see Table 2) means that a total of 3.22ng/L ($2.3x10^{-11}$ M) of Ba would potentially be present in the reactor. Since this concentration is four orders of magnitude less than the mean Ba concentration of US surface waters (43μg/L)[143], there is no report in the literature of toxicity of barium on *Shewanella oneidensis* MR-1, and Toray carbon paper is commonly used as an electrode in MFCs,[144] I assumed that the concentration was negligible and that it posed no toxicity issues for *Shewanella oneidensis* MR-1. Addtionally, since the salts used for the phosphate buffer in this experiment (see Materials and Methods) provided a much higher concentration (mM range) of Na and K in the solution, I assumed as well that the 50ppm concentration in CMF would also present no toxicity issues for *Shewanella oneidensis* MR-1.

Finally, given CNF's areal wt. of 40g/m^2 (see Table 2) and the potential presence of 50ppm of Fe means that for the 1cm^2 CNF electrode an additional 0.4μg (7nM) could be available to the CNF biofilm. When compared to the Fe provided by the addition of the trace element solution (0.1mg $FeSO_4$-$7H_2O$ in 10mL or 0.36μM for the 1L reactor), the additional Fe provided by the CNF electrode to *Shewanella oneidensis* MR-1, if available to the bacteria, is assumed to be negligible.

6.5.6 Biofilm formation

The drastic differences in biofilm formation by *S. oneidensis* MR-1 (see Figure 18) are less surprising when we consider that it can also respire electrodes as a planktonic biomass and that single physical mutations to *S. oneidensis* MR-1 have been shown to have profound effects on biofilm formation. For example, previous studies of biofilm formation by *S.oneidensis* MR-1 showed that the presence of the flagellum, swimming motility, presence of a mannose-sensitive hemagglutinin type IV pilus, and pilus retraction played a significant role in the ability for *S. oneidensis* MR-1 to form a biofilm. Specifically, the lack of a flagellum decreased the concentration of biomass (decreased biofilm formation), the lack of motility prevented the formation of a pronounced three dimensional biofilm architecture (bulk structure), the mutants defective in mannose-sensitive hemagglutinin type IV pilus biosynthesis had defects in initial attachment and the mutant defective in pilus retraction displayed poor propagation of the biofilm. [131] In addition, another study showed that mutants lacking the gene pilD (indicated in Type IV pilin production) and the protein secretion genes gspG and gspD produced less current in MFCs relative to the wild-type *S. oneidensis* MR-1. The images of the electrodes used in those microbial fuel cell experiments with the mutant lacking pilD revealed a lack of biofilm as compared to the wild- type.[145] These previous studies provide a foundation from which to investigate how morphology affects different phases of biofilm formation at a molecular and genetic level but, more importantly they highlight that small changes in how a cell interacts with its environment can have significant consequences for the entire biofilm. As the change in an substratum structure has affected biofilm formation in studies with mixed cultures [122-124] it is important to examine the differences in electrodes morphology here for this pure culture.

6.5.7 Impact of electrode morphology

A single bacterium of *S. oneidensis* MR-1 attaching to the surface of CNF would be in contact with multiple nanofibers (Figure 19 (a), (c), (e)) but would cover only a portion of a single microfiber of CMF (Figure 19 (b), (d), (f)). Since the bacteria adhere to the features of the electrode it is important that the space between the features of each electrode be within a distance that bacteria can effectively collaborate. This distance, while not established quantitatively, has been shown to influence biofilm formation in medical studies.[122] That same influence is mimicked here as the tighter spacing/morphology of the CNF electrode spurs on better biofilm formation.

Ultimately, the CNF electrode generated more current (Figure 16), exhibited a voltammogram that showed the current was being generated by a biofilm (Figure 17), and showed substantial coverage by bacteria when examined under a SEM after the experiment (Figure 17). Since the electrodes were exposed in the same reactor at the same time, differences in current production are best explained by differences in the nature of the electrode materials.

The advantage typically associated with CNF is the increased surface area[146] , better kinetics [147], and high conductivity [148]. In this case however, the advantage of using CNF electrodes was its electrode surface morphology that was more amenable to bacterial colonization and biofilm formation. This supports the novel idea that adjusting the size of the electrode constituent material to one that is more amenable for bacterial colonization and growth was important because it produced a more substantial biofilm-anode and led to an increased current production.

6.6 CONCLUSION

In this experiment, *S. oneidensis* MR-1 produced significantly more current with CNF than CMF. The examination of sterile electrodes showed that CNF and CMF differed in morphology, surface area, size of the constituent material, and conductivity. After accounting for differences in surface area, size of the constituent material, and electrode conductivity the results suggests surprisingly that the morphology (i.e. tighter spacing/size of the features) of the electrode surface of CNF is what enables the formation of electricity producing biofilms by *S. oneidensis* MR-1 relative to CMF. It may be that CNF morphology provides a preferential surface for colonization or a more habitable environment for biofilm growth yet these are subjects for future biofilm studies. In either case, changing the electrode morphology seems to play an important role in biofilm-electrode formation and current production for *Shewanella onedensis* MR-1.

7.0 THE EFFECTS OF CARBON ELECTRODE SURFACE MORPHOLOGY ON BIOFILM-ANODE PERFORMANCE (BY *GEOBACTER SULFURREDUCENS*) USING PLATELETS AS A CONSTITUENT MATERIAL (GRAPHENE-NANOPLATELETS)

In order to further validate the claim that electrode surface morphology plays a significant role in the performance of a biofilm-anode I chose to test the hypothesis using a different carbon-based constituent material for the electrode. I chose a plate-based nanomaterial (graphene-nanoplatelets) as the constituent for the electrode and decided to use *Geobacter sulfurreducens* as the innoculant. *Geobacter sulfurreducens* was chosen because it typically produces a substantial amount of current and its bio-electrochemical physiology has been well studied. The use of a different electrode constituent material would afford us a completely different morphology type and the higher performing bacterial strain would serve to magnify differences in biofilm-anode current production. Additionally the materials used in this experiment were sourced from the same manufacturer and fabricated in the same way thus eliminating the need to address differences in material chemistry.

7.1 SUMMARY

The use of nano-materials, like graphene, as electrodes is an important development in bioelectrochemical research. Given an electrode material, anode-respiring bacteria will typically optimize their metabolism and biofilm structure and produce current. However, different electrodes produce different optimized biofilms and not all optimized biofilms are equal in mass and current production. Determining how electrodes affect biofilm-electrode current production is crucial for technology development, especially for new materials like graphene. Graphene-nanoplatelet-based electrodes provide an opportunity to determine whether increases in current density from graphene type materials are a result of its heightened reactivity, increased surface area, or if general parameters such as surface morphology play a significant role. More importantly graphene-nanoplatets allow us to examine the effect of the morphology on biofilm-electrode performance from a plate-based electrode constituent material.

Here I examine the effect of electrode morphology (i.e. altering the size of graphene-nanoplatelets) on biofilm-electrode current production in a microbial fuel cell inoculated with *Geobacter sulfurreducens*. Using current production profiles, cyclic voltammetry, electrochemical impedance spectroscopy, the Nernst-Monod conduction model and the current understanding of bioelectrochemical physiology of *Geobacter sulfurreducens* I am able to determine that surface morphology, more than surface area, plays a fundamental role in current production by biofilm-electrodes that use graphene nanoplatelets.

7.2 INTRODUCTION

Since increases in performance (i.e. current production) can be attributed to an increase in surface area, electrode reactivity, electrode surface morphology, or the bacterial physiology, isolating what significantly affects current production from biofilm-electrodes, especially when using highly productive strains such as *Geobacter sulfurreducens*, remains a complex challenge and an important aspect of bioelectrochemical research.

Multiple studies have demonstrated that the modification of electrodes can improve performance (i.e. current production or acetate synthesis) of biofilm-electrodes.[47, 109, 111, 149] The use of conductive polymers [53], porphyrins [54-55], metal catalysts[48, 52, 56], and different carbon based electrodes[109, 150-151] have all shown increased current densities in their respective systems. Even for electrodes based on the same material there have been differences in biofilm-electrode current production.[124]

Many of these studies have attributed increased current density to an enhanced electrochemical activity (e.g. reduction in the activation energy barrier) [52, 152-154] or an increase in surface area[113]. As a result, there has been a particular focus on employing nano-materials such as carbon nanotubes [117, 155], nanostructured polymers[156], and nanoparticles[2, 152] in order to take advantage of their enhanced electrical, physical, and chemical properties that would increase

both surface area and reactivity. One material presently being studied for use in bio-electrochemical systems is graphene.[151]

The promise of graphene, introduced as an engineering material in 2004[157], is a primary focus for nano-materials because of its superior physical and electrical properties. Its heightened electrical conductivity, mechanical strength, and chemical reactivity have a host of research groups studying different applications.[158] Graphene is a single atom-thick layer of carbon which makes it very versatile for engineering applications. Coupled with the fact that it is a carbon-based material of which there is an abundant supply, this material could potentially enhance current production from biofilm-electrodes cost effectively.

Biofilms grown on graphene-based electrodes could potentially take advantage of its high conductivity and reactivity[159] to decrease both the ohmic and electron transfer resistances.[160-161] Graphene has already been used to develop sensors[162] and increase biofilm conductivity.[163] It has been incorporated into bio-cathodes [163], used as an anode sponge[151], generated by the reduction of graphene oxide by *Shewanella*[164], and used as a biosensor.[162]

The major issue with understanding graphene's effect on biofilm-electrode performance is that it is difficult to distinguish between the contributions from its reactivity, increased surface area and surface morphology. The challenge of isolating the influence of each of the electrode's properties in a complex bio-electrochemical system is compounded by the fact that the bio-electrochemical physiology for most bacterial strains continues to be understood[165] and that it changes with environmental conditions.[166] Despite the findings in the literature, the variations

between experiments (e.g. catalyst and electrode materials, fuel cell setup, bacterial strain, operational conditions) make it difficult to determine what is fundamentally happening between the bacteria and electrode.

In order to better understand the benefits of incorporating nano-materials such as graphene into biofilm-electrodes, it is important to determine whether graphene enhances biofilm-electrode current production via its heightened reactivity, increased surface area or surface morphology. One can tease out these different effects by combining electrode fabrication methods that allow the alteration of the constituent material size and a bacterial strain, whose physiology is well-documented,[165-167] in a MFC experiment. Using graphene nano-platelets which can be manipulated to control for platelet size, bulk resistivity, surface area, and pressed into a paper electrode presents one such option.

Studies on the bio-electrochemical physiology of *Geobacter sulfurreducens* provide important insights such as the fact that biofilm expansion and not increased colonization is the primary contributor for increased current generation during the initial stages of biofilm-electrode development. Additionally, it was shown that following initial attachment, growth rates on electrodes are similar to those of planktonic cells respiring Fe (III)-citrate thus precluding that the electrode is deficient as an electron acceptor.[166] Another finding suggests that electron transfer between cells and the electrode is not the limiting step in the electron transfer process because the diffusional limitation seen in the electron transfer analysis is indicative of the transfer of electrons to the biofilm-electrode interface being slower than the transfer across the interface.[166] These findings, along with the use of the aforementioned graphene-nanoplatelet

electrodes, can enable one to learn how graphene-nano platelets affect biofilm-anode current production in MFCs.

Here I evaluate the effect of graphene nano-platelets on MFC performance using *Geobacter sulfurreducens*. When simultaneously tested under the same conditions graphene nano-platelet electrodes that differ mainly in the size of the constituent platelets manifested differences in current production. Cyclic voltammetry (CV) was used to qualitatively monitor the evolution of the biofilm-anode while Electrochemcial Impedance Spectroscopy (EIS) was used to determine the solution and polarization resistance. From these results I found that the electrode with less surface area performs significantly better and are able to extrapolate that the surface morphology is responsible for the differences in performance.

7.3 MATERIALS AND METHODS

7.3.1 Electrodes

Graphene Nano-platelet electrodes were custom designed (see Table 3) and procured from XG Sciences (Lansing MI, USA). The nano-platelets were incorporated into a cellulose based scaffold to form a paper-like sheet. GNP-50μm was made using H-50 particles and GNP-1μm was made using C-300 grade particles. Both were manufactured to have the same in-plane conductivity. GNP-50μm, GNP-1μm and the cellulose paper (control) were evaluated in the MFCs. The electrodes were cut to 1cm^2 squares and used as MFC anodes. MFC cathodes were

made of 1 cm^2 graphite felt (GC-14, Electrolitica) squares. Platinum wires connected the electrodes to a Keithley meter.

7.3.2 Culture and Media

NBAF medium

Geobacter sulfurreducens (ATCC: PCA 51573) was initially grown in anoxic NB medium[168] supplemented with 15mM acetate and 40mM fumarate.

FWFA (200ml bottles)

A solution containing (per liter) 2.5g sodium bicarbonate ($NaHCO_3$), 0.25g ammonium chloride (NH_4Cl), 0.06g sodium phosphate monobasic/monohydrate (NaHPO4 x H_2O), 0.1g potassium chloride (KCl), 10mL vitamin mix (45-46), 10mL mineral mix(44), 40mL of 1 M fumerate solution ($C_4H_4O_4$), 1.36 sodium acetate tri-hydrate (CHCOONa x $3H_2O$).

FWA (200ml bottles)

A solution containing (per liter) 2.5g sodium bicarbonate ($NaHCO_3$), 0.25g ammonium chloride (NH_4Cl), 0.06g sodium phosphate monobasic/monohydrate ($NaHPO_4$ x H_2O), 0.1g potassium chloride (KCl), 10mL vitamin mix (45-46), 10mL mineral mix (44), 1.36 sodium acetate tri-hydrate (CHCOONa x $3H_2O$).

Geobacter sulfurreducens was grown in NBAF medium and then transferred into FWFA (10% innoculum) when inoculating the MFCs. After current generation FWA was flowed

through the reactor. All solutions were autoclaved and all solutions used as a growth medium were sparged with 80:20 mix of N_2:CO_2 gas to maintain anaerobic conditions.

7.3.3 Microbial Fuel Cell Assembly and Operation

The MFCs, with 10ml volumes for both the anode and cathode chambers, were gas sterilized for 12 hrs using ethylene and assembled in a sterile container. Anode and cathodes were placed into the MFCs and a proton exchange membrane (Nafion 117, 1.25" x 1.25") was inserted between them. A Ag/AgCl reference electrode was inserted into the anode chamber for electrochemical measurements and a 560 ohm resistor served as the electrical load between the half-cells. The reactors were connected to a personal computer via a Keithley meter which collected voltage data every hour.

The growth media (described above) and catholyte were recycled through the reactors using a peristaltic pump (Cole Parmer) at a rate of 0.5ml/min. After the potential stabilized, the anode bottles were inoculated with 20ml of PCA 51573 from lab stock culture. When the OD_{600} (Optical Density at 600nm) reached 0.2 (exponential growth phase) FWFA media was replaced with FWA media and was pumped through (no recycle) the anode chamber at a reduced rate of 0.1ml/min. The catholyte was composed of a solution containing (per liter) 3.63g Trizma Base (T6066), 0.25g ammonium chloride (NH_4Cl), 0.06g sodium phosphate monobasic/monohydrate ($NaHPO_4$ x H_2O), 0.1g potassium chloride (KCl), and 10mL of 1 M potassium ferricyanide ($C_6N_6FeK_3$).

7.3.4 Electrochemical Measurements

Electrochemical impedance spectroscopy was used to describe the internal resistance experienced by each anode. Measurements were taken before inoculation and after current had reached a maximum. A Solartron Analytical 1252A Frequency Response Analyzer and Solartron SI 1287 Electrochemical Interface was used to conduct the tests. The working reference and working electrode leads were shorted and connected to the anode. The reference electrode lead was connected to the Ag/AgCl electrode placed in the anode chamber and the counter electrode lead was connected to the cathode. The excitation signal had an amplitude of 10mV with an initial frequency of 300kHz and a final frequency of 0.1Hz. The electrodes were also evaluated before and after inoculation using cyclic voltammetry. CV scans were conducted from -0.8V to 0.3V at a scan rate of 10mV/s.

7.3.5 SEM Images

Images of sterile graphene nano-platelet electrodes were taken using a JSM-6510LV SEM set at 20kV. Magnifications of x45, x 330, and x5000 were captured and used for visual comparison.

7.4 RESULTS AND DISCUSSION

7.4.1 Electrode characterizations

The electrodes were manufactured by pressing graphene-nanoplatelets into a cellulose scaffold. The in-plane conductivities were designed to be the same so that the main differences between the electrodes would be the sizes of the constituent material and the total surface area. These are confirmed by the results in Table 3. From a bio-electrochemical perspective, the differences that are important for current production from a biofilm-electrode which should be accounted for are the differences in reactivity, surface area and surface morphology. Since both electrodes are made from graphene-nanoplatelets, any increase in reactivity would be due to an increase in surface area or the number of reactive sites and not due to a change in the chemistry of the reaction. As a result the important parameters to be considered further in this study are narrowed down to the surface area and surface morphology.

Table 3. Electrode Properties for Graphene-Nanoplatelet electrodes.

Property	GNP-1μm	GNP-50μm
Nano-platelet thickness (nm)	~2	11-15
Particle Size distribution with Avg. Diameter (μm)	1-2 (based on <um particles)	~50
Electrical Conductivity-Parallel to Surface (S/m)	2.2×10^5	2.2×10^5
Electrical Conductivity through plane (S/m)	2.8	33
Surface Area (m2/g)	300	50
Bonding	sp^2	sp^2

7.4.2 Current Density

Current production, as seen in Figure 21 started within 24 hours after inoculation. Current rose exponentially over the next few days for both electrodes. After a week of operation GNP-50μm and GNP-1μm were steadily generating 0.8 mA/cm^2 and 0.5 mA/cm^2 respectively. The reactors were inoculated at the same time using the same method and the same strain suggesting that the differences in current production are due to the differences in the electrode materials. It is important to note that while GNP-1μm boasted the highest electrode surface area it does not generate the most current. Also important is the fact that GNP-1μm reached 300 $\mu A/cm^2$ first, a point after which it has been shown that cell-doubling, and not further electrode colonization, is responsible for additional increases in current production.[166]

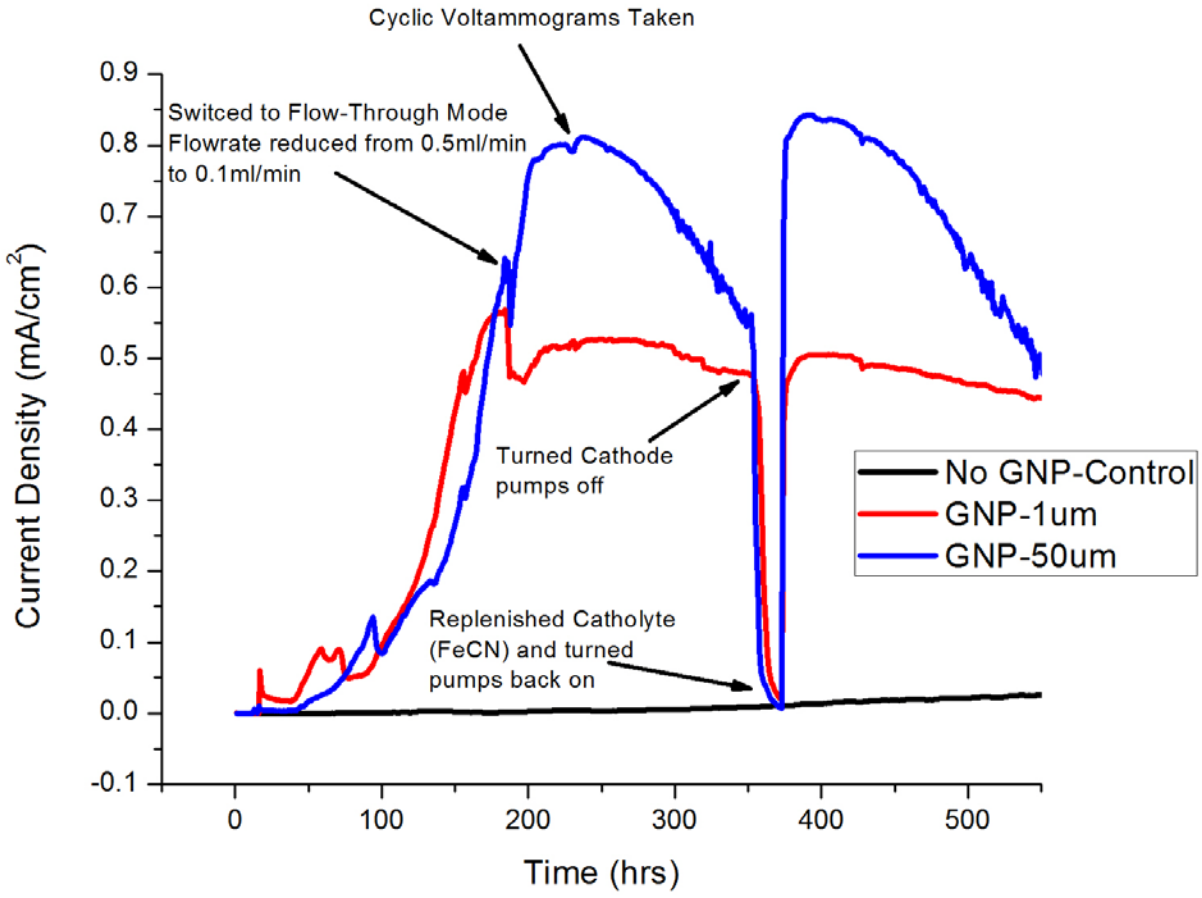

Figure 21. Current Density from MFCs inoculated with *Geobacter sulfurreducens*. GNP-50µm(blue) and GNP-1µm (red) were tested for a duration of three weeks with FeCN as the catholyte. Maximum current densities are 0.8mA/cm^2 and 0.5mA/cm^2 for GNP-50µm and GNP-1µm respectively.

The MFCs were run for a total of three weeks. GNP-50μm outperforms GNP-1μm through the entirety of the experiment, almost doubling the current production from GNP-1μm. At ~180th hr the MFCs were put into flow through mode. The flowrate was reduced from 0.5ml/min to 0.1ml/min at which point the current production for GNP-1μm leveled off while current production continued to increase exponentially for GNP-50μm. The reactors were being fed from the same bottle so differences in media or flow conditions could not explain the disparity in performance.

It was assumed that the limit to maintaining the highest level of current production would be the depleting concentration of FeCN in the catholyte. At the ~350th hr the pumps feeding the catholyte were turned off. The catholyte solution was then replenished and the pumps reactivated. Immediately, current production recovered for both MFCs. The current density in the second half of the experiment followed the same discharge profile as the first half thus confirming that GNP-50μm significantly outperforms GNP-1μm. There are two other important things to note, 1) replenishing the catholyte enabled GNP-50μm to return to peak current production, demonstrating that the catholyte was the limiting factor for current production for GNP-50μm and 2) the current production for GNP-1μm remained constant even after replacing the catholyte. This demonstrates that the limiting reaction for GNP-1μm was the current production from the biofilm-anode.

7.4.3 Cyclic Voltammetry

The results from all CV measurements are shown in Figure 22. Figure 22A and B show the CVs before inoculation and during peak current production (~230th hr) for GNP-50μm and GNP-1μm respectively. The initial CVs were taken when no bacteria were present in the system so the higher charging current (i.e. capacitance) shown by GNP-50μm is due to the electrostatic interaction with the solution and not with any interactions of the biofilm-electrode interface. Since electrostatic interactions did not inhibit biofilm colonization for either electrode, as noted by the early onset of current production for both electrodes, the shifts in CVs can be used to examine the expansion of the biofilm on the electrode.

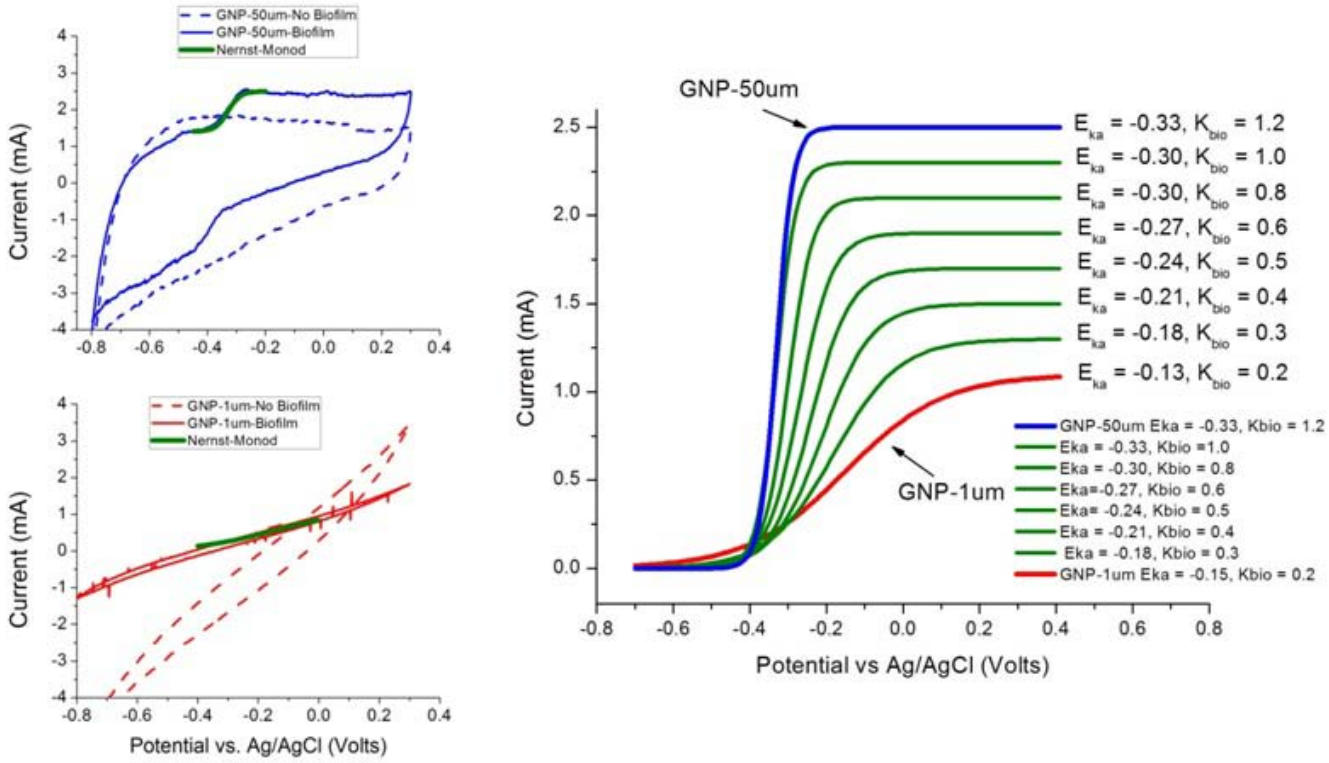

Figure 22. Cyclic Voltammograms from MFCs inoculated with *Geobacter sulfurreducens*. CVs taken before inoculation and at peak current production are shown for (A) GNP-50µm and (B) GNP-1µm with graphical fit of Nernst-Monod model shown in green. Inset (C) compares the Nernst-Monod fits from both (A) and (B) and describes the biofilm electrode evolution in terms of half-saturation potential Eka (volts) and biofilm conductivity kbio (mS/cm).

As a biofilm expands on the anode, current production will increase because of an increase in the number of respiring bacteria. The growth of bacteria increases the concentration of redox proteins that functionalize the anode and moves the electrode's open circuit potential closer to the mid-point potential of the redox proteins (e.g. outer membrane cytochromes) being employed by the bacteria. This is illustrated by the fact that the open-circuit potential for both GNP-1μm and GNP-50μm shifted from positive potentials to about -400mV vs Ag/AgCl at peak current production.

The development of the biofilm-anode also creates an upward shift in the CV relative to the initial CV and ultimately, for a fully developed biofilm-anode, turns into a sigmoidal curve following the Nernst-Monod model.[33] This sigmoidal curve is indicative of a biofilm-anode that is limited or governed by the bacterial metabolism.[126] For *Geobacter sulfurreducens* this limitation is thought to be a diffusion limitation of electrons to the terminal redox centers.[166]

The CVs for both electrodes shift to the left during peak current production. The shifts demonstrate the reduction in the electron transfer resistance and which is expected as a biofilm expands on the anode.[169-170] The decrease in electron transfer resistance is due to the fact that the number of protein conformational changes decreases with the amount of adsorbed proteins.[171] The reason is that as the biofilm grows and the concentration of proteins increases, the proteins are less likely to denature because of the spatial and electrostatic confinement provided by surrounding proteins and are thus more likely to be conjugated to the electrode surface. As a result, as the concentration of proteins attached to the electrode increases both the open circuit potential and mid-point potential shifts to more negative values (i.e. to the left in the CV). The

shift to the left and the sigmoidal curve are more pronounced in Figure 22A for GNP-50μm indicating the presence of a more developed biofilm and thus explaining the higher current production.

Each CV during peak current production was graphically fitted with the Nernst-Monod conduction-based model[126] and the values of the half-saturation potential (E_{ka}) and biofilm conductivity (k_{bio}) were extracted. In Figure 22C both of the modeled CVs are compared. In addition, the E_{ka} and k_{bio} values were used to linearly interpolate the electrochemical evolution of the biofilm-anode from the lower performing GNP-1μm to the higher performing GNP-50μm. This was done since the anodes were not poised at a specific potential. The values are given in the figure and demonstrate the expected gradual changes for E_{ka} and k_{bio} as a biofilm-anode develops from the state of GNP-1μm to the state of GNP-50μm. Essentially, as the biofilm-anode grows the E_{ka} decreases from -0.13V to -0.33V and k_{bio} increases from 0.2 to 1.2 mS/cm. These changes are expected as a biofilm grows and as proteins (i.e. c-type cytochromes) accumulate at the bacterial outer membrane [167] or in the biofilm matrix.[172] The differences in E_{ka} and k_{bio} values help qualify and explain the large differences in current production between GNP-50μm and GNP-1μm and thus confirming the notion that GNP-50μm has a more complete biofilm-anode.

7.4.4 Electrochemical Impedance Spectroscopy (EIS)

EIS was used to measure the distribution of resistances in the MFC before inoculation. The resulting spectra are shown in Figure 23. Using the simplified Randles cell as an equivalent circuit model (Figure 23 inset) the solution resistance for the MFCs for both GNP-1μm and

GNP-50μm are ~10ohms. The polarization resistances which can be extracted from the y-intercept of the model spectra show that the resistance for GNP-50μm (~10 ohms) is slightly smaller than the polarization resistance for GNP-1μm (~50 ohms). These differences can be attributed to differences in through plane conductivity (~33S/m for GNP-50μm and ~2.8 S/m for GNP-1μm) and are negligible for several reasons: 1) GNP-1μm was the first electrode to produce a substantial amount of current (80μA/cm^2 at 50th hr in Figure 21.) so the increased polarization resistance did not inhibit colonization or electron transfer from *Geobacter sulfurreducens* and 2) the differences in polarization resistance could not account for the disparity in peak current production

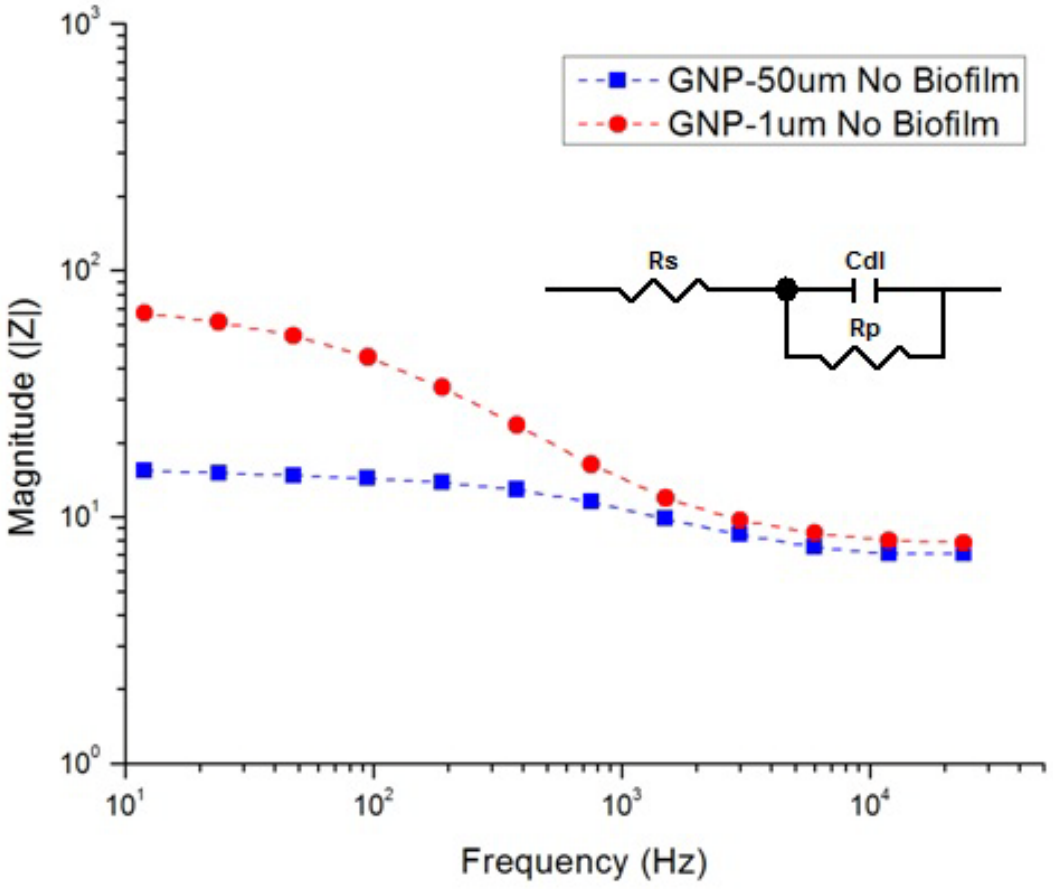

Figure 23. Electrochemical Impedance Spectra of the anode before inoculation. Spectra was generated using an excitation signal amplitude of 10mV with an initial frequency of 300kHz and a final frequency of 0.1Hz. Figure inset is a depiction of the Randles circuit used to model the spectra where Rs = solution resistance, Cdl = doubly layer capacitance, and Rp = polarization resistance.

7.4.5 SEM Images

The SEM images in Figure 24 illustrate the differences in surface morphology for the graphene nano-platelet electrodes. The roughness created by the intersection of nano-platelets is disclosed at a different magnification for each electrode. A comparison of Figure 24A and C show that at the larger scales GNP-50μm has a rougher surface while the finer resolution of Figure 24B and D highlights the smaller particles, higher surface area and roughness of GNP-1μm. The difference in surface area (GNP-1μm ~ 300m^2/g) and GNP-50μm ~ 50 m^2/g) is best exemplified in Figure 24B and D. Figure 24E was inset to provide an overview of the composition of a nano-platelet electrode at a lower magnification.

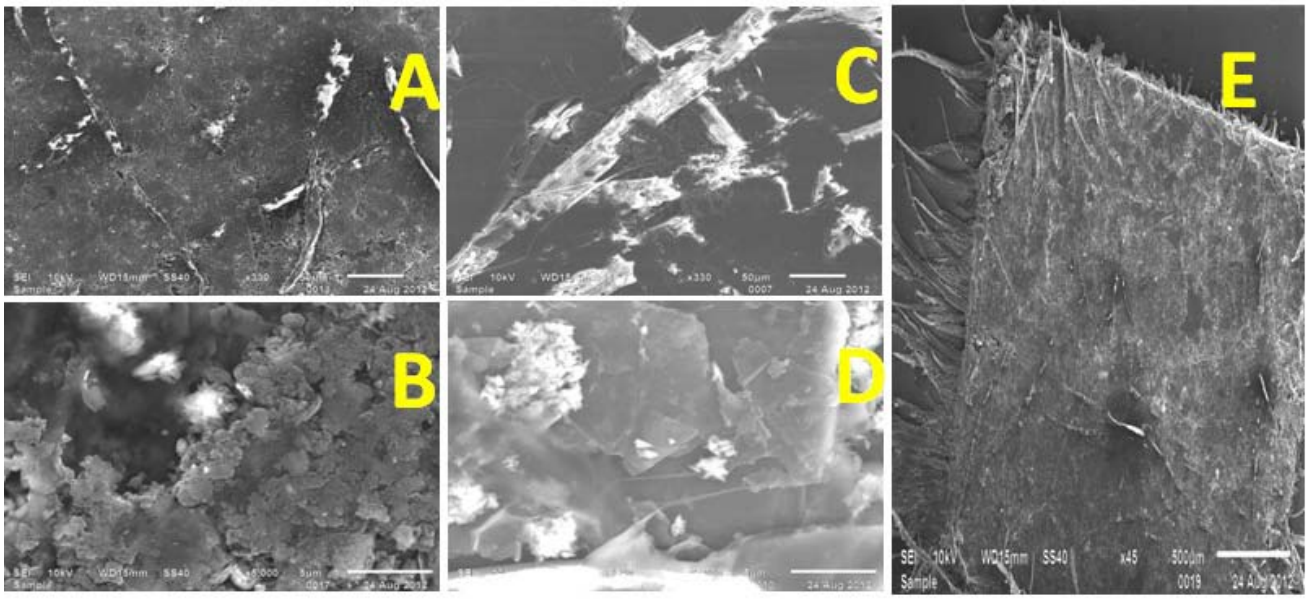

Figure 24. SEM Images of sterile graphene-nano-platelet electrodes used to demonstrate differences in surface morphology. (A) GNP-1µm (B) Magnified image of GNP-1µm (C) GNP-50µm (D) magnified image of GNP-50µm and (E) large scale image of the electrode material as a whole.

Ultimately, both electrodes were made from graphene-nanoplatelets and tested simultaneously under the same conditions leaving the explanation for the differences in current production to be justified by the differences in surface area or surface morphology. The current production profiles demonstrated that both electrodes had well developed biofilms. Although GNP-1μm had the highest surface area of graphene exposed it failed to produce the most current thus demonstrating that surface area was not the limiting factor for these electrodes. Additionally, after the catholyte was replaced, only GNP-50μm reached the peak current production of 0.8 mA/cm^2 during the three week experiment showing that while GNP-50μm was cathode limited GNP-1μm was limited by the biofilm-anode reaction.

The shifts in the CV and the graphical use of the Nernst-Monod model to quantify the differences in half-saturation potential (Eka) and the biofilm conductivity (kbio) confirm that GNP-50μm had the more complete biofilm-electrode. The EIS results showed similar polarization resistances but neither resistance inhibited colonization since the open-circuit potential for both electrodes at peak current production was ~ -400mV vs Ag/AgCl. The results illustrate that when electrodes are made of a highly reactive plate-shaped material (e.g. graphene-nanoplatelets) the electrode surface morphology plays a critical role in biofilm-electrode formation.

7.5 CONCLUSION

I presented an analysis of graphene-nanoplatelets electrodes that differed in the size of the constituent material, surface area, and surface morphology. Testing them simultaneously under the same MFC conditions I found that the electrode with much less surface area (GNP-50μm) exhibited a higher current production. Quantifying the solution and polar resistances of both electrodes with EIS and qualifying the development of the biofilm-electrode in terms of E_{ka} and k_{bio} (i.e. Nernst-Monod model) I demonstrate that the biofilm on the electrode with less surface area (GNP-50μm) has a more developed biofilm. After ruling out chemical reactivity and surface area as reasons for the improved performance I conclude that it is the surface morphology that plays a critical role in developing a biofilm-electrode for peak performance for graphene-nanoplatelet electrodes.

8.0 SUMMARY AND OUTLOOK

In summary, I have shown that incorporating platinum nanoparticles throughout both the anode and the cathode electrodes provides a more efficient use of the platinum catalyst, relative to surface deposition, for increasing MFC current density because it increases the catalyst surface area. Specifically, the incorporation of platinum nanoparticles increased the mass-specific current density for the anodic reaction and cathodic reactions by a factor of 1.5 and 4 respectively. The fact that increasing catalyst surface area is an effective method for increasing MFC current density is surprising given that hydrogen fuel cells produce current densities 2-3 orders of magnitude greater with similar Pt loadings. This is an important consideration for the field should one pursue MFC catalyst research. The novel nanofabrication methods used to incorporate platinum nanoparticles throughout the electrode are described in this thesis and can easily be used as the foundation for further studies with platinum catalysts and or as a framework for evaluating the efficient use of other potential catalysts in MFCs.

The influence of carbon-based electrodes on MFC performance was also evaluated by electrochemically characterizing the effect of different electrode constituent materials at the micro and nano scale (i.e. carbon fibers and graphene-nanoplatelets) using anode-respiring pure cultures whose physiologies were well-studied in bioelectrochemical systems. The electrode materials provided two different electrode architectures and their morphology was adjusted by

changing the size of the constituent material. Given the bacterial physiology of the pure cultures (*Shewanella oneidensis* MR-1 and *Geobacter sulfurreducens*), MFC results showed that the surface morphology of the electrodes plays a role in current production from biofilm-anodes. For *Shewanella oneidensis* MR-1 it was suggested that the tighter spacing of the electrode morphology enables both colonization and growth of an anode-respiring biofilm which increased current production. For *Geobacter sulfurreducens* the morphology offered by the larger diameter graphene-nanoplatelets enabled better biofilm growth after the initial colonization relative to the smaller diameter graphene-nanoplatelets. In both experiments, it was shown for the first time that the influence of a carbon-based electrode on MFC current production by *S.* oneidensis MR-1 and *Geobacter sulfurreducens* extends beyond the typical electrochemical parameters of electron transfer kinetics, electron conductivity, and surface area and uniquely includes surface morphology. These results expand the understanding of the significance of the abiotic electrode on MFC current production and provide the foundation for further study on biofilm formation and the optimization of carbon electrode designs to enhance MFC current production.

The study, development and manipulation of bioelectrochemical systems such as microbial fuel cells (MFCs) has enabled scientists and engineers to electrochemically "plug" into the bacterial metabolism to generate electricity from organic substrates (e.g. wastewater)[19], synthesize materials/fuels (e.g. microbial electrosynthesis of acetate)[173], monitor the remediation of radioactive waste (e.g. uranium)[174-175], and detect contaminants in the environment (e.g. arsenic)[176]. At the heart of these technologies is the biofilm-electrode in which a bacterial biofilm colonizes an electrode/current collector to form a composite material capable of executing the aforementioned processes in either a respiratory or oxidative role. Given that the biofilm-

electrode is the fundamental platform for these applications, it would be important to continue to develop the understanding of how nanofabrication methods and electrode materials increase MFC current production and manipulate the biofilm-electrode interface.

8.1 FUTURE WORK

Continuous development for MFCs and bioelectrochemical research will be both fundamental and applied. Future fundamental work built upon the experiments with platinum should focus on understanding the chemical interaction between the bacterial electron transport mechanism and the catalyst. Understanding the chemical interaction will help in minimizing the size of the catalyst nanoparticles for current production thus increasing the efficient use of catalysts even further. Applied research can focus on using the nanofabrication methods presented above as a framework for testing new materials and increasing the efficient use of more inexpensive alternatives.

Future work with carbon materials should continue exploring the connection between biofilm-electrode formation and electrode surface morphology. It would be important to first correlate the size of the constituent material to both biomass on the electrode and current density. After the most effective size for increasing current density is selected and the amount of biomass consistently produced by this material has been determined, it would be important to understand the effect of the spacing between the constituent materials and the ratio of constituent interconnections to geometric surface area on the three-dimensional morphology of the biofilm and on total biomass. The size of the constituent material, the spacing between the materials and

the ratio of constituent interconnections are suggested because they may be able to adequately describe the electrode surface morphology in a quantitative form. Moreover, these metrics could eventually be the design parameters used in optimizing carbon electrode surface morphologies for biofilm-electrode applications.

From a fundamental perspective, using transcriptomics to see the composition and concentration of proteins being expressed during biofilm formation of pure cultures would be important. These studies may be able to isolate which proteins signal for and initiate biofilm colonization during anode respiration. Subsequently understanding the structure and functions of these proteins could then allow for a study that examines how these proteins are inhibited or assisted by the electrostatic and hydrophobic nature of carbon electrode surfaces. These studies could provide a deeper insight into the rate of colonization and the rate of biofilm growth on carbon-based electrodes.

APPENDIX A

ELECTRODE DESIGN, FABRICATION AND CHARACTERIZATION

A.1 ELECTRODE FABRICATION

The design and fabrication of the platinum carbon electrodes took place in the Nanoelectronics Device Laboratory (NEDL) and in collaboration with University of Texas-Dallas NanoInstitute (UTD) and Sungkyunkwan Advanced Institute of Nanotechnology at Sungkyunkwan University in Suwon, South Korea (SKK). The designs of the electrodes vary mainly in catalyst concentration and architecture of the carbon substratum. Electrodes were fabricated using the following methods:

Electron beam evaporation of platinum onto carbon paper from Toray Industries (NEDL)

Using commercially available carbon paper (TGPH-120,E-Tek, USA) and an electron-beam evaporator (VE-180, Thermionics laboratory inc, USA) a uniform Pt film was deposited with a thickness in the range of 1000Å to 250Å following a manual procedure provided by the manufacturer. (www.thermionics.com).

Fabrication of carbon nanotubes in a sheet via co-deposition with SWNT (UTD)

Single- wall carbon nanotubes (SWNT) made by the high pressure carbon monoxide (HiPco) was be sourced from Unidym Inc. (Sunnyvale, CA). 15 mg of SWNT was be placed in aqueous surfactant solution and subjected to probe sonication (Fisher Scientific Model 500) for about 25 minutes in 5 min cycles. The surfactants used were Triton-X 100 or Pluronic X (Aldrich) and in concentrations of approximately 0.1g per 50mL of water. An ice batch was used or the bathwater was changed after each cycle to avoid overheating.

The solution was then diluted with one liter of water and decanted. A vacuum filter apparatus with a 47mm diameter filter (Millipore, 10-micron MITEX PTFE membrane filters) was used to filter the solution. A 1000 mL of water was passed through the filter until all foam disappeared followed by a second 1000 ml solution of 30% methanol. The methanol solutions were dilute to prevent a methanol oxygen reaction using nPt as the catalyst. The vacuum filtration apparatus was disassembled, and another 10-micron MITEX PTFE membrane filter was placed on top of the carbon nanotube sheet to form a “sandwich”. The vacuum apparatus was reassembled and the vacuum continually applied for one hour to maintain a flat and uncurled sheet. It is important to note that the size and shape of the SWNT sheet prepared in this way is limited only by the size and shape of the membrane filter used. It is also important to note that Multi-walled nanotube sheets can be fabricated in the same way.

Carbon nanofiber mat synthesis (SKKU)

Pyromellitic dianhydride (PMDA, Sigma Aldrich) and oxydianiline (ODA) was dried in a vacuum oven at room temperature. 4g of ODA was dissolved into 21g of DMF solution (99.8%) and stored at 5°C. 4.4g of PMDA was added to the mixture and stirred using a magnetic stir bar for 30 minutes. 1 wt% of tri-ethly amine (TEA) was added to the sample to form PAA and was stored at -5°C to maintain the solution properties. The synthesized PAA/catalyst solution was electrospun into a nanofiber onto a cylinder covered with aluminum foil and placed 15cm from the depositing syringe (2cm x 10cm). The PAA nanofiber mat was then converted in polyimide (PI) using a process previously described in the literature. The PI nanofiber mat was fired and pressed between two plates of alumina under a 3-sccm argon gas flow at 1000°C and maintained for 1 hour. This method describes the process of self-fabricating carbon nanofiber sheets however, there are also viable commercial products that can be used in its place.

A.2 ELECTRODE CHARACTERIZATION

Table A1. Electrode Characterization techniques

	Technique	Objective	Equipment Description
1	SEM	*Evaluate catalyst coverage, electrode morphology, and biofilm coverage*	*LEO 1530VP Field emission microscope*
2	AFM	*Confirm the thickness of Pt*	*PSIA Advanced Scanning Probe XE-100*
3	TEM	*Examine the distribution of platinum*	*JEOL 2100F TEM/STEM*
5	Conductivity	*Quantify the change in conductivity*	*Signatone 1160 Series) with Signatone probes (Model S-926) and a semiconductor device analyzer (Agilent Tech B1500A)*
6	Amp-I-t	*Compare current density of each electrode*	*CH Instruments 1040A multi- channel Potentiostat*
7	CV	*Compare surface area, electron transfer kinetics, and rate respiration on each electrode relative to potential*	*CH Instruments 1040A multi- channel potentiostat*

Notes:

SEM = scanning electron microscopy

AFM = atomic force microscopy

TEM = transmission electron microscopy

Amp-It = Amperometric- (I-t curves)

CV = cyclic voltammetry

These types of characterizations are analogous to those used in determining catalytic effects of materials and composites. The SEM, AFM, and TEM microscopes are available in the NanoFabrication and Characterization (NFCF) facility at the University of Pittsburgh. Additionally, the conductivity of the electrode using a 4-point probe method

SEM

SEM was used to provide a micro-level profile of the electrode and a visual inspection of the surface area. While surface area analysis permits one to calculate the total surface area of the electrode the SEM will reveal how much of it as actually available to the bacteria. In addition, inspection of the biofilm-anodes after cultivation in the MFC lets us inspect the network of bacteria assembled on the electrode. These networks are a part of the biofilm matrix which is essential to operating efficient, high energy producing MFCs. Upon dismantling the MFCs, electrode samples ($<1cm^2$) were cut and the biofilm was fixed using a paraformaldehyde solution and rinsed with phosphate buffer (0.1M). Electrodes were allowed to dessicate and were then imaged.

AFM

AFM was used to determine the thickness of the catalyst layer. AFM may also be used to probe connections within the biofilm and potentially between the bacteria and electrode. Electrodes can be sampled before and after MFC operations. Electrodes were cut to ~1mm2 , dried and imaged. Images of dummy wafers were used to monitor the catalyst thickness and the biofilm-anodes can be prepared similar to SEM samples.

TEM

TEM enabled us to determine size, distribution and adhesion of the catalyst at the nanoscale. Samples were ground into powders, suspended in ethanol, sonicated, dropped onto a TEM grid and then imaged. Cross-sectional images help determine the thickness and adhesion of the catalyst on the electrode and plan view images were used to determine the alignment of the lattice structures for both catalyst and electrode. Since platinum and carbon have different densities and packing orders, electron diffraction images are expected to be distinct. Carbon is expected to exhibit an amorphous ring and platinum will exhibit a polycrystalline structure. Combining Bright field and Dark field techniques allow one to separate structures that exhibit specific orientations. Bright field illustrates all structures and dark field illustrates only those that embody specific orientations.

Conductivity

Conductivity of 1cm x 1cm electrode samples were determined using a Probe station (Signatone 1160 Series) with Signatone probes (Model S-926) and a semiconductor device analyzer (Agilent Tech B1500A). Using the standard 4-probe technique we were able to preclude the contact resistance from the measurement allowing us a useful and accurate comparison.

A.3 ELECTRODE EVALUATION

Ultimately, the experimental setup (MEC, pure culture, single chamber) and evaluation techniques control for all relevant parameters that can affect biofilm-anode performance. Each electrode is adequately profiled and evaluated so as to account for any changes in performance be it electrochemical or physical. From these results we were able to correlate surface catalyst loading and physical electrode parameters to MEC performance. These correlations help in optimizing electrode designs using e-beam evaporation, provide an insight into the effect of composite electrodes on the biofilm-anode, and provide a framework for understanding novel materials and or depositions methods.

BIBLIOGRAPHY

1. Reinhardt, G., Energy Opportunities in Wastewater and Biosolids. *Water Environment Research Foundation* **2009**.

2. Sanchez, D. V. P.; Huynh, P.; Kozlov, M. E.; Baughman, R. H.; Vidic, R. D.; Yun, M., Carbon Nanotube/Platinum (Pt) Sheet as an Improved Cathode for Microbial Fuel Cells. *Energy & Fuels* **2010,** *24* (11), 5897-5902.

3. Potter, M. C., Electrical Effects Accompanying the Decomposition of Organic Compounds. *Proceedings of the Royal Society of London. Series B, Containing Papers of a Biological Character* **1911,** *84* (571), 260-276.

4. Cohen, B., The Bacterial Culture as an Electrical Half-Cell. *J. Bacteriol. Thirty-second Annual Meeting of the Society of American Bacteriologists* **1931,** *21* (1), 18-19.

5. Delduca, M. G., Friscoe, J. M. And Zurilla, R. W. , Developments in Industrial Microbiology *American Institute of Biological Sciences* **1963,** *4*, 81-84.

6. Karube, I.; Matsunaga, T.; Tsuru, S.; Suzuki, S., Continous hydrogen production by immobilized whole cells of Clostridium butyricum. *Biochimica et Biophysica Acta (BBA) - General Subjects* **1976,** *444* (2), 338-343.

7. Karube, I.; Matsunaga, T.; Tsuru, S.; Suzuki, S., Biochemical fuel cell utilizing immobilized cells of clostridium butyricum. *Biotechnology and Bioengineering* **1977,** *19* (11), 1727-1733.

8. Bennetto, H. P.; Stirling, J. L.; Tanaka, K.; Vega, C. A., Anodic reactions in microbial fuel cells. *Biotechnology and Bioengineering* **1983,** *25* (2), 559-568.

9. Thurston, C. F.; Bennetto, H. P.; Delaney, G. M.; Mason, J. R.; Roller, S. D.; Stirling, J. L., Glucose Metabolism in a Microbial Fuel Cell. Stoichiometry of Product Formation in a Thionine-mediated Proteus vulgaris Fuel Cell and its Relation to Coulombic Yields. *J Gen Microbiol* **1985,** *131* (6), 1393-1401.

10. Bennetto, H. P., Electricity Generation by Micro-organisms Biotechnology Education. *Biotechnology Education* **1990,** *1* (4), 163-168.

11. Allen, R.; Bennetto, H., Microbial fuel-cells. *Applied Biochemistry and Biotechnology* **1993,** *39-40* (1), 27-40.

12. Ramani, V., Fuel Cells. *The Electrochemical Society Interface* **2006**, 41.

13. Lovley, D. R., Microbial fuel cells: novel microbial physiologies and engineering approaches. *Current Opinion in Biotechnology* **2006,** *17* (3), 327-332.

14. Rabaey, K.; Verstraete, W., Microbial fuel cells: novel biotechnology for energy generation. *Trends in Biotechnology* **2005,** *23* (6), 291-298.

15. Development of a Microbial Fuel Cell for Sustainable Wastewater Treatment (No. U1R06). *Water Environment Research Foundation* **2010,** *U1R06*.

16. Pham, T.; Rabaey, K.; Aelterman, P.; Clauwaert, P.; De Schamphelaire, L.; Boon, N.; Verstraete, W., Microbial Fuel Cells in Relation to Conventional Anaerobic Digestion Technology. *Engineering in Life Sciences* **2006,** *6* (3), 285-292.

17. Van Lier, J. B., High-rate anaerobic wastewater treatment: diversifying from end-of-the-pipe treatement to resource-oriented conversion techniques. *Water Science and Technology* **2008,** *57*, 1137-1148.

18. Logan, B., Scaling up microbial fuel cells and other bioelectrochemical systems. *Applied Microbiology and Biotechnology* **2010,** *85* (6), 1665-1671.

19. Logan, B. E.; Hamelers, B.; Rozendal, R.; Schroder, U.; Keller, J.; Freguia, S.; Aelterman, P.; Verstraete, W.; Rabaey, K., Microbial fuel cells: Methodology and technology. *Environmental Science and Technology* **2006,** *40* (17), 5181-5192.

20. Bard, A. J.; Faulkner, L. R., *Electrochemical Methods : Fundamentals and Applications*. 2nd ed.; John Wiley & Sons Inc.: New York, NY, 2001.

21. Pant, D.; Van Bogaert, G.; Diels, L.; Vanbroekhoven, K., A review of the substrates used in microbial fuel cells (MFCs) for sustainable energy production. *Bioresource Technology* **2010,** *101* (6), 1533-1543.

22. Lee, H.-S.; Parameswaran, P.; Kato-Marcus, A.; Torres, C. I.; Rittmann, B. E., Evaluation of energy-conversion efficiencies in microbial fuel cells (MFCs) utilizing fermentable and non-fermentable substrates. *Water Research* **2008,** *42* (6-7), 1501-1510.

23. Parameswaran, P.; Torres, C. I.; Lee, H. S.; Krajmalnik-Brown, R.; Rittmann, B. E., Syntrophic interactions among anode respiring bacteria (ARB) and Non-ARB in a

biofilm anode: electron balances. *Biotechnology and Bioengineering* **2009,** *103* (3), 513-523.

24. Schroder, U., Anodic electron transfer mechanisms in microbial fuel cells and their energy efficiency. *Physical Chemistry Chemical Physics* **2007,** *9* (21), 2619-2629.

25. Torres, C. I.; Marcus, A. K.; Lee, H.-S.; Parameswaran, P.; Krajmalnik-Brown, R.; Rittmann, B. E., A kinetic perspective on extracellular electron transfer by anode-respiring bacteria. *FEMS Microbiology Reviews* **2010,** *34* (1), 3-17.

26. Lanthier, M.; Gregory, K. B.; Lovley, D. R., Growth with high planktonic biomass in Shewanella oneidensis fuel cells. *FEMS Microbiology Letters* **2008,** *278* (1), 29-35.

27. Marsili, E.; Baron, D. B.; Shikhare, I. D.; Coursolle, D.; Gralnick, J. A.; Bond, D. R., Shewanella secretes flavins that mediate extracellular electron transfer. *Proceedings of the National Academy of Sciences* **2008,** *105* (10), 3968-3973.

28. Rabaey, K.; Boon, N.; Höfte, M.; Verstraete, W., Microbial Phenazine Production Enhances Electron Transfer in Biofuel Cells. *Environmental Science & Technology* **2005,** *39* (9), 3401-3408.

29. Rabaey, K.; Boon, N.; Siciliano, S. D.; Verhaege, M.; Verstraete, W., Biofuel Cells Select for Microbial Consortia That Self-Mediate Electron Transfer. *Appl. Environ. Microbiol.* **2004,** *70* (9), 5373-5382.

30. Delaney, G. M.; Bennetto, H. P.; Mason, J. R.; Roller, S. D.; Stirling, J. L.; Thurston, C. F., Electron-transfer coupling in microbial fuel cells. 2. performance of fuel cells containing selected microorganism - mediator - substrate combinations. *Journal of chemical technology and biotechnology. Biotechnology* **1984,** *34* (1), 13-27.

31. Newman, D. K.; Kolter, R., A role for excreted quinones in extracellular electron transfer. *Nature* **2000,** *405* (6782), 94-97.

32. Pham, T.; Boon, N.; Aelterman, P.; Clauwaert, P.; De Schamphelaire, L.; Vanhaecke, L.; De Maeyer, K.; Höfte, M.; Verstraete, W.; Rabaey, K., Metabolites produced by <i>Pseudomonas</i> sp. enable a Gram-positive bacterium to achieve extracellular electron transfer. *Applied Microbiology and Biotechnology* **2008,** *77* (5), 1119-1129.

33. Marcus, A. K.; Torres, C. I.; Rittmann, B. E., Conduction-based modeling of the biofilm anode of a microbial fuel cell. *Biotechnology and Bioengineering* **2007,** *98* (6), 1171-1182.

34. El-Naggar, M. Y.; Gorby, Y. A.; Xia, W.; Nealson, K. H., The Molecular Density of States in Bacterial Nanowires. *Biophysical Journal* **2008,** *95* (1), L10-L12.

35. Gorby, Y. A.; Beveridge, T. J.; Wiley, W. R., *Composition, Reactivity, and Regulation of Extracellular Metal-Reducing Structures(Nanowires) Produced by Dissimilatory Metal Reducing Bacteria*. 2005; p Medium: ED.

36. Gorby, Y. A.; Yanina, S.; Mclean, J. S.; Rosso, K. M.; Moyles, D.; Dohnalkova, A.; Beveridge, T. J.; Chang, I. S.; Kim, B. H.; Kim, K. S.; Culley, D. E.; Reed, S. B.; Romine, M. F.; Saffarini, D. A.; Hill, E. A.; Shi, L.; Elias, D. A.; Kennedy, D. W.; Pinchuk, G.; Watanabe, K.; Ishii, S. I.; Logan, B.; Nealson, K. H.; Fredrickson, J. K., Electrically conductive bacterial nanowires produced by Shewanella oneidensis strain MR-1 and other microorganisms. *Proceedings of the National Academy of Sciences* **2006,** *103* (30), 11358-11363.

37. Leang, C.; Qian, X.; Mester, T.; Lovley, D. R., Alignment of the c-Type Cytochrome OmcS along Pili of Geobacter sulfurreducens. *Appl. Environ. Microbiol.* **2010,** *76* (12), 4080-4084.

38. Nakamura, R.; Kai, F.; Okamoto, A.; Newton, Greg j.; Hashimoto, K., Self-Constructed Electrically Conductive Bacterial Networks13. *Angewandte Chemie* **2009,** *121* (3), 516-519.

39. Ntarlagiannis, D.; Atekwana, E. A.; Hill, E. A.; Gorby, Y., Microbial nanowires: Is the subsurface â€œhardwiredâ€□? *Geophys. Res. Lett.* **2007,** *34*.

40. Reguera, G.; Mccarthy, K. D.; Mehta, T.; Nicoll, J. S.; Tuominen, M. T.; Lovley, D. R., Extracellular electron transfer via microbial nanowires. *Nature* **2005,** *435* (7045), 1098-1101.

41. Reguera, G.; Nevin, K. P.; Nicoll, J. S.; Covalla, S. F.; Woodard, T. L.; Lovley, D. R., Biofilm and nanowire production leads to increased current in Geobacter sulfurreducens fuel cells. *Applied and Environmental Microbiology* **2006,** *72* (11), 7345-7348.

42. Richter, H.; Nevin, K. P.; Jia, H.; Lowy, D. A.; Lovley, D. R.; Tender, L. M., Cyclic voltammetry of biofilms of wild type and mutant Geobacter sulfurreducens on fuel cell anodes indicates possible roles of OmcB, OmcZ, type IV pili, and protons in extracellular electron transfer. *Energy & Environmental Science* **2009,** *2* (5), 506-516.

43. Alwarappan, S.; Joshi, R. K.; Ram, M. K.; Kumar, A., Electron transfer mechanism of cytochrome c at graphene electrode. *Applied Physics Letters* **2010,** *96* (26), 263702-3.

44. Gerasimov, J. Y.; Lai, R. Y., An electrochemical peptide-based biosensing platform for HIV detection. *Chemical Communications* **2010,** *46* (3), 395-397.

45. Odenthal, K. J.; Gooding, J. J., An introduction to electrochemical DNAbiosensors. *Analyst* **2007,** *132* (7), 603-610.

46. Qiao, Y.; Bao, S.-J.; Li, C. M., Electrocatalysis in microbial fuel cells-from electrode material to direct electrochemistry. *Energy & Environmental Science* **2010,** *3* (5), 544-553.

47. Liu, Y.; Harnisch, F.; Fricke, K.; Schröder, U.; Climent, V.; Feliu, J. M., The study of electrochemically active microbial biofilms on different carbon-based anode materials in microbial fuel cells. *Biosensors and Bioelectronics* **2010,** *25* (9), 2167-2171.

48. Park, H. I.; Mushtaq, U.; Perello, D.; Lee, I.; Cho, S. K.; Star, A.; Yun, M., Effective and Low-Cost Platinum Electrodes for Microbial Fuel Cells Deposited by Electron Beam Evaporation. *Energy & Fuels* **2007,** *21* (5), 2984-2990.

49. Scott, K.; Rimbu, G. A.; Katuri, K. P.; Prasad, K. K.; Head, I. M., Application of Modified Carbon Anodes in Microbial Fuel Cells. *Process Safety and Environmental Protection* **2007,** *85* (5), 481-488.

50. Xuyen, N. T.; Sanchez, D. P. V.; Kim, T. H.; Park, H. I.; Yun, M.; Lee, Y. H., Diffusion-limited reduction of organometallic compound on carbon nanofiber mat for catalytic applications. *Journal of Materials Chemistry* **2010,** *20* (26), 5468-5473.

51. Harnisch, F.; Wirth, S.; Schröder, U., Effects of substrate and metabolite crossover on the cathodic oxygen reduction reaction in microbial fuel cells: Platinum vs. iron(II) phthalocyanine based electrodes. *Electrochemistry Communications* **2009,** *11* (11), 2253-2256.

52. Rosenbaum, M.; Zhao, F.; Quaas, M.; Wulff, H.; Schröder, U.; Scholz, F., Evaluation of catalytic properties of tungsten carbide for the anode of microbial fuel cells. *Applied Catalysis B: Environmental* **2007,** *74* (3-4), 261-269.

53. Niessen, J.; Schröder, U.; Rosenbaum, M.; Scholz, F., Fluorinated polyanilines as superior materials for electrocatalytic anodes in bacterial fuel cells. *Electrochemistry Communications* **2004,** *6* (6), 571-575.

54. Zhao, F.; Harnisch, F.; Schröder, U.; Scholz, F.; Bogdanoff, P.; Herrmann, I., Application of pyrolysed iron(II) phthalocyanine and CoTMPP based oxygen reduction catalysts as cathode materials in microbial fuel cells. *Electrochemistry Communications* **2005,** *7* (12), 1405-1410.

55. Cheng, S.; Liu, H.; Logan, B. E., Power Densities Using Different Cathode Catalysts (Pt and CoTMPP) and Polymer Binders (Nafion and PTFE) in Single Chamber Microbial Fuel Cells. *Environmental Science & Technology* **2005,** *40* (1), 364-369.

56. Park; Park, D.; Zeikus; Zeikus, J., Impact of electrode composition on electricity generation in a single-compartment fuel cell using Shewanella putrefaciens. *Applied Microbiology and Biotechnology* **2002,** *59* (1), 58-61.

57. Selembo, P. A.; Merrill, M. D.; Logan, B. E., The use of stainless steel and nickel alloys as low-cost cathodes in microbial electrolysis cells. *Journal of Power Sources* **2009,** *190* (2), 271-278.

58. Yuan, Y.; Kim, S., Polypyrrole-coated reticulated vitreous carbon as anode in microbial fuel cell for higher energy output. *Bulletin of the Korean Chemical Society* **2008,** *29* (1), 168-172.

59. Zou, Y.; Xiang, C.; Yang, L.; Sun, L.-X.; Xu, F.; Cao, Z., A mediatorless microbial fuel cell using polypyrrole coated carbon nanotubes composite as anode material. *International Journal of Hydrogen Energy* **2008,** *33* (18), 4856-4862.

60. Schröder, U.; Nießen, J.; Scholz, F., A Generation of Microbial Fuel Cells with Current Outputs Boosted by More Than One Order of Magnitude. *Angewandte Chemie International Edition* **2003,** *42* (25), 2880-2883.

61. Anderson, M. L.; Stroud, R. M.; Rolison, D. R., Enhancing the Activity of Fuel-cell Reactions by Designing Three-dimensional Nanostructured Architectures: Catalyst - modified Carbon−Silica Composite Aerogels. *Nano Letters* **2002,** *2* (3), 235-240.

62. Formo, E.; Lee, E.; Campbell, D.; Xia, Y., Functionalization of Electrospun TiO2 Nanofibers with Pt Nanoparticles and Nanowires for Catalytic Applications. *Nano Letters* **2008,** *8* (2), 668-672.

63. Hsin, Y. L.; Hwang, K. C.; Yeh, C.-T., Poly(vinylpyrrolidone)-Modified Graphite Carbon Nanofibers as Promising Supports for PtRu Catalysts in Direct Methanol Fuel Cells. *Journal of the American Chemical Society* **2007,** *129* (32), 9999-10010.

64. Liu, S.-H.; Yu, W.-Y.; Chen, C.-H.; Lo, A.-Y.; Hwang, B.-J.; Chien, S.-H.; Liu, S.-B., Fabrication and Characterization of Well-Dispersed and Highly Stable PtRu Nanoparticles on Carbon Mesoporous Material for Applications in Direct Methanol Fuel Cell. *Chemistry of Materials* **2008,** *20* (4), 1622-1628.

65. Lin, Y.; Cui, X.; Yen, C. H.; Wai, C. M., PtRu/Carbon Nanotube Nanocomposite Synthesized in Supercritical Fluid: A Novel Electrocatalyst for Direct Methanol Fuel Cells. *Langmuir* **2005,** *21* (24), 11474-11479.

66. Bensebaa, F.; Farah, A. A.; Wang, D.; Bock, C.; Du, X.; Kung, J.; Le Page, Y., Microwave Synthesis of Polymer-Embedded Pt−Ru Catalyst for Direct Methanol Fuel Cell. *The Journal of Physical Chemistry B* **2005,** *109* (32), 15339-15344.

67. Kim, S. J.; Park, Y. J.; Ra, E. J.; Kim, K. K.; An, K. H.; Lee, Y. H.; Choi, J. Y.; Park, C. H.; Doo, S. K.; Park, M. H.; Yang, C. W., Defect-induced loading of Pt nanoparticles on carbon nanotubes. *Applied Physics Letters* **2007,** *90* (2).

68. Yu, W.; Tu, W.; Liu, H., Synthesis of Nanoscale Platinum Colloids by Microwave Dielectric Heating. *Langmuir* **1998,** *15* (1), 6-9.

69. Li, D.; Mccann, J. T.; Gratt, M.; Xia, Y., Photocatalytic deposition of gold nanoparticles on electrospun nanofibers of titania. *Chemical Physics Letters* **2004,** *394* (4–6), 387-391.

70. Niesz, K.; Grass, M.; Somorjai, G. A., Precise Control of the Pt Nanoparticle Size by Seeded Growth Using EO13PO30EO13 Triblock Copolymers as Protective Agents. *Nano Letters* **2005,** *5* (11), 2238-2240.

71. Wen, Z.; Wang, Q.; Li, J., Template Synthesis of Aligned Carbon Nanotube Arrays using Glucose as a Carbon Source: Pt Decoration of Inner and Outer Nanotube Surfaces for Fuel-Cell Catalysts. *Advanced Functional Materials* **2008,** *18* (6), 959-964.

72. Di Noto, V.; Negro, E.; Gliubizzi, R.; Lavina, S.; Pace, G.; Gross, S.; Maccato, C., A Pt–Fe Carbon Nitride Nano-electrocatalyst for Polymer Electrolyte Membrane Fuel Cells and Direct-Methanol Fuel Cells: Synthesis, Characterization, and Electrochemical Studies. *Advanced Functional Materials* **2007,** *17* (17), 3626-3638.

73. Xuyen, N. T.; Ra, E. J.; Geng, H.-Z.; Kim, K. K.; An, K. H.; Lee, Y. H., Enhancement of Conductivity by Diameter Control of Polyimide-Based Electrospun Carbon Nanofibers. *The Journal of Physical Chemistry B* **2007,** *111* (39), 11350-11353.

74. Chang, I. S.; Jang, J. K.; Gil, G. C.; Kim, M.; Kim, H. J.; Cho, B. W.; Kim, B. H., Continuous determination of biochemical oxygen demand using microbial fuel cell type biosensor. *Biosensors and Bioelectronics* **2004,** *19* (6), 607-613.

75. A. Balows; H. G. Truper; M. Dworkin; Harder, W.; K. H. Schleifer, *The Acetogenic Bacteria. In:The Prokaryotes*. 2 ed.; Springer: New York, 1992.

76. Hoster, H.; Iwasita, T.; Baumgartner, H.; Vielstich, W., Pt-Ru model catalysts for anodic methanol oxidation: Influence of structure and composition on the reactivity. *Physical Chemistry Chemical Physics* **2001,** *3* (3), 337-346.

77. Suzuki, H.; Shintaku, M.; Sato, T.; Tamano, M.; Mastsuura, T.; Hori, M.; Kaito, C., Experimental Evidence of Stability of Pt Clusters on and in Carbon Particles. *Japanese Journal of Applied Physics* **2005,** *44* (19).

78. Xuyen, N. T.; Jeong, H. K.; Kim, G.; So, K. P.; An, K. H.; Lee, Y. H., Hydrolysis-induced immobilization of Pt(acac)2 on polyimide-based carbon nanofiber mat and formation of Pt nanoparticles. *Journal of Materials Chemistry* **2009,** *19* (9), 1283-1288.

79. Battiston, G. A.; Gerbasi, R.; Porchia, M.; Gasparotto, A., Metal Organic CVD of Nanostructured Composite TiO2-Pt Thin Films: A Kinetic Approach. *Chemical Vapor Deposition* **1999,** *5* (1), 13-20.

80. Fiddy, S. G.; Newton, M. A.; Campbell, T.; Dent, A. J.; Harvey, I.; Salvini, G.; Turin, S.; Evans, J., Particle development and characterisation in Pt(acac)2 and Pt(acac)2/GeBu4 derived catalysts supported upon porous and mesoporous SiO2: effect of reductive environment, and support structure. *Physical Chemistry Chemical Physics* **2002,** *4* (5), 827-834.

81. Utriainen, M.; Kröger-Laukkanen, M.; Johansson, L.-S.; Niinistö, L., Studies of metallic thin film growth in an atomic layer epitaxy reactor using M(acac)2 (M=Ni, Cu, Pt) precursors. *Applied Surface Science* **2000,** *157* (3), 151-158.

82. Somorjai, G. A.; Blakely, D. W., MECHANISM OF CATALYSIS OF HYDROCARBON REACTIONS BY PLATINUM SURFACES. *Nature* **1975,** *258* (5536), 580-583.

83. Somorjai, G. A.; Contreras, A. M.; Montano, M.; Rioux, R. M., Clusters, surfaces, and catalysis. *Proceedings of the National Academy of Sciences* **2006,** *103* (28), 10577-10583.

84. Zoski, C. G., *Handbook of Electrochemistry*. Elsevier: Amsterdam, The Netherlands, 2007.

85. Sheppard, S.-A.; A. Campbell, S.; R. Smith, J.; W. Lloyd, G.; C. Walsh, F.; R. Ralph, T., Electrochemical and microscopic characterisation of platinum-coated perfluorosulfonic acid (Nafion 117) materials[dagger]. *Analyst* **1998,** *123* (10), 1923-1929.

86. Ishikawa, Y.; Liao, M.-S.; Cabrera, C. R., Oxidation of methanol on platinum, ruthenium and mixed Pt–M metals (M=Ru, Sn): a theoretical study. *Surface Science* **2000,** *463* (1), 66-80.

87. Kua, J.; Goddard, W. A., Oxidation of Methanol on 2nd and 3rd Row Group VIII Transition Metals (Pt, Ir, Os, Pd, Rh, and Ru):Application to Direct Methanol Fuel Cells. *Journal of the American Chemical Society* **1999,** *121* (47), 10928-10941.

88. Vielstich, W.; Lamm, A.; Gasteiger, H. A., *Handbook of Fuel Cells: Fundamentals, Technology, Applications*. Wiley-VCH: England, 2003; Vol. 2, ch. 41, p 3826.

89. Zhao, Y.; Fan, L.; Zhong, H.; Li, Y.; Yang, S., Platinum Nanoparticle Clusters Immobilized on Multiwalled Carbon Nanotubes: Electrodeposition and Enhanced Electrocatalytic Activity for Methanol Oxidation. *Advanced Functional Materials* **2007,** *17* (9), 1537-1541.

90. Pham, T. H.; Aelterman, P.; Verstraete, W., Bioanode performance in bioelectrochemical systems: recent improvements and prospects. *Trends in Biotechnology* **2009,** *27* (3), 168-178.

91. Sharma, T.; Mohana Reddy, A. L.; Chandra, T. S.; Ramaprabhu, S., Development of carbon nanotubes and nanofluids based microbial fuel cell. *International Journal of Hydrogen Energy* **2008,** *33* (22), 6749-6754.

92. Ahn, Y.; Logan, B. E., Effectiveness of domestic wastewater treatment using microbial fuel cells at ambient and mesophilic temperatures. *Bioresource Technology* **2010,** *101* (2), 469-475.

93. Zhao, F.; Harnisch, F.; Schroder, U.; Scholz, F.; Bogdanoff, P.; Herrmann, I., Challenges and Constraints of Using Oxygen Cathodes in Microbial Fuel Cells. *Environmental Science & Technology* **2006,** *40* (17), 5193-5199.

94. Du, Z.; Li, H.; Gu, T., A state of the art review on microbial fuel cells: A promising technology for wastewater treatment and bioenergy. *Biotechnology Advances* **2007,** *25* (5), 464-482.

95. Torres, C. I.; Kato Marcus, A.; Rittmann, B. E., Proton transport inside the biofilm limits electrical current generation by anode-respiring bacteria. *Biotechnology and Bioengineering* **2008,** *100* (5), 872-881.

96. Rozendal, R. A.; Hamelers, H. V. M.; Rabaey, K.; Keller, J.; Buisman, C. J. N., Towards practical implementation of bioelectrochemical wastewater treatment. *Trends in Biotechnology* **2008,** *26* (8), 450-459.

97. Torres, C. I.; Marcus, A. K.; Rittmann, B. E., Proton transport inside the biofilm limits electrical current generation by anode-respiring bacteria. *Biotechnology and Bioengineering* **2008,** *100* (5), 872-881.

98. Genies, L.; Bultel, Y.; Faure, R.; Durand, R., Impedance study of the oxygen reduction reaction on platinum nanoparticles in alkaline media. *Electrochimica Acta* **2003,** *48* (25-26), 3879-3890.

99. Oh, S.-E.; Logan, B. E., Proton exchange membrane and electrode surface areas as factors that affect power generation in microbial fuel cells. *Applied Microbiology and Biotechnology* **2006,** *70* (2), 162-169.

100. Zhang, M.; Fang, S.; Zakhidov, A. A.; Lee, S. B.; Aliev, A. E.; Williams, C. D.; Atkinson, K. R.; Baughman, R. H., Strong, Transparent, Multifunctional, Carbon Nanotube Sheets. *Science* **2005,** *309* (5738), 1215-1219.

101. Zhang, T.; Zeng, Y.; Chen, S.; Ai, X.; Yang, H., Improved performances of *E. coli*-catalyzed microbial fuel cells with composite graphite/PTFE anodes. *Electrochemistry Communications* **2007,** *9* (3), 349-353.

102. Gil, G.-C.; Chang, I.-S.; Kim, B. H.; Kim, M.; Jang, J.-K.; Park, H. S.; Kim, H. J., Operational parameters affecting the performannce of a mediator-less microbial fuel cell. *Biosensors and Bioelectronics* **2003,** *18* (4), 327-334.

103. Park, H. I.; Sanchez, D.; Cho, S. K.; Yun, M., Bacterial Communities on Electron-Beam Pt-Deposited Electrodes in a Mediator-Less Microbial Fuel Cell. *Environmental Science & Technology* **2008,** *42* (16), 6243-6249.

104. Dresselhaus, M. S.; Eklund, P. C., Phonons in carbon nanotubes. *Advances in Physics* **2000,** *49* (6), 705 - 814.

105. Torres, C. S. I.; Krajmalnik-Brown, R.; Parameswaran, P.; Marcus, A. K.; Wanger, G.; Gorby, Y. A.; Rittmann, B. E., Selecting Anode-Respiring Bacteria Based on Anode Potential: Phylogenetic, Electrochemical, and Microscopic Characterization. *Environmental Science & Technology* **2009,** *43* (24), 9519-9524.

106. Bond, D. R.; Lovley, D. R., Electricity Production by *Geobacter sulfurreducens* Attached to Electrodes. *Appl. Environ. Microbiol.* **2003,** *69* (3), 1548-1555.

107. Kim, B. H.; Park, H. S.; Kim, H. J.; Kim, G. T.; Chang, I. S.; Lee, J.; Phung, N. T., Enrichment of microbial community generating electricity using a fuel-cell-type electrochemical cell. *Applied Microbiology and Biotechnology* **2004,** *63* (6), 672-681.

108. Franks, A. E.; Malvankar, N.; Nevin, K. P., Bacterial biofilms: the powerhouse of a microbial fuel cell. *Biofuels* **2010,** *1* (4), 589-604.

109. Chaudhuri, S. K.; Lovley, D. R., Electricity generation by direct oxidation of glucose in mediatorless microbial fuel cells. *Nat Biotech* **2003,** *21* (10), 1229-1232.

110. Reguera, G.; Nevin, K. P.; Nicoll, J. S.; Covalla, S. F.; Woodard, T. L.; Lovley, D. R., Biofilm and Nanowire Production Leads to Increased Current in *Geobacter sulfurreducens* Fuel Cells. *Appl. Environ. Microbiol.* **2006,** *72* (11), 7345-7348.

111. Tsai, H.-Y.; Wu, C.-C.; Lee, C.-Y.; Shih, E. P., Microbial fuel cell performance of multiwall carbon nanotubes on carbon cloth as electrodes. *Journal of Power Sources* **2009,** *194* (1), 199-205.

112. Li, F.; Sharma, Y.; Lei, Y.; Li, B.; Zhou, Q., Microbial Fuel Cells: The Effects of Configurations, Electrolyte Solutions, and Electrode Materials on Power Generation. *Applied Biochemistry and Biotechnology* **2010,** *160* (1), 168-181.

113. Logan, B.; Cheng, S.; Watson, V.; Estadt, G., Graphite Fiber Brush Anodes for Increased Power Production in Air-Cathode Microbial Fuel Cells. *Environmental Science & Technology* **2007,** *41* (9), 3341-3346.

114. Morozan, A.; Stamatin, I.; Stamatin, L.; Dumitru, A.; Scott, K., Carbon electrodes for microbial fuel cells. *Journal of Optoelectronics and Advanced Materials* **2007,** *9* (1), 221-224.

115. Cheng, S.; Logan, B. E., Ammonia treatment of carbon cloth anodes to enhance power generation of microbial fuel cells. *Electrochemistry Communications* **2007,** *9* (3), 492-496.

116. Dumas, C.; Mollica, A.; Féron, D.; Basséguy, R.; Etcheverry, L.; Bergel, A., Marine microbial fuel cell: Use of stainless steel electrodes as anode and cathode materials. *Electrochimica Acta* **2007,** *53* (2), 468-473.

117. Qiao, Y.; Li, C. M.; Bao, S.-J.; Bao, Q.-L., Carbon nanotube/polyaniline composite as anode material for microbial fuel cells. *Journal of Power Sources* **2007,** *170* (1), 79-84.

118. Zeng, L.; Zhang, L.; Li, W.; Zhao, S.; Lei, J.; Zhou, Z., Molybdenum carbide as anodic catalyst for microbial fuel cell based on Klebsiella pneumoniae. *Biosensors and Bioelectronics* **2010,** *25* (12), 2696-2700.

119. Dewan, A.; Beyenal, H.; Lewandowski, Z., Scaling up Microbial Fuel Cells. *Environmental Science & Technology* **2008,** *42* (20), 7643-7648.

120. Andersson, S.; Nilsson, M.; Dalhammar, G.; Rajarao, G. K., Assessment of Carrier Materials for Biofilm Formation and Denitrification. *Vatten* **2008,** (64), 201-207.

121. Ebrahimi, S.; Fernández Morales, F. J.; Kleerebezem, R.; Heijnen, J. J.; Van Loosdrecht, M. C. M., High-rate acidophilic ferrous iron oxidation in a biofilm airlift reactor and the role of the carrier material. *Biotechnology and Bioengineering* **2005,** *90* (4), 462-472.

122. Kappell, G. M.; Grover, J. P.; Chrzanowski, T. H., Micro-scale surface-patterning influences biofilm formation. *Electronic Journal of Biotechnology* **2009,** *12* (3).

123. Chen, S.; He, G.; Carmona-Martinez, A. A.; Agarwal, S.; Greiner, A.; Hou, H.; Schröder, U., Electrospun carbon fiber mat with layered architecture for anode in microbial fuel cells. *Electrochemistry Communications* **2011,** *13* (10), 1026-1029.

124. He, G.; Gu, Y.; He, S.; Schröder, U.; Chen, S.; Hou, H., Effect of fiber diameter on the behavior of biofilm and anodic performance of fiber electrodes in microbial fuel cells. *Bioresource Technology* **2011,** *102* (22), 10763-10766.

125. Baron, D.; Labelle, E.; Coursolle, D.; Gralnick, J. A.; Bond, D. R., Electrochemical Measurement of Electron Transfer Kinetics by *Shewanella oneidensis* MR-1. *Journal of Biological Chemistry* **2009,** *284* (42), 28865-28873.

126. Torres, C. S. I.; Marcus, A. K.; Parameswaran, P.; Rittmann, B. E., Kinetic Experiments for Evaluating the Nernst−Monod Model for Anode-Respiring Bacteria (ARB) in a Biofilm Anode. *Environmental Science & Technology* **2008,** *42* (17), 6593-6597.

127. Rittman, B. E.; Mccarty, P. L., *Environmental Biotechnology: Principles and Applications*. McGraw Hill: New York, NY, 2001.

128. Katsikogianni, M.; Missirlis, Y. F., Concise review of mechanisms of bacterial adhesion to biomaterials and of techniques used in estimating bacteria-material interactions. *European Cells and Materials* **2004,** *8*, 37-57.

129. Pavithra, D.; Mukesh, D., Biofilm formation, bacterial adhesion and host response on polymeric implants—issues and prevention. *Biomedical Materials* **2008,** *3* (3), 034003.

130. Maissel, L. I.; Glang, R., *Handbook of thin film technology*. McGraw-Hill: 1970.

131. Thormann, K. M.; Saville, R. M.; Shukla, S.; Pelletier, D. A.; Spormann, A. M., Initial Phases of Biofilm Formation in *Shewanella oneidensis* MR-1. *Journal of Bacteriology* **2004,** *186* (23), 8096-8104.

132. Hirst, J., Elucidating the mechanisms of coupled electron transfer and catalytic reactions by protein film voltammetry. *Biochimica et Biophysica Acta (BBA) - Bioenergetics* **2006,** *1757* (4), 225-239.

133. Malvankar, N. S.; Tuominen, M. T.; Lovley, D. R., Biofilm conductivity is a decisive variable for high-current-density *Geobacter sulfurreducens* microbial fuel cells. *Energy & Environmental Science* **2012,** *5* (2), 5790-5797.

134. Liu, C.; Gorby, Y. A.; Zachara, J. M.; Fredrickson, J. K.; Brown, C. F., Reduction kinetics of Fe(III), Co(III), U(VI), Cr(VI), and Tc(VII) in cultures of dissimilatory metal-reducing bacteria. *Biotechnology and Bioengineering* **2002,** *80* (6), 637-649.

135. Carpentier, W.; De Smet, L.; Van Beeumen, J.; Brigé, A., Respiration and Growth of Shewanella oneidensis MR-1 Using Vanadate as the Sole Electron Acceptor. *Journal of Bacteriology* **2005,** *187* (10), 3293-3301.

136. Middleton, S. S.; Latmani, R. B.; Mackey, M. R.; Ellisman, M. H.; Tebo, B. M.; Criddle, C. S., Cometabolism of Cr(VI) by Shewanella oneidensis MR-1 produces cell-associated reduced chromium and inhibits growth. *Biotechnology and Bioengineering* **2003,** *83* (6), 627-637.

137. Wang, H.; Law, N.; Pearson, G.; Van Dongen, B. E.; Jarvis, R. M.; Goodacre, R.; Lloyd, J. R., Impact of Silver(I) on the Metabolism of Shewanella oneidensis. *Journal of Bacteriology* **2010,** *192* (4), 1143-1150.

138. Hau, H. H.; Gilbert, A.; Coursolle, D.; Gralnick, J. A., Mechanism and Consequences of Anaerobic Respiration of Cobalt by Shewanella oneidensis Strain MR-1. *Applied and Environmental Microbiology* **2008,** *74* (22), 6880-6886.

139. Goldstein, J. I.; Newbury, D. E.; Echlin, P.; Joy, D. C.; Lyman, C. E.; Lifshin, E.; Sawyer, L.; Michael, J. R., *Scanning Electron Microscopy and X-ray Microanalysis*. 3rd ed.; Kluwer Academic/Plenum Plublishers: New York, NY, 2003.

140. Rahaman, M. S. A.; Ismail, A. F.; Mustafa, A., A review of heat treatment on polyacrylonitrile fiber. *Polymer Degradation and Stability* **2007,** *92* (8), 1421-1432.

141. Campbell Jr, F., *Manufacturing Processes for Advanced Composites*. Elsevier: New York, NY, 2004.

142. Liu, J.; Wang, P. H.; Li, R. Y., Continuous carbonization of polyacrylonitrile-based oxidized fibers: Aspects on mechanical properties and morphological structure. *Journal of Applied Polymer Science* **1994,** *52* (7), 945-950.

143. National Research Council, U. S. *Drinking Water and Health*; Washington D.C., 1977.

144. Minteer, S. D.; Atanassov, P.; Luckarift, H. R.; Johnson, G. R., New materials for biological fuel cells. *Materials Today* **2012,** *15* (4), 166-173.

145. Bretschger, O.; Obraztsova, A.; Sturm, C. A.; Chang, I. S.; Gorby, Y. A.; Reed, S. B.; Culley, D. E.; Reardon, C. L.; Barua, S.; Romine, M. F.; Zhou, J.; Beliaev, A. S.; Bouhenni, R.; Saffarini, D.; Mansfeld, F.; Kim, B.-H.; Fredrickson, J. K.; Nealson, K. H., Current Production and Metal Oxide Reduction by *Shewanella oneidensis* MR-1 Wild Type and Mutants. *Applied and Environmental Microbiology* **2007,** *73* (21), 7003-7012.

146. Mcdonough, J. R.; Choi, J. W.; Yang, Y.; La Mantia, F.; Zhang, Y. G.; Cui, Y., Carbon nanofiber supercapacitors with large areal capacitances. *Applied Physics Letters* **2009,** *95* (24).

147. Wu, L.; Zhang, X.; Ju, H., Detection of NADH and Ethanol Based on Catalytic Activity of Soluble Carbon Nanofiber with Low Overpotential. *Analytical Chemistry* **2006,** *79* (2), 453-458.

148. Ra, E. J.; Raymundo-Piñero, E.; Lee, Y. H.; Béguin, F., High power supercapacitors using polyacrylonitrile-based carbon nanofiber paper. *Carbon* **2009,** *47* (13), 2984-2992.

149. Zhang, T.; Nie, H.; Bain, T. S.; Lu, H.; Cui, M.; Snoeyenbos-West, O. L.; Franks, A. E.; Nevin, K. P.; Russell, T. P.; Lovley, D. R., Improved cathode materials for microbial electrosynthesis. *Energy & Environmental Science* **2013,** *6* (1), 217-224.

150. Chen, S.; Hou, H.; Harnisch, F.; Patil, S. A.; Carmona-Martinez, A. A.; Agarwal, S.; Zhang, Y.; Sinha-Ray, S.; Yarin, A. L.; Greiner, A.; Schroder, U., Electrospun and solution blown three-dimensional carbon fiber nonwovens for application as electrodes in microbial fuel cells. *Energy & Environmental Science* **2011,** *4* (4), 1417-1421.

151. Xie, X.; Yu, G.; Liu, N.; Bao, Z.; Criddle, C. S.; Cui, Y., Graphene-sponges as high-performance low-cost anodes for microbial fuel cells. *Energy & Environmental Science* **2012,** *5* (5), 6862-6866.

152. Fan, Y.; Xu, S.; Schaller, R.; Jiao, J.; Chaplen, F.; Liu, H., Nanoparticle decorated anodes for enhanced current generation in microbial electrochemical cells. *Biosensors and Bioelectronics* **2011,** *26* (5), 1908-1912.

153. Lowy, D. A.; Tender, L. M.; Zeikus, J. G.; Park, D. H.; Lovley, D. R., Harvesting energy from the marine sediment–water interface II: Kinetic activity of anode materials. *Biosensors and Bioelectronics* **2006,** *21* (11), 2058-2063.

154. Michaelidou, U.; Ter Heijne, A.; Euverink, G. J. W.; Hamelers, H. V. M.; Stams, A. J. M.; Geelhoed, J. S., Microbial Communities and Electrochemical Performance of Titanium-Based Anodic Electrodes in a Microbial Fuel Cell. *Applied and Environmental Microbiology* **2011,** *77* (3), 1069-1075.

155. Xie, X.; Ye, M.; Hu, L.; Liu, N.; Mcdonough, J. R.; Chen, W.; Alshareef, H. N.; Criddle, C. S.; Cui, Y., Carbon nanotube-coated macroporous sponge for microbial fuel cell electrodes. *Energy & Environmental Science* **2012,** *5* (1), 5265-5270.

156. Qiao, Y.; Bao, S.-J.; Li, C. M.; Cui, X.-Q.; Lu, Z.-S.; Guo, J., Nanostructured Polyaniline/Titanium Dioxide Composite Anode for Microbial Fuel Cells. *ACS Nano* **2007,** *2* (1), 113-119.

157. Novoselov, K. S.; Geim, A. K.; Morozov, S. V.; Jiang, D.; Zhang, Y.; Dubonos, S. V.; Grigorieva, I. V.; Firsov, A. A., Electric Field Effect in Atomically Thin Carbon Films. *Science* **2004,** *306* (5696), 666-669.

158. Geim, A. K.; Novoselov, K. S., The rise of graphene. *Nat Mater* **2007,** *6* (3), 183-191.

159. Sharma, R.; Baik, J. H.; Perera, C. J.; Strano, M. S., Anomalously Large Reactivity of Single Graphene Layers and Edges toward Electron Transfer Chemistries. *Nano Letters* **2010,** *10* (2), 398-405.

160. Wang, Q. H.; Jin, Z.; Kim, K. K.; Hilmer, A. J.; Paulus, G. L. C.; Shih, C. J.; Ham, M. H.; Sanchez-Yamagishi, J. D.; Watanabe, K.; Taniguchi, T.; Kong, J.; Jarillo-Herrero, P.; Strano, M. S., Understanding and controlling the substrate effect on graphene electron-transfer chemistry via reactivity imprint lithography. *Nature Chemistry* **2012,** *4* (9), 724-732.

161. Yuan, Y.; Zhou, S.; Zhao, B.; Zhuang, L.; Wang, Y., Microbially-reduced graphene scaffolds to facilitate extracellular electron transfer in microbial fuel cells. *Bioresource Technology* **2012,** *116* (0), 453-458.

162. Mohanty, N.; Berry, V., Graphene-Based Single-Bacterium Resolution Biodevice and DNA Transistor: Interfacing Graphene Derivatives with Nanoscale and Microscale Biocomponents. *Nano Letters* **2008,** *8* (12), 4469-4476.

163. Zhuang, L.; Yuan, Y.; Yang, G.; Zhou, S., In situ formation of graphene/biofilm composites for enhanced oxygen reduction in biocathode microbial fuel cells. *Electrochemistry Communications* **2012,** *21* (0), 69-72.

164. Salas, E. C.; Sun, Z.; Lüttge, A.; Tour, J. M., Reduction of Graphene Oxide via Bacterial Respiration. *ACS Nano* **2010,** *4* (8), 4852-4856.

165. Vargas, M.; Malvankar, N. S.; Tremblay, P.-L.; Leang, C.; Smith, J. A.; Patel, P.; Synoeyenbos-West, O.; Nevin, K. P.; Lovley, D. R., Aromatic Amino Acids Required for Pili Conductivity and Long-Range Extracellular Electron Transport in Geobacter sulfurreducens. *mBio* **2013,** *4* (2).

166. Marsili, E.; Sun, J.; Bond, D. R., Voltammetry and Growth Physiology of Geobacter sulfurreducens Biofilms as a Function of Growth Stage and Imposed Electrode Potential. *Electroanalysis* **2010,** *22* (7-8), 865-874.

167. Nevin, K. P.; Kim, B.-C.; Glaven, R. H.; Johnson, J. P.; Woodard, T. L.; Methé, B. A.; Didonato, R. J., Jr.; Covalla, S. F.; Franks, A. E.; Liu, A.; Lovley, D. R., Anode Biofilm Transcriptomics Reveals Outer Surface Components Essential for High Density Current Production in <italic>Geobacter sulfurreducens</italic> Fuel Cells. *PLoS ONE* **2009,** *4* (5), e5628.

168. Coppi, M. V.; Leang, C.; Sandler, S. J.; Lovley, D. R., Development of a Genetic System forGeobacter sulfurreducens. *Applied and Environmental Microbiology* **2001,** *67* (7), 3180-3187.

169. Borole, A. P.; Aaron, D.; Hamilton, C. Y.; Tsouris, C., Understanding Long-Term Changes in Microbial Fuel Cell Performance Using Electrochemical Impedance Spectroscopy. *Environmental Science & Technology* **2010,** *44* (7), 2740-2745.

170. Ramasamy, R. P.; Ren, Z.; Mench, M. M.; Regan, J. M., Impact of initial biofilm growth on the anode impedance of microbial fuel cells. *Biotechnology and Bioengineering* **2008,** *101* (1), 101-108.

171. Malmsten, M., Formation of Adsorbed Protein Layers. *Journal of Colloid and Interface Science* **1998,** *207* (2), 186-199.

172. Rollefson, J. B.; Stephen, C. S.; Tien, M.; Bond, D. R., Identification of an Extracellular Polysaccharide Network Essential for Cytochrome Anchoring and Biofilm Formation in Geobacter sulfurreducens. *Journal of Bacteriology* **2011,** *193* (5), 1023-1033.

173. Nevin, K. P.; Hensley, S. A.; Franks, A. E.; Summers, Z. M.; Ou, J.; Woodard, T. L.; Snoeyenbos-West, O. L.; Lovley, D. R., Electrosynthesis of Organic Compounds from Carbon Dioxide Is Catalyzed by a Diversity of Acetogenic Microorganisms. *Applied and Environmental Microbiology* **2011,** *77* (9), 2882-2886.

174. Williams, K. H.; Bargar, J. R.; Lloyd, J. R.; Lovley, D. R., Bioremediation of uranium-contaminated groundwater: a systems approach to subsurface biogeochemistry. *Current Opinion in Biotechnology* (0).

175. Williams, K. H.; Nevin, K. P.; Franks, A.; Englert, A.; Long, P. E.; Lovley, D. R., Electrode-Based Approach for Monitoring In Situ Microbial Activity During Subsurface Bioremediation. *Environmental Science & Technology* **2009,** *44* (1), 47-54.

176. Ju, A., Using electroative bacteria, students design toxin snesor. *Cornell Chronicle* 2012.